

***Studies on the structural, electrical and
magnetic properties of composites
based on spinel ferrites***

Thesis submitted to

COCHIN UNIVERSITY OF SCIENCE & TECHNOLOGY

In partial fulfilment of the requirements for the award of the degree of
DOCTOR OF PHILOSOPHY

By

Malini K.A

Department of Physics

Cochin University of Science and Technology

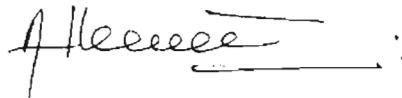
Cochin – 682 022, INDIA

May 2001

Dedicated to my Loving Parents...

CERTIFICATE

Certified that the thesis entitled "*Studies on the structural, electrical and magnetic properties of composites based on spinel ferrites*" is based on the bonafide research work carried out by Mrs. Malini K.A. under my guidance, at the Physics Department, Cochin University of Science & Technology, Cochin - 682 022, and has not been included in any other thesis submitted previously for the award of any degree.



Dr. M. R. Anantharaman

(Supervising Guide)

Dept. of Physics -

Cochin University of Science and Technology

Cochin-22

DECLARATION

I hereby declare that the work presented in this thesis entitled "*Studies on the structural, electrical and magnetic properties of composites based on spinel ferrites*" is based on the original research work carried out by me under the guidance and supervision of Dr. M.R.Anantharaman, Sr. Lecturer, Department of Physics, Cochin University of Science & Technology, Cochin-682 022 and has never been included in any other thesis submitted previously for the award of any degree.

Cochin - 22

30-05-2001



Malini K.A.

CONTENTS

Page No.

Preface

Chapter 1. Introduction

1.1. Evolution of Modern Magnetic Materials.....	01
1.2. Applications of magnetism.....	04
1.3. Magnetic Composites.....	06
1.4. Ferrites.....	07
1.5. Magnetic Nanocomposites	08
1.6. Rubber Ferrite Composites.....	09
1.7. Present Study	10

Chapter 2. Theory and Materials

2.1. Different kinds of Magnetic ordering	13
2.1.1 Diamagnetism.....	14
2.1.2 Paramagnetism.....	15
2.1.3 Ferromagnetism	15
2.1.4 Antiferromagnetism	16
2.1.5 Ferrimagnetism	16
2.2. Important theories of Magnetism.....	16
2.2.1 Langevin theory of paramagnetism.....	16
2.2.2 Weiss Molecular Field theory.....	18
2.2.3 Exchange Interaction.....	19
2.2.4 Neel's Two sublattice theorem.....	20
2.3. Superparamagnetism.....	23
2.4. Spinel ferrites.....	27
2.5. Electrical properties of spinel ferrites.....	29
2.6. Materials	30
2.6.1 Magnetic iron oxide.....	30

2.6.2	Nickel Zinc ferrites.....	30
2.6.3	Ion exchange resins.....	31
2.6.4	Natural Rubber Matrix.....	32

Chapter 3. Experimental Techniques

3.1.	Different schemes of preparation of magnetic nanocomposites	35
3.2.	Preparation of nanocomposites by ion exchange method.....	36
3.3.	Differential Scanning Calorimetry.....	37
3.4.	Vibrating sample magnetometry.....	38
3.5.	Iron Content Estimation.....	40
3.6.	Mössbauer Spectroscopy.....	40
3.7.	ESR Spectroscopy.....	43
3.8.	Preparation of ceramic nickel zinc ferrite samples.....	45
3.9.	Structural Evaluation of Ceramic NZF.....	46
3.10.	Incorporation of $Ni_{1-x}Zn_xFe_2O_4$ in natural rubber matrix	47
3.11.	Cure Characteristics.....	49
3.12.	Evaluation of hardness of the prepared RFCs.....	50
3.13.	Evaluation of Mechanical properties.....	50
3.14.	Dielectric measurements	51
3.15.	AC conductivity measurements.....	54

Chapter 4. Effect of cycling on the magnetisation of magnetic nanocomposites and decomposition studies on the composites

4.1.	Introduction.....	56
4.2.	Optimisation of the preparation conditions	57
4.3.	XRD studies.....	60
4.4.	Magnetic Studies.....	65
4.5.	Fe Content estimation	67
4.6.	Mössbauer studies.....	67
4.7.	Conclusion	69

Chapter 5. Low Temperature studies on magnetic nanocomposites

5.1. Introduction.....	70
5.2. Low temperature magnetisation studies.....	73
5.3. Mössbauer Studies.....	74
5.4. ESR studies on the nanocomposites samples.....	83
5.5. Conclusion.....	86

Chapter 6. Magnetic and Processability Studies on RFCs

6.1. Introduction.....	88
6.2. Structural Evaluation.....	89
6.3. Cure Characteristics.....	95
6.4. Magnetic Measurements.....	98
6.4.1 Ceramic samples.....	98
6.4.2 Composite samples.....	100
6.4.3 Tailoring of magnetic properties.....	103
6.5. Conclusion.....	107

Chapter 7. Dielectric and Mechanical properties of RFCs

7.1. Introduction.....	109
7.2. Dielectric Measurements.....	110
7.2.1 Ceramic samples.....	110
7.2.2 Dielectric properties of Blank Natural rubber.....	117
7.2.3 Dielectric properties of RFCs.....	118
7.3. Mechanical Properties.....	125
7.4. Hardness Measurements.....	127
7.5. Conclusion.....	128

Chapter 8. AC conductivity studies on RFCs

8.1. Introduction.....	129
8.2. Frequency dependence of AC conductivity.....	130
8.2.1 Ceramic samples.....	130
8.2.2 Blank Natural rubber.....	132
8.2.3 Composite samples.....	133
8.3. Compositional dependence.....	134

8.3.1 Ceramic Samples.....	134
8.3.2 Composite samples.....	135
8.4. Loading dependence.....	136
8.5. Temperature dependence.....	137
8.5.1 Ceramic Samples.....	137
8.5.2 Blank Natural rubber.....	139
8.5.3 Composite samples.....	139
8.6. Activation energy for conduction.....	141
8.7. Conclusion.....	142

Chapter 9. Summary and Conclusion.....143

References

Annexure I. Studies on the influence of dopants on the properties of maghemite (M.Phil Dissertation work)

Annexure II. List of publications/communicated papers

Preface

Magnetism and magnetic materials play very important role in the day to day life of human beings. They have a vital role in making life more humane. The principle of magnetism is applied in making a multitude of devices which are essentially passive energy storage devices. They find extensive applications in devices like inductor cores, circulators, isolators, refrigerator door seals, EMI shields and storage media, to mention a few.

Ferrites are a class of ferrimagnetic materials and the last century has witnessed tremendous amount of research activity in the area of ferrites. This has lead to the development and establishment of many theories and models in addition to or complementing those obtained from research on metallic materials. Efforts to improve upon or to replace the existing devices by materials with superlative properties have been a canonical attribute of scientists and engineers. In this pursuit new materials and new theories take birth. Magnetism and magnetic materials also witnessed a similar revolution with the discovery of magnetic nanocomposites and magnetic nanomaterials.

Early 90's witnessed a surge of activities in the nanostructured materials. Though Richard Feynman had predicted way back in 50's that in the 21st century engineering applications will be at the nanoscale, Feynman's prediction that "There is plenty of room at the bottom" has come true. Now, considerable attention is being paid to this area worldwide. Nanoparticles exhibit superlative properties when compared to their coarser cousins. As Rustham Roy, one of the pioneers in the nanophysics, has rightly said "It's really a new ball game at the nanolevel". At the nanoscopic scale many underlying principles that govern the properties are different. New theories are to be drawn or formulated to explain the behaviour of these materials. In this work too, efforts are made to explain or postulate the nanoscale behaviour of the magnetic composites.

Magnetic nanocomposites are known to exhibit remarkable properties compared to their bulk counterparts. Magnetic nanocomposites with magnetic nanoparticles dispersed in polymer matrices have gained considerable attention

because of their wide ranging applications. Below a critical size they become single domain as against the multidomain in bulk. These composites exhibit phenomena like superparamagnetism, quantum tunneling of magnetization and magnetocaloric effect. Moreover, they are also found to possess large coercivities. They have the potential to make new devices like image sensors, magnetic refrigerators and ferrofluids.

Ceramic magnetic materials used in devices have the inherent drawback in that, they are not easily machinable to obtain complex shapes. Plastic magnets or elastomer magnets have the advantages of flexibility and mouldability. They are light weight and low cost. Hence plastic magnets or rubber ferrite composites have the potential in replacing the ceramic type of magnetic materials for applications where flexibility is an important criterion. Moreover, they are also important because of their microwave absorbing properties.

Spinel ferrites are a major class in itself among the ferrite materials because of their high resistivity and appropriate permeability and permittivity. They also have the unique advantage of being tailored and so their properties can be altered by a judicious choice of the constituents and appropriate preparative techniques.

This thesis mainly deals with the preparation and studies on magnetic composites based on spinel ferrites prepared both chemically and mechanically. Rubber ferrite composites (RFC) are chosen because of their mouldability and flexibility and the ease with which the dielectric and magnetic properties can be manipulated to make them as useful devices. Natural rubber is chosen as the matrix because of its local availability and possible value addition. Moreover, NR represents a typical unsaturated nonpolar matrix. The work can be thought of as two parts. Part I concentrates on the preparation and characterisation of nanocomposites based on $\gamma\text{-Fe}_2\text{O}_3$. Part II deals with the preparation and characterisation of RFCs containing Nickel zinc ferrites.

In the present study magnetic nanocomposites have been prepared by ion exchange method and the preparation conditions have been optimised. The in situ incorporation of the magnetic component is carried out chemically. This method is selected as it is the easiest and simplest method for preparation of nanocomposite. Nanocomposite samples thus prepared were studied using VSM, Mossbauer

spectroscopy, Iron content estimation, and ESR spectroscopy. For the preparation of RFCs, the filler material namely nickel zinc ferrite having the general formula $Ni_{1-x}Zn_xFe_2O_4$, where x varies from 0 to 1 in steps of 0.2 have been prepared by the conventional ceramic techniques. The system of $Ni_{1-x}Zn_xFe_2O_4$ is chosen because of their excellent high frequency characteristics. After characterisation they are incorporated into the polymer matrix of natural rubber by mechanical method. The incorporation is done according to a specific recipe and for various loadings of magnetic fillers and also for all compositions. The cure characteristics, magnetic properties and dielectric properties of these composites are evaluated. The ac electrical conductivity of both ceramic nickel zinc ferrites and rubber ferrite composites are also calculated using a simple relation. The results are correlated.

A general introduction to magnetic materials and magnetic composites and a brief review of the history of magnetic materials along with an outline of the different applications and importance of magnetic composites is cited in **CHAPTER 1**. This chapter introduces the two systems under the present study, namely, chemically and mechanically prepared composites with special emphasis on their importance and applications.

CHAPTER 2 deals with various fundamental theories and phenomena that are central to this work. It also explains the spinel structure of ferrites and crystal chemistry of ferrites. Different magnetic ordering with special emphasis on superparamagnetism is discussed and dealt with in this chapter.

Various experimental techniques including preparative conditions and analytical tools employed for characterisation of the composites at various stages are discussed in **CHAPTER 3**. Different schemes for the synthesis of nanocomposites with particular reference to ion exchange method are also listed in this chapter. This is followed by a description of the different characterisation techniques adopted for this system at various stages. This include an outline of magnetic measurements, iron content estimation, Electron Spin Resonance spectroscopy (ESR), Differential Scanning Calorimetry (DSC) and Mossbauer spectroscopy. Preparation of ceramic nickel zinc ferrites belonging to the series $Ni_{1-x}Zn_xFe_2O_4$ by ceramic technique and their incorporation in Natural rubber matrix and characterisation techniques used at various stages are also cited in this experimental chapter. Cure characteristics of these rubber ferrite composites were

carried out by using a Gottfert Elastograph. Vulcanisation of these samples were done on an electrically heated hydraulic press up to their respective cure time. Dielectric studies of these powder samples and rubber ferrite composites were done using a dielectric cell and an impedance analyser (model: HP4285A) in the frequency range 100KHz to 8MHz. The acquisition of data is fully automated by employing a software package called LABVIEW which in turn is based on the principle of virtual instruments(VI). From the capacitance value obtained for different frequencies, dielectric constant was calculated by using the parallel plate capacitance method. From the dielectric data the ac electrical conductivity of these samples were also evaluated. Magnetic properties of ceramic $\text{Ni}_{1-x}\text{Zn}_x\text{Fe}_2\text{O}_4$ and the rubber ferrite composites were carried out by using Vibrating sample magnetometer (VSM) model: (EG&G PAR 4500).

Synthesis of magnetic nanocomposites are explained in detail in **CHAPTER 4**. This chapter also deals with the optimisation of the preparation conditions and effect of cycling on the magnetic properties of the prepared composites. The ion content is estimated for the cycled samples. The results are correlated.

CHAPTER 5 deals with the low temperature magnetic studies on the nanocomposites prepared. ESR and Mossbauer studies were used as analytical tools to interpret the results obtained at low temperatures.

Structural and magnetic properties of ceramic fillers, cure characteristics and processability of RFCs and the magnetic properties of RFCs are dealt with in **CHAPTER 6**. The processability of the composites are studied and the variation of magnetisation and coercivity with composition for different filler loadings are compared and correlated. The correlation of the properties are carried out with a view to tailoring materials with specific magnetic properties. A general equation was formulated to predict the magnetic properties of the composites from the known values of the magnetisation of the filler material. The measured and calculated values are compared and correlated.

The dielectric properties of ceramic $\text{Ni}_{1-x}\text{Zn}_x\text{Fe}_2\text{O}_4$ and rubber ferrite composites containing $\text{Ni}_{1-x}\text{Zn}_x\text{Fe}_2\text{O}_4$ were evaluated and the results are discussed in **CHAPTER 7**. The frequency, composition, loading and temperature dependence of dielectric constant are studied and explained. Semi empirical mixture equations are proposed to correlate the dielectric properties of the

composites with various loadings. Correlation of the properties indicate that the magnetic and electrical properties can be modified appropriately by judicious choice of composition(x) and an appropriate amount of the filler. The temperature dependence of the dielectric constant of the ceramic samples as well as the RFCs and the dielectric properties of the blank natural rubber are also discussed in this chapter.

CHAPTER 8 explains the calculation of ac electrical conductivity (σ_{ac}) using the data available from the dielectric measurements by employing a simple relationship for both ceramic $Ni_{1-x}Zn_xFe_2O_4$ and also for rubber ferrite composites. The variation of σ_{ac} with frequency, composition, temperature and loading are discussed and explained in detail in this chapter. From the temperature dependence of σ_{ac} the activation energy for conduction was also calculated and is given in this chapter.

In **CHAPTER 9** the conclusions drawn from the studies on both chemically and mechanically prepared composites are listed. The observations and results are discussed and compared for both systems. Commercial importance and possibility for applications of these composites are also discussed in this chapter. This chapter also gives the description of future works possible in the system under investigation.

Finally the Dissertation work carried out during the M.Phil. Course is given as an Annexure(Annexure I).

Acknowledgement

Not much in this thesis would have come to fruition without the interaction and support of many people. I have great pleasure to acknowledge them and all their help.

The investigations in this thesis have been carried out under the supervision of Dr. M. R. Anantharaman, Sr. Lecturer, Dept. of Physics, Cochin University of Science and Technology. I express my deep sense of gratitude for his excellent guidance, competent advice and constant encouragement without which the successful completion of this work would not have been possible.

I am thankful to Dr. Elizabeth Mathai, Head of the Department of Physics, Prof. K. P. Rajappan Nair, Prof. M. Sabir and Prof. K. Babu Joseph, former Heads of Department of Physics, for providing me the necessary facilities.

With pleasure I thank all faculty members especially Dr. S. Jayalekshmi and Dr. B. Pradeep and all non-teaching staff of the Department of Physics for their help throughout the course of this work.

I also express my deep sense of gratitude to Prof. Philip Kurian, Department of PS & RT, Cochin University of Science and Technology, for fruitful discussions and guidance during various stages of this work and for allowing me to use their laboratory for sample preparation. I am thankful to Dr. A. Kuraiyose, former Head of the department of PS&RT for permitting me to use their laboratory and library facilities. I also thank the other faculty members, technical staff and research scholars of polymer science department for their help during this work.

With pleasure I express my sincere thanks to Prof. V.N. Sivasankara Pillai Director, School of Environmental Sciences, for his timely help and advice in the initial stages of this work. I also thank Mr. M. Balachandran, Research Scholar, School of Environmental Science for his help.

With great pleasure I express my sincere thanks to Prof. A. Narayanasamy, Mr. C. N. Chinnasamy, Mr. N. Ponpandian, Mr. Justin Joseph and Miss. Latha. B of the Department of Nuclear Physics, Guindy campus, Madras University, for the valuable discussions and for helping with the magnetic measurements. My thanks are also due to Dr. P. A. Joy, Dr. S. D. Kulkarni, and Dr. S. K. Date of Physical Chemistry Division, NCL Pune, Mrs. Geetha Sreenivasan, Ms. Vrinda Viswanathan and Mr. Paul Davis of IIT, Mumbai,

Acknowledgement

Prof. Ajay Gupta, Dr. Alok Banerjee and Dr. B. Dasannacharya of IUC DAET Indore for their help in various stages of this work.

I would like to thank Dr. Jacob Philip, Former Head and the technical staff of the Department of Instrumentation, for their help in completing this work. I also express my sincere thanks to Prof. Madhavan Pillai (former Head) and Dr. P. A Unnikrishnan of Chemistry Department for their help.

I thankfully acknowledge the financial assistance from University Grants Commission (UGC) and Council for Scientific and Industrial Research (CSIR), Govt. of India, in the form of the fellowship (CSIR award No. F.No.9/239(243)/97/EMR-I). I also thank Department of Science and Technology (GOI) for the project sanctioned to Dr. M. R. Anantharaman.

Words are insufficient to express my gratitude to my colleagues, Mr. C. Joseph Mathai, Ms. S. Sindhu, Mr. S. Saravanan, Mr. Santhosh D Shenoy, Mr. E. M. Mohammed, Mr. M. A. Solomon, Mr. Mathew George and Mrs. Prema K.H. for their support throughout my research career. I thank them for the creative suggestions and lively moments in the lab. Without their support I wouldn't have completed this work. I also thank my former labmates Mrs. Girija Nair, Mr. S. Jagatheesan and others for their love and support.

All my friends in the Department especially Mr. Shaji S, Mr. Saji Augustine and Ms. Viji Varghese owe special thanks for the joyful and friendly atmosphere they provided for me. I thank Ms. Manju T for helping me in the finishing stages of my work. I also thank my dear friends Latha, Ani and Valsu for the support, encouragement and love given to me throughout my research life. I also thankfully remember all those who have been my teachers and all classmates in my entire academic life.

At this moment I remember with love and thanks, the inspiration, love and the blessings of my parents, father in law, mother in law, sisters, brother and brother in laws. I sincerely thank them and all other family members for their blessings. I also thank the support and inspiration I received from my husband Mr. Jayaram and my little son Appu.

There are innumerable friends and well wishers who have helped directly or indirectly in the completion of this work and I thank them individually for their help and support.

Last but not least I thank God Almighty for all His Blessings.


Malini K. A.

CHAPTER 1

INTRODUCTION

Magnetic materials are pervasive throughout our society. They are used, for instance, in magnetic recording media and devices, in motors, in transformers, on credit cards, as permanent magnets, as magnetic sensors on cheques, in theft control devices, in automotive and small engine timing devices, in xerographic copiers, in magnetic resonance imaging (MRI) machines, in microwave communications, in magnetic separation, and in magnetic cooling. Virtually they pervade all human activities. Magnetic materials include metals, ceramics and polymers at different size scales ranging from large castings to particulates, thin films, multilayers and nanocomposites.

1.1 Evolution of Modern Magnetic Materials

Magnetism was known from antiquity, but the scientific study of its nature did not begin in right earnest until the Renaissance. Research on magnetism received the required impetus during the eighteenth and early nineteenth centuries. Hans Christian Oersted in 1819, André Marie Ampère in 1820, and Michael Faraday in 1821 established the relationship between electricity and magnetism. Ampère's (1827) account of his electrodynamic theory showed that magnetism and electromagnetism were the same force, and both can be produced by electrical currents.

In the 1900's Edward M. Purcell and Felix Bloch, both American physicists developed a way to measure the magnetic field of the nuclei, which was the first step to the well known Magnetic Resonance Imaging (MRI). The French Physicist Paul Langevin (1872- 1946) studied temperature dependence of magnetic properties. Pierre Ernst Weiss (1865 – 1940) modified Langevin's theory by postulating the internal molecular field.

Niel Bohr's theory of atomic structure provided an understanding of the periodic table and shed light on the magnetic properties of transition elements, such as iron and the rare earths or in compounds containing these elements. The spin of electrons and the subsequent magnetic property was discovered by Samuel Abraham Goudsmit (1902 – 1978) and George Engene Uhlenbeck (1900 – 1988). 1970's witnessed the discovery of superconducting magnets, which can be considered as one of the landmarks in modern science(1-8).

The discovery of Giant Magneto Resistance (GMR) in 1988, in structures of alternating magnetic and nonmagnetic thin layers, was the accumulation of several decades of intensive research in thin film magnetism and improvements in epitaxial growth techniques developed mainly in semiconductor materials (5).

In 1995, a different class of high magnetoresistive materials was discovered in which the nonmagnetic layer separating the two ferromagnetic layers is made with an ultrathin insulating material, such as an aluminum oxide layer $< 20 \text{ \AA}$ thick. The gradual improvement of GMR and other materials have made them attractive for nonvolatile magnetic random access memory (MRAM) applications. MRAM is the newest technique, concerning the storage of bits for a certain period. One of the most important characteristics of MRAM, is the fact that it uses the spin of an electron, rather than the charge, to indicate the presence of a "1" or a "0". The potential to make MRAM a high density, high speed, and low power, general purpose memory prompted intense research on this materials.

Late nineties also witnessed the birth of the new era of nanomaterials. As the size of magnetic elements scales below 20 nm, a superparamagnetic phase emerges in which the room temperature thermal energy overcomes the magnetostatic energy well of the element, resulting in zero hysteresis. In other words, although the element itself is a single-domain ferromagnet, the ability of an individual magnetic "dot" to store magnetization orientation information is lost when its dimension is below a threshold. On the other hand, suitably prepared alloys of immiscible ferromagnetic and nonmagnetic metals that contain single-domain ferromagnetic grains in a nonmagnetic matrix have been shown to exhibit GMR characteristics. Nanometric magnetic materials exhibit many other

remarkable properties other than GMR. Thus it is a new era of miniaturization, that has opened up with the nanoscaling of the magnetic materials(5-7).

A very exciting consequence of ultrascaled magnetic particles is quantum tunneling of the magnetization direction of a collection of spins. There is no simple Schrödinger equation that describes this process, since it is not an elementary particle that is tunneling but a collective coordinate.

Another interesting type of nanomagnetic structure is nanometer ferromagnetic wires fabricated using conventional nanolithography, nanoimprint lithography, AFM/MFM direct writing, groove deposition, and electrodeposition into pores of template polymer membranes. Such nanowires of either single layer or multilayers may provide new approaches to very small magnetoresistive sensors, ultrahigh-density hard disks, and other extensions of conventional applications(10).

Recently, molecular magnetism is receiving much attention with the development of a variety of synthesis techniques largely adapted from biology and chemistry. Magnetic materials prepared from molecules, not atoms or ions, have enabled the establishment of a diverse new class of magnets with magnetic ordering temperatures well above room temperature. As a class, molecule-based magnets are anticipated to exhibit a collection of technologically important attributes that include: modulation/tuning of properties via organic chemistry methodologies, compatibility with polymers for composites, low density, flexibility, transparency, low temperature processibility, insulating, solubility, high coercivity, high strength, low environmental contamination, biocompatibility, high magnetic susceptibilities and permeabilities, high magnetizations, low magnetic anisotropy and semiconducting behavior. Many of these nonmagnetic characteristics are not available with conventional atom-based magnets. Natural and artificial ferritin proteins are examples molecular magnets. Another example of molecular magnetism is a cobalt-iron-cyanide-based Prussian blue analog (11-13).

1.2 Applications of Magnetism

Magnetism and magnetic materials find applications in almost all realms of human life. They play a vital role in making life more sophisticated and humane. The most important use of magnets in the home, is the electric motors. All electric motors use electromagnets. These motors run refrigerators, vacuum cleaners, washing machines, compact disc players, blenders, drills, race cars etc. Audiotape and videotape players have electromagnets called *heads* that record and read information on tapes covered with tiny magnetic particles. Magnets in speakers transform the signal into a sound by making the speakers vibrate. An electromagnet called a deflection yoke in TV picture tubes helps form images on a screen. (4-10)

The magnets used in the industry and business are mostly electromagnetic powered devices, such as cranes, cutters, fax machines, computers etc. Generators in power plants rely on magnets like the ones found in electric motors to produce electricity. Transformers are devices that use electromagnetics to change high-voltage electricity to low-voltage electricity needed in homes and businesses. In transportation, systems that use electromagnetics are trains, subways, trolleys, monorails, escalators, elevators etc. Scientists and engineers have developed trains that use electromagnetism to float it above the track. They use the force of a magnet to levitate the train. It eliminates friction so it has an advantage of higher speeds over ordinary trains.

In Science and medicine, bending magnets are very powerful magnets that help control beams of atomic particles which is boosted into high speed devices called particle accelerators. Magnetic bottles are created to hold plasmas which is so hot they would melt any container made of ordinary material, So they hold it in a magnetic field, (magnetic bottles). Magnetic resonance imaging (MRI) is the technique used primarily in medical settings to produce high quality images of the inside of the human body. MRI is based on the principles of nuclear magnetic resonance (NMR), a spectroscopic technique used by scientists to obtain microscopic chemical and physical information about molecules. The principle of MRI is applicable in the human body because we are all filled with small

biological magnets, the most abundant and responsive of which is the nucleus of the hydrogen atom, the proton. The principle of MRI takes advantage of the random distribution of protons which possess fundamental magnetic properties

Dilute magnetic semiconductors are appealing materials for magneto-optical devices. Ferromagnetic semiconductors are obtained by doping magnetic impurities into host semiconductors. They are key materials for spin electronics (spintronics) in which the correlation between the charge and spin of electron is used to bring about spin dependent electronic functionality such as GMR and spin field effect transistor(5). Among such materials reported so far GaAs has a T_c of about 100K.

Manipulation of magnets with electric current is an integral part of everyday technology. It is the operating principle behind the electric motors and determines how information is written on magnetic memory devices. This concept of moving electric charges developing a magnetic field which exerts force on magnets is an old understanding. There is another mechanism by which an electric current can reorient magnets and for very small devices this mechanism is more powerful than current induce magnetic fields. This new mechanism is called spin transfer and this is based on the interaction of the magnet with the intrinsic spin of the electrons(6).

Magnetic nanocomposites find lot of applications because of their remarkable properties. They are used as magnetic recording media, colour imaging, ferrofluids, catalysts etc. Magnetic nanocomposite consisting of iron oxide embedded in polymer matrices are found to be behaving like transparent magnets with remarkable electrical and optical properties. Flexible magnets or rubber ferrite magnets find applications in many devices because of their easy mouldability and microwave absorbing properties(14-15).

Magnetic ceramics or ferrites, are very well established groups of magnetic materials. Research activity on ferrites, especially intense in the last 50 years, has led to establishment of many theories and models in addition to or complementing those obtained from research on metallic materials. Magnetic ceramics participate in virtually every application areas. Ferrites have become a reference material; developments associated with other new magnetic materials, such as the extra

hard rare earth inter metallics or the extra-soft amorphous ribbons are often assessed by comparison with ferrites.

Eventhough magnetic ceramics are very well established, but improvements and innovations continue to take place; many new and exciting applications, theories and preparation technologies are currently under development. Ferrites are complex because they combine two complex areas; ceramic microstructures and magnetic phenomena. Ceramic microstructures, formed as a result of physico-chemical processes such as solid state sintering are affected by a large number of interacting variables. The quantum mechanical nature of their magnetic properties makes them difficult to comprehend since they are entirely different to macroscopic everyday experience. The study of ferrites; their synthesis/fabrication; establishing the relationship between crystal structure, texture and physical properties and the modeling of magnetic interactions, is of necessarily interdisciplinary.

1.3 Magnetic Composites

The designer's demand for light weight and improved properties for different applications and the solid-state theory's predictions of extremely high potential of composite materials have resulted in vast research interest on composite materials especially on magnetic composites(16).

In the broadest sense, composites are mixtures of chemicals. They are composed of two or more materials. Usually, composites are the result of embedding fibers, particles, or layers of one material in a matrix of another material. Thus composites are designed to exploit the best properties of both components to produce a material that surpasses the performance of the individual parts.

Polymer matrix composites are the most commonly used of the advanced composite materials. These materials can be fashioned into a variety of shapes and sizes. They provide great strength and stiffness along with a resistance to corrosion.

Magnetic composites in which magnetic component is embedded in nonmagnetic matrix have gained considerable interest in recent year as they can have the magnetic properties of the filler as well as the mechanical and physical properties of the matrix(17-18). The most important advantage of composite materials is that one can tailor materials depending on their applications by suitable selection of the filler and the matrix. The chemical and physical properties of composites can be tailored to meet the needs of each individual application. The vast potential of composites will never be completely exploited until a time comes when it is no longer possible to design revolutionary new composite materials.

The study of composite materials assumes significance not only from the application point of view, but also from the fundamental point of view. It will be of interest to study the effect of the components on various properties of the composites. A systematic study in this respect will help in tailoring materials for various applications. Also the studies on magnetic nanocomposites will help in understanding the physics behind small scale particles.

This thesis is on the preparation and characterization of some magnetic composites based on spinel ferrites. The systems under study can be divided into two, depending on their method of preparation namely, chemically prepared composites and mechanically prepared composites. In the chemically prepared composites it is assumed that the magnetic component incorporated is in the nanometer range and hence they are called magnetic nanocomposites and the mechanically prepared composites has rubber as one of the component and is called rubber ferrite composite(RFC). The common feature of these two systems is that the magnetic components in both these systems belong to the spinel ferrite systems. Since the focal theme of the present work centers on composites containing spinel ferrite, a brief description about ferrites in general and spinel ferrites in particular will be given in the ensuing paragraphs.

1.4 Ferrites

Ferrites are mixed metal oxides with iron oxides (Fe^{3+}) as their main component. They exhibit spontaneous magnetisation and phenomena like magnetic saturation and hysteresis. Ferrites can generally be classified in to three

groups namely spinels, Garnets and Magneto-plumbites. Spinel ferrites have a cubic structure with general formula $MO.Fe_2O_3$, where M is a divalent metal ion like Mn, Ni, Fe, Co, Mg etc. Garnets have a complex cubic structure having a general formula $Ln_3^{III}Fe_eO_{12}$. The third type magneto-plumbite is having a hexagonal structure with general formula $MO.Fe_{12}O_{18}$. The most important in the group of magneto plumbite is barium ferrite $BaO.Fe_{12}O_{18}$, which is a hard ferrite(1,2,5,8).

Spinel ferrites are important over conventional magnetic materials because of their wide variety of applications. They have low electrical conductivities when compared to other magnetic materials and hence they find wide use in microwave applications. The present system under study namely Nickel zinc ferrites have very good permittivity and permeability values. Systems similar to $Ni_{1-x}Zn_xFe_2O_4$ also have the unique advantage that their magnetic and dielectric properties can be tailored for various applications. Gamma ferric oxide is another important member of the spinel ferrite family. $\gamma-Fe_2O_3$ has a vacancy ordered spinel structure with general formula $Fe^{3+} \left[Fe_{\frac{5}{3}}^{3+} \Gamma_{\frac{1}{3}} \right] O_4^{2-}$ where Γ represent the vacancies concentrated on B sites. This has the advantage of modifying the magnetic properties by addition of suitable dopants.(1,2)

1.5 Magnetic Nanocomposites

As already mentioned as the size becomes smaller and smaller properties of materials become different from that of their bulk counterparts. The discovery of nanoscopic materials have opened up new vistas in the frontier areas of material science and technology. The recent advances in nanotechnology has made it possible to devise newer materials with novel chemical, magnetic and electrical properties(19,20). Particles possessing nanometric dimensions, lying in the range 1-10nm are found to be exhibiting superior physical properties with respect to their coarser sized cousins. The properties of nanostructured materials are determined by the complex interplay among the building blocks and the interfaces between them.

Single nanosized magnetic particles are mono-domains and one expects that also in magnetic nanophase materials the grains correspond with domains,

while boundaries on the contrary to disordered walls. Magnetic nano-composites have been used for mechanical force transfer (ferrofluids), for high density information storage and magnetic refrigeration(20-23). Multilayers and other types of materials containing nanocomposites are found to exhibit properties like GMR and magnetocaloric effect. A research team led by Ron Ziolo (21) has developed a composite material consisting of 5 to 10-nm magnetic iron-oxide particles lodged in a polymer matrix. This nanocomposite material consists of tiny magnetic particles dispersed in a lightweight, insulating polymer solid. They serve as transparent magnets and also can be converted into magnetic fluids. Other than serving as a lossless transformer, the nanomagnets could act as miniature switches or sensors in smart materials, or as a form of microwave shielding. Also, the material is expected to have novel acoustic, thermal, and optical properties. Besides these the magnetic nanocomposites can find applications in medical diagnostics, digital information storage, leak free sealing and detection and sensing devices(19-23).

1.6 Rubber Ferrite Composites (RFCs)

Flexible magnets(include plastic magnets and rubber magnets) are compounds of polymers with magnetic fillers. Rubber ferrite composites are composite materials of ferrite fillers and natural/synthetic matrix. They are light in weight, soft, elastic, stable, flexible, easy to be processed and energy-saving. The application field ranges from electronic & electric industry, motor stators and rotors, information technology, printing and decoration etc. The size, shape and magnetization pattern can be manufactured according to user's need(24,33).

In magnetic polymers the magnetic powder as well as the polymer chosen affect the processability and other physical properties of the final product. In tailoring composites for various applications it is necessary to select the proper filler and matrix. The polymer matrix must have appropriate mechanical and chemical properties. The macroscopic properties of the composite magnetopolymers is influenced by the interactions between the filler and the matrix. It may also be noted that systematic study of such composites can help tailor materials for various applications.

Incorporation of polycrystalline ferrites in elastomer matrixes will lead to flexible rubber ferrite composites or RFC(34-36). An appropriate selection of

magnetic filler and matrix can result in RFCs with required properties for different application. For plastic magnets it is easy to see that the properties of the polymer matrices, especially viscoelasticity may affect the processability as well as magnetic property. Rubber ferrite composites (RFCs) can be synthesized by the incorporation of ferrite powders in natural or synthetic rubber like butyl or nitrile rubber matrixes. This can not only bring in economy but also can produce flexible magnets. The impregnation of magnetic filler in the matrix imparts magnetic properties into the matrix and modifies the dielectric properties of the matrix. The microwave absorbing properties of elastomer warrants an appropriate dielectric strength and a desirable magnetic property. This can be achieved by synthesizing RFC wherein appropriate amount of fillers are incorporated into the rubber matrix. Factors like percolation limits or nature of the matrix, like saturated/ unsaturated / polar rubber all influences the final properties of the composites. In principle the macroscopic parameters of the composites would be influenced by the interaction between the filler and the matrix. The effect of fillers in modifying the properties is to be understood properly in explaining the various properties of the composites.

The Rubber Ferrite Composites find applications in microwave and anti radar applications(27-31). They are found to be very good microwave absorbers and are useful for EMI shielding. Here their lightweight, low cost and flexibility are added advantages. Depending on the filler characteristics as well as filler loading one can vary the properties of these composites. Also addition of carbon black is known to modify the dielectric as well as microwave absorbing properties of the RFCs. Thus these composites are ideal for applications where desired permittivity and permeability are one of the criteria.

1.7 Present Study

In the present study attempts are made to prepare magnetic composites by chemical as well as mechanical means. In the magnetic nanocomposites synthesis the incorporation of the magnetic component is made by chemical methods and in RFC preparation the precharacterised magnetic filler namely Nickel zinc ferrite ($\text{Ni}_{1-x}\text{Zn}_x\text{Fe}_2\text{O}_4$ for various x) were embedded into natural rubber matrix. In preparing composites the choice of the magnetic filler and the optimal size and shape of the filler particles are very important. A judicious choice of the magnetic

filler with the appropriate recipe can give a combination of dielectric and magnetic properties suited for various applications.

Gamma iron oxide is a commercially important magnetic material. Almost 90-99% of the recording industry use $\gamma\text{-Fe}_2\text{O}_3$ and materials derived from $\gamma\text{-Fe}_2\text{O}_3$ as the recording media. It is important from the fundamental point of view also. It contains only one cation, namely the triply charged iron ion. They have high electrical resistivity which means that the electrons are localized. Because of these properties $\gamma\text{-Fe}_2\text{O}_3$ can be considered as a prototype for the study of ferrimagnetism. The main problem encountered in the study of $\gamma\text{-Fe}_2\text{O}_3$ and $\gamma\text{-Fe}_2\text{O}_3$ based system is the difficulty in their preparation. In the present study of composite magnetic materials it is envisaged to incorporate $\gamma\text{-Fe}_2\text{O}_3$ into a polymer matrix of sulphonated polystyrene and study their magnetic characteristics.

Nickel zinc ferrite is an important member in the class of general ferrites, because of their various properties. For example they exhibit a wide range of permeability, coercive force and magnetic and electric loss. Their magnetic and electrical properties can be varied depending on the composition. They are also important because of their relatively high resistivity at carrier frequencies and sufficiently low loss for microwave applications. They find application in many electronic devices. Hence in this work it is proposed to prepare nickel zinc ferrite belonging to the series $\text{Ni}_{1-x}\text{Zn}_x\text{Fe}_2\text{O}_4$, where x varies from 0 to 1 in steps of 0.2. It will also be interesting to study the variations in magnetic, dielectric and conducting properties with respect to the change in composition and also the structural properties. Synthesis of composites based on nickel zinc ferrites is of interest to physicists and electrical engineers because the addition of fillers modifies the magnetic and dielectric properties of the matrix considerably.

In the first case attempt is made to incorporate $\gamma\text{-Fe}_2\text{O}_3$ into a polymer matrix of sulphonated polystyrene by the ion exchange method. By employing this method it is possible to incorporate magnetic component in situ into the matrix. The preparation conditions have been optimized and the prepared samples were characterized. X ray diffraction techniques, vibrating sample magnetometry, Fe content estimation, Mossbauer spectroscopy and Electron Spin Resonance spectroscopy techniques were used for the characterization at various stages.

In the second part, Nickel zinc ferrite ($\text{Ni}_{1-x}\text{Zn}_x\text{Fe}_2\text{O}_4$ for various x from 1=0 to 1 in steps of 0.2) were prepared by conventional ceramic technique were characterised and were then incorporated into natural rubber matrix for various loadings of the filler. The structural, magnetic, mechanical and electrical characterization of these ceramic filler as well RFC have been carried out and the results are correlated.

The objectives of the proposed work can be listed as follows

- Preparation of magnetic nanocomposites by ion exchange method
- Structural and Magnetic characterization of the composites
- Low temperature studies (magnetic, ESR and Mossbauer) on these nanocomposites sample.
- Preparation of ceramic nickel zinc ferrite belong to the series $\text{Ni}_{1-x}\text{Zn}_x\text{Fe}_2\text{O}_4$
- Preparation of rubber ferrite composites containing NZF in NR
- Evaluation of cure parameters of RFCs
- Mechanical, Electrical and magnetic characterization of prepared samples
- Correlation of properties.

CHAPTER 2

THEORY AND MATERIALS

In any systematic study it is necessary to know the fundamental theories that deal with the subject or material under study. This chapter deals with the different theories and phenomena that are dealt with in this work. It also explains the spinel structure of ferrites and crystal chemistry of ferrites. Different magnetic ordering with special emphasis on superparamagnetism is discussed and dealt with in this chapter. A brief account of the electrical properties of ferrites is also given in this chapter. An account of the materials that form part of this work are also dealt with in this chapter.

2.1 Different Kinds of Magnetic ordering (Magnetism)

Depending on the magnetic structure, materials exhibit different kinds of magnetic ordering or arrangement of spins. The origin of magnetism can be attributed to the orbital and spin motion of electrons(1-3). Magnetic moments of important magnetic atoms such as iron cobalt and nickel are caused by spin motion of electrons.

The magnetic moment per unit volume or the magnetization M of a substance and the magnetic flux density is related by the relation

$$B = M + \mu_0 H \dots\dots\dots(2.1)$$

where H is the applied field and μ_0 is the magnetic permeability of free space.

The ratio $\frac{B}{H} = \mu \dots\dots\dots(2.2)$

is called the absolute permeability and

$$\frac{M}{H} = \chi \dots\dots\dots(2.3)$$

is called absolute susceptibility.

$$\mu \text{ and } \chi \text{ are related by the expression } \mu = 1 + \chi \dots\dots\dots(2.4)$$

The observed value of relative susceptibility of a material varies from 10^{-5} for very weak magnetic materials to 10^6 for very strong magnetic materials. In some cases it takes negative values. The magnetic susceptibility χ , defined as the ratio M/H is a useful property for characterizing magnetic materials. Based on the values of χ exhibited by different materials magnetism can be divided into the following categories. They are

Diamagnetism

Paramagnetism

Anti ferromagnetism

Ferromagnetism and

Ferrimagnetism.

Other kinds of magnetism like Superparamagnetism, metamagnetism and parasitic magnetism etc are not included in this general list since they can be considered as derivatives from one of the above(1-3,8,37-42).

Magnetic moment tends to align along the applied field direction because; a parallel configuration leads to a decreased magnetic energy given by

$$E_p = -\mu \cdot H = -\mu H \cos\theta \dots\dots\dots (2.5)$$

Where μ is the magnetic moment, θ is the angle between magnetic moment and field, E_p is the magnetic potential energy.

2.1.1 Diamagnetism

Diamagnetism is a non-cooperative phenomenon and is universal in nature. Diamagnetism is caused by the orbital motion of electrons. In diamagnetic materials the constituent atoms or molecules have all their electrons paired up in such a way that their magnetic dipole moments cancel each other. Hence there are no dipoles to be aligned by the field. In fact, an applied magnetic field is opposed by changes in the orbital motion of the electrons of a diamagnetic substance. This property can be understood as an example of Lenz's law, which states that an applied magnetic field produces a field that opposes its cause. A small negative χ

value characterizes a diamagnetic material. Negative χ is a result of Lenz's law. Superconductors are also perfect diamagnets with $\chi = -1$.

2.1.2 Paramagnetism

Paramagnetism results out of the increasing difficulty of ordering the magnetic moments of the individual atoms along the direction of the magnetic field as the temperature is raised. Paramagnets have a relative magnetic permeability, μ_r , greater than 1 and the susceptibility, χ , is positive. Paramagnets are governed by Curie's law, which states that χ is proportional to $1/T$, T being the absolute temperature. Paramagnetic structures usually contain transition metals or rare earth materials that possess unpaired electrons.

2.1.3 Ferromagnetism

A ferromagnetic substance has a net magnetic moment even in the absence of the external magnetic field. This is because of the strong interaction between the magnetic moments of the individual atoms or electrons in the magnetic substance that causes them to line up parallel to one another. If the many individual magnetic dipole moments produced in a material are appreciable, there can be long-range interactions. This leads to large-scale areas of magnetism called domains. In ferromagnetic materials, the dipoles within a domain are all aligned and the domains tend to align with an applied field. Ferromagnets can have a magnetic permeability of several thousands. The energy expended in reorienting the domains from the magnetized back to the demagnetized state manifests itself in a lag in response, known as hysteresis. An important property of ferromagnets is the Curie temperature, θ . Above the Curie temperature ferromagnets become paramagnets, since there is sufficient thermal energy to destroy the interaction between atoms that creates domains. They then have a susceptibility given by the Curie-Weiss law,

$$\chi = \frac{C}{(T - \theta)}, \dots\dots\dots(2.6) \quad \text{where } C \text{ is the Curie constant.}$$

Iron, Cobalt and Nickel are all examples of ferromagnetic materials. Chromium Dioxide is another material which exhibits ferromagnetism.

2.1.4 Antiferromagnetism

Substances in which the magnetic moments interact in such a way that it is energetically favorable for them to line up antiparallel are called antiferromagnets. They exhibit a very small positive susceptibility.

The response of antiferromagnetic substances to an applied magnetic field depends up on the temperature. At low temperatures, the arrangement of the atomic dipoles is not affected, and the substance does not respond to an applied magnetic field. As the temperature is increased, some atoms are loosened and align with the magnetic field. This results in a weak magnetism in the substance. There is a temperature analogous to the Curie temperature called the Néel temperature, above which antiferromagnetic order disappears. Above the Néel temperature the effect decreases because of greater movement of the atoms. Oxides of Manganese, Cr_2O_3 etc are some examples of antiferromagnetic materials.

2.1.5 Ferrimagnetism

Ferrimagnets are a form of antiferromagnet in which the opposing dipoles are not equal so they do not cancel out. These materials display a spontaneous magnetization, very small compared to ferromagnets. Ferrimagnets are good insulators, making them very useful in preventing energy losses due to eddy currents in transformers.

Ferrites are typical examples of ferrimagnets and naturally occurring magnetite is a typical example of this category of materials.

Having seen the primary forms of magnetism it would be appropriate to delve into the various theories governing these phenomena exhibited by magnetic materials.

2.2 Important Theories of Magnetism

2.2.1 Langevin theory of paramagnetism

Langevin's theory gives a classical explanation for paramagnetism (1-3,8,37-42). This is based on the reduction in magnetic energy given by equation 2.5 and a probability of Boltzman form $e^{-E_p/kT}$

The Langevin's equation for Magnetisation is

$$M = N\mu \left(\coth a - \frac{1}{a} \right) \dots\dots\dots(2.7) \text{ where } \mathbf{a} \text{ is the ratio } \frac{\mu H}{kT}$$

Right hand side of equation 2.7 is called Langevin function

$$L(a) = \left(\coth a - \frac{1}{a} \right) = \frac{a}{3} - \frac{a^3}{45} + \frac{2a^5}{945} - \dots\dots\dots(2.8)$$

For large applied field or low temperature $L(a)=1$ and $M_0=N\mu$, this is known as saturation because $N\mu$ corresponds to maximum magnetization state when all magnetic moments are aligned parallel to the field. However saturation is not achieved in paramagnets even for the largest field that can be applied. When a is small $L(a)=a/3$ and hence

$$M = \frac{N\mu\mu H}{3kT}$$

or

$$\chi = \frac{N\mu^2}{3kT} = \frac{C}{T}, \dots\dots\dots(2.9)$$

This is called Curie law, where $C = \frac{N\mu^2}{3k}$ is the Curie constant.

If quantum mechanics is applied in this case, instead of continuous distribution of available energies discrete energy level system is to be considered. Then the general expression for magnetisation M takes the following form

$$M = \frac{(2J+1)}{2J} \coth\left(\frac{2J+1}{2J}a^1\right) - \frac{1}{2J} \coth\left(\frac{a^1}{2J}\right) \dots\dots\dots(2.10) \text{ where}$$

$$a^1 = \frac{gJ\mu_B H}{kT}$$

Right hand side of equation 2.10 is called Brillouin function.

When $J=\infty$ classical Langevin expression is obtained.

$J=1/2$ is the spin only case and equation becomes $M=\tanh a^1$

For small values of a^1

$$\chi = \frac{N\mu_{\text{eff}}^2}{3kT} = \frac{C}{T} \dots\dots\dots(2.11).$$

Thus the Curie law can also be derived from the Brillouin function except that the magnetic moment μ is replaced by μ_{eff} which is equal to

$\mu_{eff} = g\mu_B [J(J+1)]^{1/2} p_{eff} \mu_B$ where p_{eff} may be regarded as the effective magnon number of the system.

2.2.2 Weiss Molecular field theory

Progress and understanding of magnetism is indebted mainly to the developments in quantum theory(1-3,8,37-42). The first modern theory of magnetism, perhaps the simplest kind of approach to ferromagnetic ordering was put forwarded by Pierre Weiss. This theory supposes that, the interaction of magnetic atom with crystal can be described by a molecular field. Weiss observed that magnitude H_e of the effective molecular field should be proportional to magnetic moment / unit volume.

$$H_e = \gamma M \dots\dots\dots(2.12)$$
 Constant of proportionality γ is called Weiss constant

In the ferromagnetic state of a solid M and H_e are large quantities without any applied field. Above Curie temperature an external field H must be applied to produce magnetization. The magnetization is self assistive with the molecular field it generates.

Hence the total magnetization can be written as

$$M = \chi_0 (H + H_e) \dots\dots\dots(2.13), \text{ for } T > T_c$$

where $\chi = \frac{C}{T}$ is the weak field susceptibility which obeys Curie Weiss law.

Using eq(2.12) in eq(2.13)

$$M = \chi_m H = \chi_0 H (1 - \gamma \chi_0)^{-1} \text{ for } T > T_c$$

$$\therefore \chi_m, \text{ the observed susceptibility is } \frac{\chi_0}{(1 - \gamma \chi_0)} = \frac{C}{T - \gamma C} \dots\dots\dots(2.14)$$

$$\therefore \chi_m = \frac{C}{(T - T_c)} \text{ for } T > T_c = \gamma C \dots\dots\dots (2.15)$$

and thus the molecular field theory directly leads to the Curie Weiss law for susceptibility above Curie point. Also we can deduce the Weiss coefficient if we

know the Curie constant and Curie temperature. From equation (2.15) it is clear that at $T=T_c$, $\chi=\infty$ and since $\chi=M/H$ this leads to the concept of spontaneous magnetization.

This molecular field theory also helps us in creating an equation for the temperature dependence of spontaneous magnetization in the ferromagnetic phase. The molecular field theory can be applied to ferrimagnets also. In the simplest case of ferrites with two sublattices as in the case of spinels the molecular field acting on each sublattice is expressed as

$$H_A = \gamma_{AA}M_A - \gamma_{AB}M_B \dots\dots\dots(2.16)$$

$$H_B = \gamma_{AB}M_B - \gamma_{BA}M_A \dots\dots\dots(2.17)$$

The negative sign accounts for the antiparallel order between the sublattices.

In the case of ferrimagnets there is a net magnetic moment since the sublattice magnetization do not cancel each other.

At temperature T the net magnetization is

$M(T) = M_{oct}(T) - M_{tetra}(T)$ where M_{oct} and M_{tetra} are the magnetization of octahedral site and tetrahedral site respectively.

For $T < T_c$ Curie Weiss expression becomes

$$\frac{1}{\chi} = \frac{T}{C} + \frac{1}{\chi_0} - \frac{b}{(T - \theta)}, \quad \text{where } \chi_0, b \text{ and } \theta \text{ are the related molecular field}$$

coefficients. At high temperature the term $\frac{b}{(T - \theta)}$ becomes negligible.

$$\text{Therefore } \frac{1}{\chi} = \frac{T}{C} + \frac{1}{\chi_0} \dots\dots\dots(2.18)$$

2.2.3 Exchange Interaction

In order to understand the magnetic ordering in a system it is necessary to know the different interactions within the system. For example in the case of a simple system with two atoms a and b, the total energy is expressed as

$$E = E_A + E_B + Q \pm J_{EX} \dots\dots\dots(2.19)$$

Where E_a and E_b are energies of electrons when they orbit their separate atoms. Q is the electrostatic coulomb interaction energy and J_{ex} is the exchange energy or exchange integral. J_{ex} arises from the exchange between electrons of the atoms, ie when 'a' electron moves around the nucleus 'b' and 'b' electron moves around the nucleus 'a'. They are indistinguishable except for their spins. Therefore spin orientation is most important. Parallel spin will give positive J_{ex} and antiparallel spins will result in negative J_{ex} . This explains the formation of antiferromagnetic ordering and ferromagnetic ordering in materials.

In 1928 Heisenberg showed that exchange energy can be expressed as

$$E_{EX} = -2J_{EX}S_1.S_2 = -2J_{EX}S_1S_2 \cos\theta \dots\dots\dots(2.20)$$

E_{ex} is the exchange energy, S_i and S_j are the total spins of adjacent atoms and J_{ex} is the exchange integral which represents the probability of exchange of electron. For $J_{ex}>0$ ferromagnetic order results in an energy minimum and $J_{ex}<0$ antiparallel spin is favoured.

Based on the Quantum theory the exchange of electrons taking place in compounds have been explained. But it is L.Neel who proposed a simple theory for explaining the ferrimagnetic ordering found in compounds. In the following section the importance of Neel theory with respect to ferrimagnetic materials is briefly highlighted.

2.2.4 Neel's two sublattice theorem

Strong quantum mechanical forces of interaction exist between the spinning electrons in the neighbouring metal ions(37-42). According to Neel this interaction is negative in ferrites, that is the forces acting between ions on A site and B site are negative. This means that the force acting to hold the neighbouring atomic magnetic axes are antiparallel or opposite in direction. Three sets of interactions namely, A-A, B-B and A-B exist in ferrites. A-A and B-B interactions are weak and A-B interaction is predominant in ferrites. The result is that the magnetic moments on A sites are held antiparallel to those on B sites and the spontaneous magnetization of the domain is therefore due to the difference of moments on A and B sites respectively. In ferrimagnets however the A and B

sublattice magnetizations are not equal and hence this results in a net spontaneous magnetization.

We expect that the exchange forces between the metal ions in a ferrimagnet will be through the oxygen ions by means of the super exchange mechanism. However molecular field theory for ferrimagnet is inherently complicated, because A and B sites are crystallographically different for ferrimagnets. That is the AA interaction in ferrimagnets will be different from the BB interaction even though the ions involved are identical. The basic reason is that an ion in the A site has different number and arrangement of neighbours than the identical ion in the B site.

Figure 2.1 shows the exchange interactions that would have to be considered in a rigorous treatment of an inverse spinel $MOFe_2O_3$. These interactions are five in all.

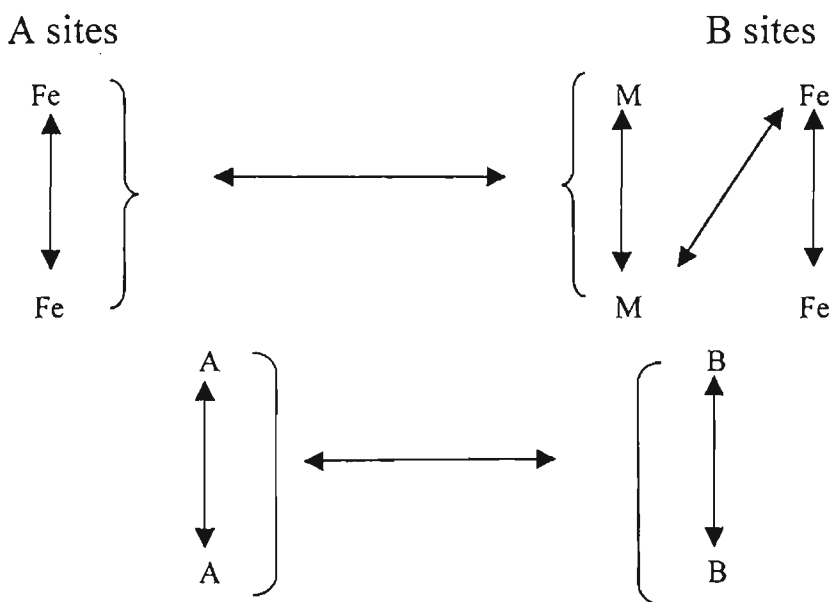


Figure 2.1 Exchange interactions

To simplify this problem Neel replaced the real ferrimagnet with a model composed of identical magnetic ions divided unequally between A and B sublattices(40). This still leaves three different interactions to be considered.

Let there be 'n' identical magnetic ions per unit volume with a fraction λ located on A sites and a fraction $\nu = 1-\lambda$ on B sites. Let μ_A be the average moment of an A ion in the direction of the field. Eventhough A and B sites are

identical, μ_A is not equal to μ_B because these ions are exposed to different molecular fields. Then magnetization of A sublattice is

$$M_A = \lambda n \mu_A$$

Put $n \mu_A = M_a$

Then $M_A = \lambda M_a$ and $M_B = \lambda M_b$ (2.21)

Neel defined the interaction within the material from the Weiss Molecular field viewpoint. The magnetic field acting upon an atom or ion is written in the form $H = H_0 + H_m$ where H_0 is externally applied field and H_m is internal or molecular field which arises due to interaction.

When molecular field concept is applied to ferrimagnetic materials we have

$$\left. \begin{aligned} H_A &= H_{AA} + H_{AB} \text{ and} \\ H_B &= H_{BB} + H_{BA} \end{aligned} \right\} \text{.....(2.22)}$$

The molecular field components may be written as

$$\left. \begin{aligned} H_{AA} &= \gamma_{AA} M_A \\ H_{AB} &= \gamma_{AB} M_B \\ H_{BB} &= \gamma_{BB} M_B \\ H_{BA} &= \gamma_{BA} M_A \end{aligned} \right\} \text{.....(2.23)}$$

Where γ 's are molecular field coefficients and M_A and M_B are magnetic moments of A and B sublattices.

$\gamma_{AB} = \gamma_{BA}$ but $\gamma_{AA} \neq \gamma_{BB}$ unless the two sublattices are identical. Neel showed that $\gamma_{AB} < 0$ favouring antiparallel arrangement of M_A and M_B gives rise to ferrimagnetism.

When size of the magnetic particles are reduced below critical size they behave differently with respect to their ferrimagnetic counterparts. This is called

superparamagnetism and this theory has greater implications as far as applications are concerned. The phenomena of superparamagnetism will be discussed below.

2.3 Superparamagnetism

As the particle diameter decreases to the order of lattice parameter, the intrinsic magnetic property such as the spontaneous magnetization, magnetocrystalline anisotropy, magnetostriction etc will become particle size dependent (8,42-47). There are three reasons for the particle size dependence of the magnetization. They are

1. The probability of thermally activated magnetisation increases as the particle volume decreases. As soon as the energy barrier for irreversible magnetization changes, KV is of the order of magnitude of kT , then hysteresis vanishes
2. Surface effects become increasingly important as the particle volume decreases. This is particularly strong in cases where the spin systems of the particles are coupled by exchange interaction to other spin systems along the particle surfaces. This phenomenon is known as exchange anisotropy and this will cause a shift in the hysteresis curve.
3. The condition for reversal of magnetization as well as the reversal mechanism depend on the particle dimension as well as the particle shape. General character of the hysteresis loop is not affected, but the coercivity is greatly affected.

Now the effect of particle size and temperature on the coercivity and magnetisation of fine particle systems will be considered.

Consider an assembly of uniaxial single domain particles each with anisotropic energy density $E = K \sin^2\theta$ where K is the anisotropy constant and θ is the angle between M_s and the easy axis of magnetisation. If the volume of each particle is V then energy barrier ΔE that must be overcome before a particle reverses its magnetization is KV ergs. In every material fluctuations due to thermal energy are continuously occurring at a microscopic level. If the single domain particle becomes small enough KV will become comparable with thermal energy and fluctuations could overcome the anisotropy forces and spontaneously reverse the magnetization from one direction to another. Each particle has a magnetic moment

$\mu = M_s V$ and if a field is applied it will tend to align the moments along the field. But the thermal fluctuations will promote randomization. This is similar to the behaviour of a normal paramagnet with the exception that the moments involved are enormously high compared to the moment in paramagnetism. The magnetic moment per atom or ion in a paramagnet is only a few Bohr magneton in a normal paramagnet, whereas a spherical particle of iron of 50 \AA in diameter has a moment of more than 10000 Bohr magneton.

If $K=0$ then each particle in the assembly has no magnetic anisotropy and classical theory of paramagnetism can be applied. Then the magnetization of the magnetic particles in a non magnetic matrix is given by

$M = n\mu L(a)$ where M is the magnetization of the assembly, n is the number of particles per unit volume of the assembly, $\mu (=M_s V)$ is the magnetic moment per particle $a = \mu H/kT$ and $n\mu = M_{sa}$ = saturation magnetization of the assembly.

If K is finite and the particles are aligned with their easy axis parallel to one another and with the field, then the moment directions are severely quantised either parallel or antiparallel to the field. Then according to quantum theory $M = n\mu \tanh a$, where the hyperbolic tangent is a special case of Brillouin function. In the third case that for nonaligned particles of finite K the moment per particles is not constant and hence the above two equations cannot be applied. But in such a case the two conditions of Superparamagnetism is satisfied. The two conditions are

1. Magnetization at two different temperatures superimpose when plotted as a function of H/T
2. There is no hysteresis.

Hysteresis will appear and Superparamagnetism disappears when particles of certain size are cooled to a particular temperature or particle size at certain temperature is increased beyond a critical size. In order to determine the critical temperature and size we must consider the rate at which thermal equilibrium is achieved.

Consider an assembly of uniaxial particles which is in an initial state of magnetization M_i by an applied field. Now the field is reduced to zero at a time $t=0$. Some particles in the assembly will reverse their magnetization as their

thermal energy is larger and the magnetization of the assembly tend to decrease. The rate of decrease at any time is proportional to the magnetization existing at that time and the Boltzmann factor $e^{-KV/kT}$

$$\text{Therefore } -\frac{dM}{dt} = f_0 M e^{\frac{-KV}{kT}} = \frac{M}{\tau} \dots\dots\dots(2.24)$$

The proportionality factor is called the frequency factor and it has a value of 10^9sec^{-1} .

The constant τ is called the relaxation time.

Rearranging the above equation and integrating we arrive at

$M_r = M_i e^{\frac{-t}{\tau}} \dots\dots\dots(2.25)$, and hence relaxation time τ can be defined as the time for remanence M_r to decrease to $1/e$ of its initial value. From equation 2.24, we can write

$$\frac{1}{\tau} = f_0 e^{\frac{-KV}{kT}} \dots\dots\dots(2.26)$$

Thus it is clear that τ is strongly dependent on V and T .

If we put relaxation time as 100sec, then from equation (2.26) we arrive at

$$\frac{KV}{kT} = 25 \dots\dots\dots(2.27)$$

Hence transition to stable state occurs when energy barrier equals $25kT$ and also the upper limit of the particle volume for Superparamagnetism for uniaxial particles is given by

$$V_p = \frac{25kT}{K} \dots\dots\dots(2.28)$$

For a particle assembly of constant size there will be particular temperature called the superparamagnetic blocking temperature, below which magnetisation will be stable. For a uniaxial particle assembly,

$$T_B = \frac{KV}{25k} \dots\dots\dots(2.29)$$

Now we can consider the effect of an applied field on the approach to equilibrium. Assume an assembly of particles with their easy axis parallel to the z

axis. Let it be initially saturated in the +z direction and let us now apply a field in the -z direction. Then the Ms in each particle will make an angle θ with the z axis. Then the total energy per particle is

$$E = V(K \sin^2 \theta + HM_s \cos \theta) \dots\dots\dots(2.30)$$

The energy barrier for reversal is the difference between the maximum and minimum values of E and it can be obtained as

$$\Delta E = KV(1 - \frac{HM_s}{2K})^2 \dots\dots\dots(2.31)$$

The particles with sizes larger than D_p are stable in zero field and will not thermally reverse in 100s. But when the field is applied the energy barrier can reduce to 25kT. This will be the coercivity and is given by

$$\Delta E = KV(1 - \frac{H_{ci}M_s}{2K})^2 = 25kT \dots\dots\dots(2.32)$$

$$H_{ci} = (\frac{2K}{M_s}) \left[1 - (\frac{25kT}{KV})^{1/2} \right] \dots\dots\dots(2.33)$$

When V is very large or T is zero $H_{ci}=(2K/M_s)$

Putting this limiting value as

$H_{ci,0}$ and substituting for 25kT/K as V_p , we get

$$h_{ci} = \frac{H_{ci}}{H_{ci,0}} = 1 - (\frac{V_p}{V})^{1/2} = 1 - (\frac{D_p}{D})^{3/2} \dots\dots\dots(2.34)$$

Similarly equation (2.33) can also be used for variation of coercivity with temperature for particles of constant size. For this we assume that particle with critical size V_p have zero coercivity at their blocking temperature T_B .

We get

$$h_{ci} = \frac{H_{ci}}{H_{ci,0}} = 1 - (\frac{T}{T_B})^{1/2} \dots\dots\dots(2.35)$$

Particles larger than V_p have finite retentivity as thermal energy cannot reverse their magnetization in 100s. To find a relation between retentivity and size we can combine equations 2.25 and 2.26 to get

$$\ln \frac{M_r}{M_i} = -\frac{t}{\tau} = -10^9 e^{-KV/kT} \dots\dots\dots(2.36)$$

substituting equation 2.28 and putting $t=100s$ we get

$$\ln \frac{M_r}{M_i} = -10^{11} e^{-25V/V_p} \dots\dots\dots(2.37).$$

Thus the above equations predict the dependence of magnetic properties of the fine particles on their size.

2.4 Spinel ferrites

The spinel ferrites belong to a family of materials which resembles the structure of the naturally occurring mineral $MgAl_2O_4$. The general formula for spinel structure can be written as AB_2O_4 . The oxygen anions have a FCC arrangement accommodating the smaller positive ions in the interstices. The available spaces are of two kinds and size known as tetrahedral (A) and octahedral (B) sites. In the mineral spinel Mg ion occupy the A site, known as tetrahedral site because the four nearest oxygen neighbours. The B site ions have six nearest oxygen ions and are called the octahedral site and is occupied by the Al ions. The general formula for spinel ferrites is written as AFe_2O_4 . (39,48)

Many different cationic combinations are possible in a spinel structure. Any three cations with a total charge of eight can form a spinel structure. However there is a limiting cation radii of 0.4 to 0.9 Å, based on the oxide ion radii. The unit cell consists of eight formula units ($8 \times AFe_2O_4$) where A is the divalent metal ion. The 32 oxygen ions form a f.c.c. lattice in which two kinds of interstitial sites are present namely, 1) 64 tetrahedral sites surrounded by 4 oxygen (A sites) and 2) 32 octahedral sites surrounded by 6 oxygen ions (B ions).

The crystal structure is best described by subdividing the unit cell into 8 octants with edge $a / 2$ as shown in Figure2.2c . The location of oxygen ions and metal ions in every octant can be easily described. The oxygen ions are arranged in identical manner in all octants. Each octant contains four oxygen ions in the body diagonal and they lie at the corners of a tetrahedron. Positions of metal ions are different in the two octants sharing a face. In the case of octants sharing only an edge the location is the same. Hence the complete picture of the location of metal ions is obtained if position of ions are drawn in two adjacent octants as shown in Figure2.2d

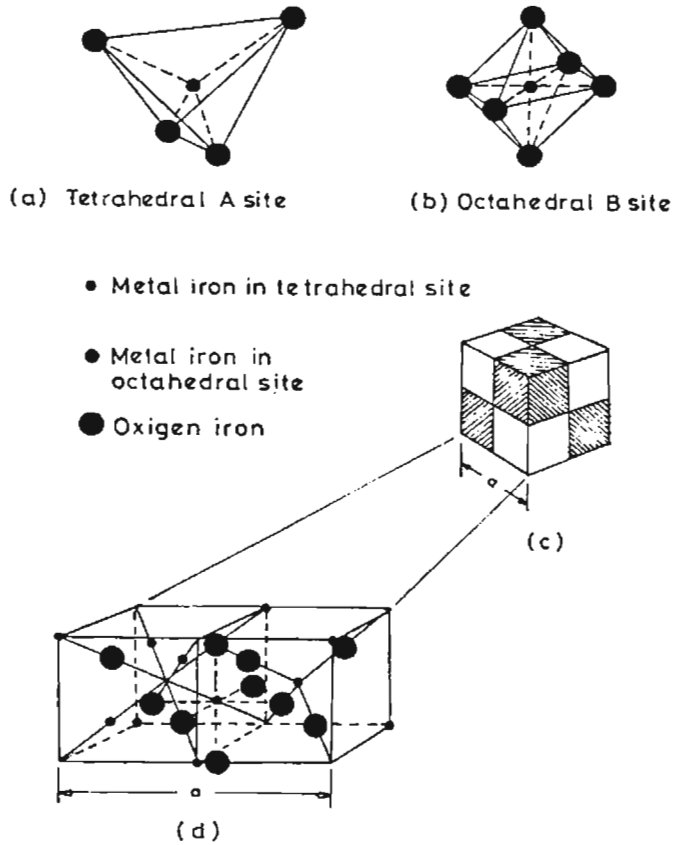


Fig.22 Cristal structure of a cubic ferrite

The distribution of metal ions is very important for an understanding of magnetic properties of these materials. Not all available sites are occupied by metal ions: Only $1/8^{\text{th}}$ of the A sites and $1/2$ of the B sites are occupied. In the case of mineral spinel Mg^{2+} ions are in A sites and Al^{3+} ions are in B sites. It is called normal spinel structure in which the divalent ions are on B sites and trivalent ions are on the A sites. If D and T describe the divalent and trivalent cations respectively then another cation distribution possible is $(\text{T})[\text{D}\text{T}\text{O}_4]$. This structure in which divalent ions are in the A sites and trivalent ions are equally distributed between A and B sites, is called an inverse spinel structure. Iron, Cobalt, Nickel ferrites have inverse structure and they are all ferrimagnetics. ZnFe_2O_4 is a

normal spinel, NiFe_2O_4 is inverse spinel. The normal and inverse structure are to be regarded as extreme cases, because X-ray and neutron diffraction have shown that intermediate structures can exist. The physical properties of spinels depend not only on the kinds of cations in the lattice but also on their distribution over the available sites. The distribution of the divalent ions on A and B sites in some ferrites can be altered by heat treatment, it depends on whether the material is quenched from a high temperature or slowly cooled. The size of the cation, valency of the cation and the oxygen parameter of the anions also are some of the factors determining the cation distribution. (48-49)

One of the important properties of ferrites is their electrical characteristics. A very short description of the electrical properties of ferrites is provided in the next section.

2.5 Electrical properties of spinel ferrites

Different materials respond differently to an electric field. They conduct electricity to lesser or greater extent. Spinel ferrites have a low electrical conductivity when compared to other magnetic materials hence they find wide use in many applications particularly in microwave frequencies. Spinel ferrites and garnets have resistivity values in the range 10^{-4} and 10^9 Ohm m at room temperature. In ferrites the low conductivity is associated with the simultaneous presence of Fe^{2+} and Fe^{3+} ions on equivalent lattice sites. The mechanism of conduction is known as hopping conduction (Verwey et al) (48,50). The extra electron on ferrous ion requires little energy to move to similarly situated adjacent ferric ion. The valence states of the two ions are interchanged. Under the influence of an electric field the extra ion can be considered to constitute the conduction current, jumping or hoping from one iron ion to the next. In such a process the mobility of the jumping electrons or holes are found to be proportional to $e^{-E_a/kT}$, where E_a is the activation energy, k Boltzman's constant and T the temperature in degree absolute. Since ferrites are semiconductors their resistivity (ρ) decreases with increase in temperature according to the relation of the form

$$\rho = \rho_0 \exp(E_a/kT)$$

where E_a is the activation energy required to cause the electron jump.

One of the important components in the composites under the present study are gamma iron oxide and nickel zinc ferrites respectively. Therefore a short account of these two ferrites is provided in the next section.

2.6 Materials

2.6.1 Magnetic iron oxide (maghemite- γ - Fe_2O_3)

Maghemite is one of the most important magnetic materials. This compound has a vacancy ordered spinel structure and is prepared by oxidising magnetite Fe_3O_4 . The Fe ions are in the trivalent state and a fraction of the cation sites are vacant. The structure of gamma ferric oxide can be written as

$\text{Fe}^{3+} \left[\text{Fe}_{\frac{2}{3}}^{3+} \Gamma_{\frac{1}{3}} \right] \text{O}_4^{2-}$ where Γ represents vacancies which are exclusively found on the octahedral sites (52).

90-95% of the recording or storage industry employ this material as one of the medium for storage.(1-3,8).

2.6.2 Nickel zinc ferrites

Ferrites are mixed oxides with general formula $\text{M}^{2+}\text{O Fe}_2\text{O}_3$ where M is a metallic ion. The best known example is Fe_3O_4 ie $\text{FeO} \cdot \text{Fe}_2\text{O}_3$. They are important technologically as they have high electrical resistivity and low eddy current loss(1-3,8). Nickel Zinc ferrite or $\text{Ni}_{1-x}\text{Zn}_x\text{Fe}_2\text{O}_4$ (NZF) is a classical example of mixed ferrite. Here x can be varied. The cation distribution is written as



These ferrites find many applications. The lattice parameter varies linearly with composition (Vegards Law). The cation radius ratio for tetrahedral sites is larger and the cation has strong influence on the lattice parameter as well as the magnetic properties of these materials.

The focal theme of the present study is on nanocomposites and it is pertinent that some salient features of the chosen matrix, namely ion exchange resins are explained. The ensuing section contains a brief overview of ion exchange resins and its properties with respect to the structure. The insitu

incorporation of an inorganic component is carried out chemically by the method of ion exchange and therefore this also is given some mention here.

2.6.3 Ion exchange resins.

Organic swellable copolymers is converted into water swellable material by the introduction of functional ionic sites. These ionic sites give the polymer ion exchange property. A cross linked polymer of styrene and divinylbenzene is a hard, insoluble resin which may be formed into tiny beads. Since the molecular network contains pendant phenyl groups (from the styrene group) these may undergo electrophilic substitution reaction and thus produce functionalized polymers. Many chemical reactions may infact be carried out on these functions which are attached to the cross linked net of polymers. When such a polymer is sulphonated an insoluble resin is resulted with sulphonyl group attached to it. Such a substance is called ion exchange resins. Figure 2.3 shows a schematic picture of the ion exchange resin of sulphonated polystyrene.

Sulphonate groups are attached to the insoluble resins, the protons are only held electrostatically and may easily migrate to an adjacent water phase as long as another positive ion from the aqueous solution can move in to take its position and balance the negative sulphonate charge. When packed in a column with water, the water can serve to exchange the cations. If a solution of NaCl is passed through the column, the passing Na ions are caught by the resin releasing proton into the solution forming HCl.

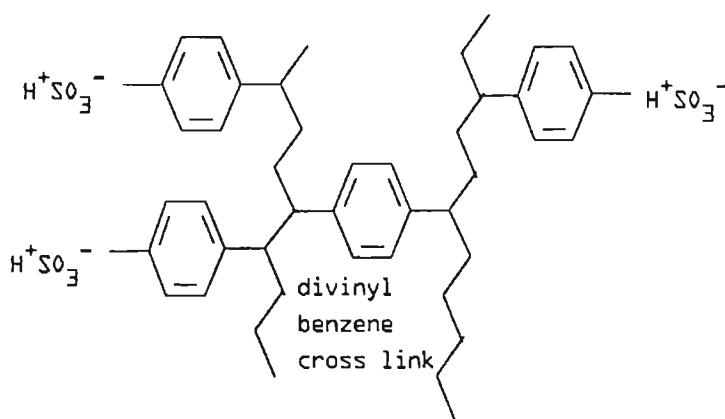


Fig.2.3 Structure of Sulphonted polystyrene.

Strongly acid anion exchangers enter into the reaction of ion exchange with the salts of acids in neutral and acidic aqueous solution. The weakly acid cation exchangers are capable of ion exchange only with cations of the salt of weak acids, the completeness of the exchange increases with increasing pH of the solution.

Strongly basic ion exchange resins are capable of ion exchange in neutral and weakly alkaline solutions. Weakly basic anion exchangers enter into exchange only in acid solution, the completeness of exchange increases with decreasing pH of the solution.

The exchange capacity of an ordinary ion exchange resin depends on both the ability of its ions to exchange with ions of the solution and the ability of displacing ions to penetrate the resin. (53-55)

In the preparation of magnetic composites by mechanical means, since Natural Rubber is chosen a brief description of different properties of this unique polymer is described for clarity and continuity. Also the need for a proper recipe for compounding and their role are also briefly mentioned.

2.6.4 Natural Rubber matrix(NR)

The use of rubber components often facilitates greater sophistication in engineering design and enables compliance and flexibility to be introduced in a controlled and generally failsafe manner. Preparation of flexible magnets will aid in moulding the magnets with desirable properties in the required shape. Here in the present study for the preparation of RFCs the natural rubber matrix, which is abundant in the state of Kerala is selected. Natural Rubber is particularly precious to the rubber industry. Both by history and by technical merits remains the reference standard for the entire industry. Natural rubbers technical assets include good processability, high strength and excellent resistance to dynamic flexing. The regularity of its chemical structure and its tendency to crystallize, makes natural rubber an irreplaceable material in rubber compounding. Natural rubber is also an important polymer from the commercial point of view. It is an unsaturated nonpolar polymer which is easily processable, light weight and inexpensive. As a poor conductor of electricity it is valuable as an electric insulator. Use of NR for technological applications is a prospective value addition to the abundantly and locally available natural resource. Natural rubbers principal weakness is its lack of

inherent resistance to environmental damage. That is, they are prone to cracks due to atmospheric oxygen or ozone.

The discovery and development of natural rubber has furnished rubber technology with a new elastomer. Natural rubber has an empirical formula C_5H_8 and a chemical structure of almost 100% cis-1,4 polyisoprene chain. The average molecular weight is $1-1.5 \times 10^6$ and number average is $3-5 \times 10^5$. due to its high stereoregularity, it crystallizes when stored at low temperature or on stretching. This gives it its unique high tensile strength and tear resistance even in the pure gum stock. Figure 2.4 illustrates the structure of natural rubber.

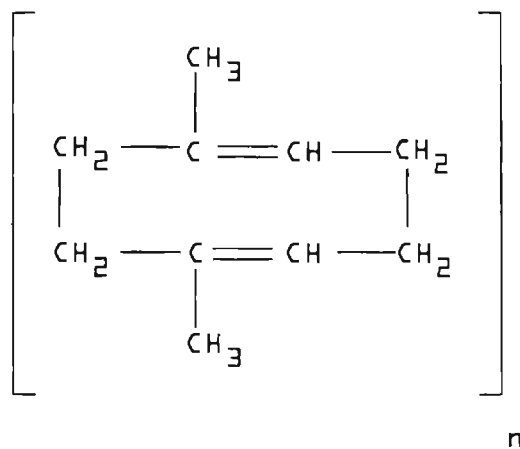


Fig. 2.4 Structure of Natural Rubber

Natural Rubber after vulcanization provides high tensile strength and high tear resistance. The strength however falls with increase in temperature.

Sulphur is added for the vulcanization of Natural Rubber. It brings about cross linking and converts rubber to form bound structure. Usually 0.5 to 5 phr (part per hundred rubber by weight) sulphur is added. Certain chemicals, termed accelerators, when used with sulfur shorten the time of vulcanization and improve the physical properties of rubber. Eventhough inorganic accelerators like white lead, lead monoxide, lime, and magnesia are used as accelerators, the organic accelerators are found to be more active. Some examples are mercapto benzothiazole disulphide (MBTS), Tetramethyl thiuram disulphide (TMTD), cyclohexyl benzthiazyl sulphenamide (CBS), zinc dibutyl carbonates(ZDC) etc.

The proportion required is relatively small, usually 0.5 to 1.0 part per 100 of rubber being sufficient. Most accelerators require the presence of zinc oxide to exert their full effectiveness, and some require an organic acid, such as stearic acid. Modern compounding formulas, therefore, usually contain zinc oxide and stearic acid. They are called activators/ co-activators. Normally a right combination of the chemicals constitute a recipe for mixing, apart from fillers, whether they are reinforcing or magnetic fillers. (51,53-55)

Some substances toughen the rubber, giving it added strength and resistance to wear. These are known as reinforcing agents. Carbon black in very finely divided form is the most common reinforcing ingredient; it is relatively cheap and is one of the most effective known. Other widely used reinforcing agents include zinc oxide, magnesium carbonate, silica, calcium carbonate, and certain clays, but all of these have less reinforcing values than carbon black.

CHAPTER 3

EXPERIMENTAL TECHNIQUES

Various experimental techniques including preparative conditions and analytical tools employed for characterisation of the composites at various stages are discussed in this chapter. Different schemes for the synthesis of nanocomposites with special emphasis on ion exchange method and characterisation techniques are listed here. The preparation of ceramic nickel zinc ferrite belonging to the series $\text{Ni}_{1-x}\text{Zn}_x\text{Fe}_2\text{O}_4$ by ceramic technique and their incorporation in Natural rubber matrix and analytical tools employed for characterisation are discussed in this chapter on experimental techniques.

3.1 Different schemes of preparation of magnetic nanocomposites

There are different schemes available for the synthesis of magnetic nanoparticles/ nanocomposites. Some of the important methods for preparation will be discussed. In the **inert gas evaporation** (20) method a metal is evaporated in an inert atmosphere at a reduced pressure and then condensed in the gas phase to form metal clusters or nanocrystals. These collect on the cold finger and can be oxidised to fine ceramic powder which is then scrapped off the cold finger and compacted. To make nanocomposites two different metals are to be evaporated and condensed at the same time.

In the **solution chemical route** (20) called spray conversion processing to make bulk quantities of cobalt/tungsten carbide particles embedded in cobalt grains, molecular mixing is accomplished by aqueous solution phase reactions between suitable precursors such as ammonium metatungstate and cobalt nitrate. The solution mixture is aerosolised and rapidly spray dried to get extremely fine mixture of tungsten and cobalt salts. These precursor powder is reduced with hydrogen and then reacted with CO in a fluidised bed reactor to yield nanophase cobalt/tungsten carbide powder. Nanocomposites with impressive properties can also be prepared by dispersing nanoscale particles of one ceramic either inside the larger grains of a second ceramic or between the grains

Rapid thermal decomposition of precursors in solution (RTDS) method is yet another synthesis scheme which can be used to make nanophase powders of NiO and Ni(OH)₂. The RTDS process applies a high temperature and pressure to a rapidly flowing solution containing dissolved precursors to synthesize ultrafine particles. Recently **solgel method** is gaining popularity and can be made use of for the dispersion of small metal or alloy particles in non-metallic matrixes.

Co-precipitation method is an effective technique employed for the preparation of nanoparticles. **High energy ball milling** is also being used extensively for the production of nanoscale particles. (20,21,56-61)

The last few techniques namely the solgel method, co-precipitation technique, ball milling etc are widely used for the production of magnetic fine particles. Another important method used for the preparation of magnetic nanocomposite is the **ion exchange method**(21,60,61). In this method the nanoscopic magnetic components are dispersed in the nonmagnetic matrix of the ion exchange resin. Here in the present study the ion exchange method will be employed to prepare magnetic nanocomposites containing dispersions of iron oxide in a nonmagnetic matrix. Therefore the details are discussed in more detail in the next section.

3.2 Preparation of nanocomposites by ion exchange method.

Nanometer sized γ -Fe₂O₃ particles were embedded in a polymer matrix by the method of ion exchange followed by reduction. The method adopted here is a modification of the preparation scheme reported by Ziolo et al[21] The polymer matrix employed is a cross linked polymer of sulphonated polystyrene and divinyl benzene, which have exchangeable H⁺ ion containing SO₃⁻H⁺ groups. The schematic of a polystyrene structure is shown in Chapter 2 (Fig.2.3)

The ion exchange resin is soaked for 24 hours in distilled water containing few drops of hydrazine hydrate which acts as the oxygen scavenger. This soaked resin is packed in the reaction column and FeSO₄ solution is added into the column. Then the ion exchange sites in the resin will be exchanged with Fe ions from this aqueous solution of ferrous sulphate. The excess Fe ions are removed by thorough washings of the column. These exchanged Fe ions are then converted into Fe(OH)₂ by the addition of an alkali solution of NaOH. This is then oxidized to yield, presumably, γ -Fe₂O₃. Drop wise addition of dilute aqueous solution of H₂O₂ is found

to accelerate the conversion to oxide. The resin is then washed with water and then dried. Instead of adding H_2O_2 , the addition of hydrazine hydrate solution is also tried. The process of preparation up to the conversion to hydroxide was carried out in an oxygen free atmosphere. This is achieved by maintaining the level of the solution above the column height.

The entire preparation scheme is depicted in Fig.3.1. Samples were prepared by using both weak and strong ion exchange resins

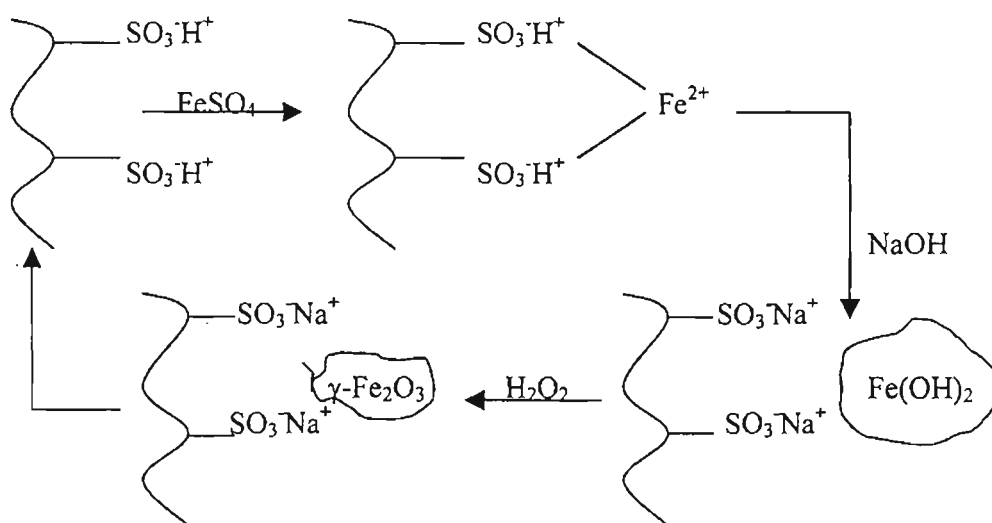


Fig.3.1 preparation Scheme for the nanocomposites

3.3 Differential scanning calorimetry (DSC)

Whenever a material undergoes a change in its physical state such as melting or transition from one crystalline state to another or whenever it reacts chemically, heat is either absorbed or liberated. Thus these thermal changes are either due to endothermic or exothermic reactions or transitions. Such changes can be caused by phase transitions, fusion, crystalline inversion etc. Generally phase transitions and dehydrations are endothermic processes whereas crystallisation, oxidation etc are exothermic reactions. Differential scanning calorimetry or DSC is an effective tool to detect such thermal changes in a material. In DSC the thermal behaviour of a sample is studied by measuring the differential heat flow required to maintain the sample material and an inert reference material at the same temperature. The term DSC was first used by Watson et al (62) to describe the instrumental set up developed by

Perkin Elmer Corporation. The curve obtained in DSC is a recording of the heat flow $\frac{dH}{dt}$ in *mcal/s* as a function of T.

Generally in DSC a peak in the upward direction, indicate an increase in enthalpy (endothermic reaction) while exothermic reaction is recorded as a peak in the opposite direction. Area enclosed by the DSC curve is proportional to enthalpy change. There are two modes used in DSC. One is the power compensated DSC and other is heat flux DSC. In the former case the sample and reference are heated by separate heaters and their temperature is increased or decreased linearly. In heat flux method the difference in heat flow into the sample and reference are noted as the sample and reference are heated linearly.

DSC-7 (Perkin - Elmer) operates in power compensation mode and with 3700 Data system, gives direct calorimetric measurements, characterisation and analysis of thermal properties of the sample. Platinum resistance heaters and thermometers are used in DSC-7 to accomplish temperature and energy measurements. Continuous and automatic adjustment of heater power necessary to keep the sample temperature identical to that of the reference holder provides a varying electrical signal equivalent to varying thermal behaviour of the sample. For standard operation DSC-7 is equipped with an insulated reservoir which allows the use of ice water coolant. The scanning rate can be varied over a wide range from 0.1⁰C to 200⁰C/min.

3.4 Vibrating Sample Magnetometry(VSM)

The magnetic characterization of both composites prepared (Magnetic nanocomposites and RFCs) as well as the ceramic Ni_{1-x}Zn_xFe₂O₄ were carried out by using Vibrating Sample Magnetometer (VSM) (model: EG & G 4500). Parameters like Saturation magnetization (σ_s), Retentivity (σ_r) and Coercivity (H_c) were obtained from this room temperature measurements. Low temperature measurements were carried out on the nanocomposite samples. The thermomagnetisation data can also be generated using a VSM.

When a sample material is placed in a uniform magnetic field, a dipole moment is induced in the sample. The amount of magnetic flux linked to any coil placed in the vicinity of this magnetic moment is given by

$$\phi = \mu_0 n \alpha M \dots\dots\dots(3.1)$$

μ_0 – permeability of free space

n - number of turns per unit length of coil

M – magnetic moment of the specimen

α - Geometric moment decided by position of moment with respect to coil as well as shape of coil.

$$\text{Anharmonic oscillator of the type } Z = Z_0 + A \exp(j\omega t) \dots\dots\dots(3.2)$$

induces an emf in the stationary detection coil. The induced emf is given by

$$V = -\frac{d\phi}{dt} = -j\omega\mu_0 nMA\left(\frac{\partial\alpha}{\partial z}\right)e^{j\omega t} \dots\dots\dots(3.3)$$

If amplitude of vibration (A), frequency and $\frac{\partial\alpha}{\partial z}$ are constant over the sample zone then induced voltage is proportional to the magnetic moment of the sample. This is the basic idea behind VSM (63-65).

In model PAR 4500 VSM the material under study is contained in a sample holder, which is centered in the region between the pole pieces of a laboratory electromagnet. A slender vertical sample rod connects the sample holder with a transducer assembly located above the magnet. The transducer converts a sinusoidal ac drive signal in to a sinusoidal vertical vibration of the sample rod and the sample is thus made to undergo a sinusoidal motion in a uniform magnetic field. Coils mounted on the pole pieces of the magnet pick up the signal resulting from the sample motion. This ac signal at the vibrating frequency is proportional to the magnitude of the moment induced in the sample. However it is also proportional to the vibration amplitude and frequency. This vibrational amplitude and frequency are kept constant by a servo system. Thus the pickup coil output accurately gives an account of the moment level of the sample.

The system is provided with facilities for low temperature measurements as well for the thermomagnetisation measurements. That is, the variation of saturation magnetisation with temperature can be studied by using this system.

3.5 Iron content Estimation

The iron content of some nanocomposite samples was estimated by a method described by Vogel (66). The method followed is the same as that used for the estimation of iron in iron ores. About 1g of the sample is weighed accurately into a beaker and digested with 100ml of 10% HCl. The digestion is continued for 2 hours on a water bath. It is allowed to cool and filtered through Whatmann No.41 filter paper. The filtrate and washings were collected and it was boiled for 10 minutes after adding 5ml of concentrated nitric acid. Ammonia is added drop wise with stirring till in excess. This was further digested for about five minutes and filtered hot through Whatman No.41 filter paper. It is then washed free of any chloride using 1% ammonium nitrate. The filter paper containing the precipitate is ignited in a silica crucible. One drop of nitric acid is added to the residual ash and heated again to red hot. This is then cooled in a desiccator and weighed. Then the weight of iron is calculated by assuming that 159.68 grams of iron oxide contains 111.68 gm of iron.

3.6 Mössbauer Spectroscopy

The Mössbauer effect is the recoil-free emission of gamma radiation from a solid radioactive material. Since the gamma emission is recoil-free, it can be resonantly absorbed by stationary atoms(67). The nuclear transitions are very sensitive to the local environment of the atom and Mössbauer spectroscopy is a sensitive probe of the different environments an atom occupies in a solid material(68). The production of gamma rays for ^{57}Fe Mössbauer spectroscopy is depicted in Fig. 3.2

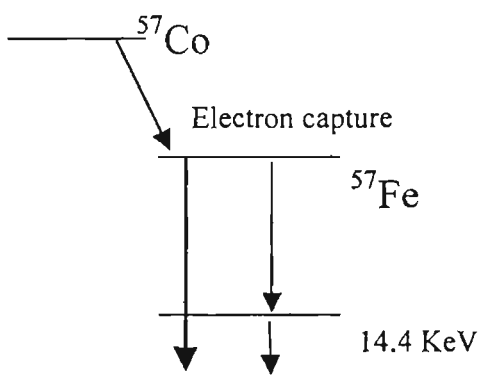


Fig 3.2 The production of gamma rays for ^{57}Fe Mössbauer spectroscopy

Approximately 90% of the ^{57}Fe nuclear excited state decays through the intermediate level to produce 14.4 keV gamma radiation. These gamma photons can then be absorbed by ^{57}Fe in a sample.

The gamma ray source is a radioactive element that is mechanically vibrated back and forth to Doppler shift the energy of the emitted gamma radiation. The diagram Fig.3.3 below shows a transmission Mossbauer experiment. As the energy of the gamma radiation is scanned by Doppler shifting, the detector records the frequencies of gamma radiation that are absorbed by the sample.

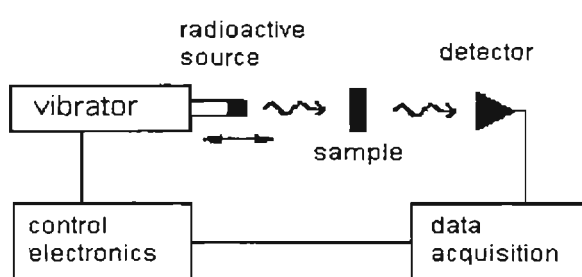


Fig.3.3 A Typical Transmission Mössbauer Experimental Setup

Mössbauer spectrum reflects the hyperfine interactions of the sample. Several parameters can be extracted from the spectrum. These parameters can be used to identify the chemical and magnetic phases present in the sample like a fingerprint.

A shift in the position of the resonance line on the Doppler scale is produced by the electric monopole interactions and this gives rise to the isomer shift (chemical shift ' δ '). By electric monopole interaction one can get an idea about the electron density in the sample. But the electric quadrupole and magnetic dipole interactions split the resonance lines originating from transition between degenerate nuclear levels. Quadrupole splitting gives an idea about the electric field gradient. Magnetic dipole interaction gives idea about the internal magnetic field of the specimen. Figure 3.4 gives an outline of the different interactions that produce different types of Mossbauer spectra.

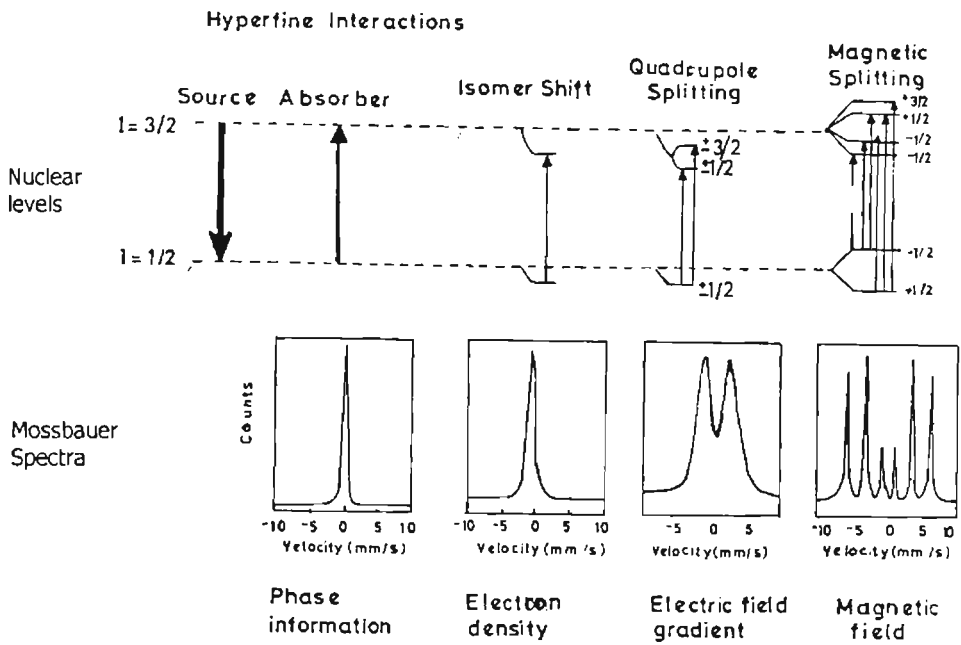


Fig 3.4 Different Interactions in a Mossbauer Spectra

Most valuable chemical information can be extracted from these Mössbauer parameters like Electric quadrupole splitting (ΔE_Q), Magnetic dipole splitting (ΔE_M), and chemical shift or isomer shift (δ). The isomer shift and the quadrupole splitting can be calculated using the following formula

$$\text{Isomer shift } (\delta) = \frac{V_1 + V_6 + V_2 + V_5}{4} \dots\dots\dots(3.4)$$

$$\text{and Quadrupole splitting } (E_q) = \frac{(V_6 - V_5) - (V_2 - V_1)}{2} \dots\dots\dots(3.5)$$

where V_1, V_2 etc are the Doppler velocities corresponding to the different lines in the sextet. Electric quadrupole interaction occurs only if there is an observable nuclear quadrupole moment and simultaneously a non zero electric field gradient at the nucleus. An atomic nucleus in the energy state E with spin quantum number $I > 0$ possesses a non zero magnetic dipole moment μ and may interact with a magnetic field H at the nucleus. The interaction is called magnetic dipole interaction or nuclear Zeeman effect. The nuclear Zeeman effect splits the nuclear state with spin quantum number I into $2I+1$ equally spaced and non degenerate substates.

The hyperfine field H_{eff} at the nucleus was calculated using the formula $H_{\text{eff}} =$ total split in mm/sec $\times 31.25 \text{ KOe}$. The total split here corresponds to the split between the extreme lines. The factor 31.25 KOe was deduced from the total split (in channels) of the iron foil spectrum for calibration. (67-69)

3.7 ESR Spectroscopy

Electron Paramagnetic Resonance (EPR), often called Electron Spin Resonance (ESR), is a branch of spectroscopy in which electromagnetic radiation (usually of microwave frequency) is absorbed by molecules, ions, or atoms possessing electrons with unpaired spins, *i.e.* electronic spin $S > 0$. (70-72).

In EPR, because of the interaction of the unpaired electron spin moment (given by two projections, $m_s = \pm 1/2$, for a free electron) with the magnetic field, the so-called Zeeman effect, different projections of the spin gain different energies as shown in fig.3.5

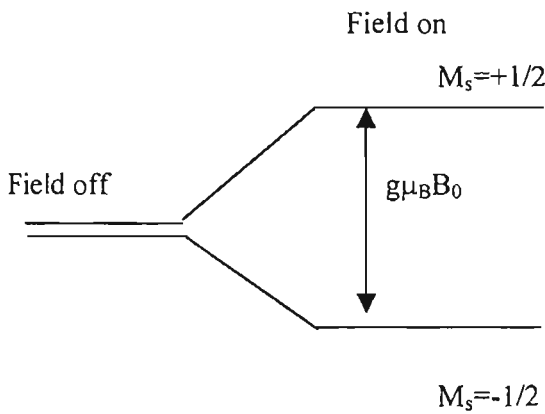


Fig. 3.5 Energy levels giving rise to ESR spectra

The energy of the levels is given by the following equation

$$E_{m_s} = g\mu_B \mathbf{B}_0 m_s \dots \dots \dots (3.6)$$

Applying the selection rule for m_s , transition between these levels will involve an energy transfer of

$$\Delta E = g\mu_B B_0 \dots\dots\dots(3.7)$$

The ESP-300 ESR spectrometer (Bruker) consists of an electromagnet with power supplies to generate and modulate a uniform magnetic field of several thousand Gauss, as well as the components that generate and detect microwave power.

A Hall probe, driven from a stable constant-current power system, with a digital multimeter (DMM) reading the Hall voltage, is used to measure the value of the magnetic field between the poles of the magnet.

The microwave system consists of a microwave power supply (on a table above the magnet) which uses a klystron. The output of the microwave power (mw) supply is connected via rectangular waveguide (10 GHz) and through a circulator to a high-Q resonant cavity. The samples to be investigated are mounted in the middle of the cavity, where magnetic component of the microwave power is maximum and is oriented perpendicular to the static field. A microwave diode, which detects the microwave power resides inside the same box as the power supply. The higher the quality of the resonant cavity the greater the microwave field can be obtained on the sample. Very polar solvents like water absorb efficiently on microwave frequencies themselves. Because of that, water samples have to be made in narrow capillaries and carefully located in the center of the cavity. Most of our measurements will be done in the 0.1 - 1.0 mW range.

There are variety of schemes for detecting resonant EPR transitions(70). To minimize the noise from the mw diode in steady state measurements, a magnetic field modulation scheme with phase sensitive detection is usually employed. As a result, the detected signal appears as a first derivative (Fig.3.6).

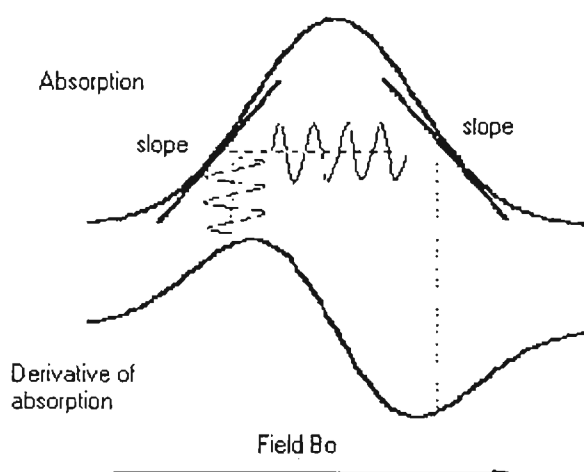


Fig. 3.6 Absorption and first Derivative of ESR Spectra

In the Bruker spectrometer there is choice between 12.5 kHz and 100 kHz modulation frequency. The amplitude of field modulation (MA) can be varied up to 40 G (4mT). Utmost care must be taken in choosing appropriate MA. If MA is too big, the width of detected signal derivative would be wider than the real width of absorption, but if it is too small, the signal intensity would be less. For most of the cases it is a good first approximation to set MA between 0.5 and 1.0 G.

The ESR spectra of the nanocomposite samples were recorded both at room temperature, at 110K and at Liquid nitrogen temperature.

3.8 Preparation of ceramic nickel zinc ferrite samples

Ferrous oxalate dihydrate is prepared from ferrous sulphate and oxalic acid solutions. For this AR grade ferrous sulphate and oxalic acid solutions are taken in appropriate molecular ratios. These are then mixed thoroughly by the dropwise addition of oxalic acid solution into the ferrous sulphate solution with constant stirring of the solutions using a magnetic stirrer. Care was taken to keep the reaction temperature to be between 60-70 degree Celsius. The precipitate is filtered, thoroughly washed and dried in an oven at 100 degree Celsius for 3 hours to yield ferrous oxalate dihydrate (FOD).

Nickel zinc ferrite ($\text{Ni}_{1-x}\text{Zn}_x\text{Fe}_2\text{O}_4$) samples with x varying from $x=0.0$ to $x=1.0$ in steps of 0.2 are prepared using the freshly prepared FOD by the usual ceramic technique⁽⁷³⁻⁷⁶⁾. For this appropriate amount of AR grade Nickel carbonate, zinc oxide and ferrous oxalate dyhydrate (FOD) are mixed thoroughly using a mortar and pestle in AR grade acetone medium. These are then prefired at 500 degree Celsius for 4 hours. These prefired samples are again mixed in acetone medium and is fired once again to obtain a homogeneous mixture. Repeated sintering and mixing were continued till single phasic spinel compound was obtained. This pre sintered powder was then finally sintered at $1000 \pm 15^\circ\text{C}$ for several hours to obtain the respective nickel zinc ferrite sample. The sintered sample is then crushed into powder form.

The pre-sintered powders were pressed in the form of cylindrical pellets having a diameter of 12mm and then they were finally sintered at around 1000°C by keeping the pellets inside the furnace for several hours. They were then allowed to cool naturally under ambient conditions and these pellets are used for electrical characterization of ceramic $\text{Ni}_{1-x}\text{Zn}_x\text{Fe}_2\text{O}_4$.

These samples were then subjected to XRD studies for the evaluation of structural parameters.

3.9 Structural evaluation of the ceramic NZF

The X ray diffractograms of these powder samples were recorded on a X-ray diffractometer (Rigaku D max-C) using Cu K_α radiation ($\lambda = 1.5405 \text{ \AA}$). This was done to ensure the formation of exact phase and to confirm that there is no impurity phase present in the prepared samples. From the diffractograms recorded, parameters like relative intensity (I/I_0), interatomic spacing (d) etc were obtained. Lattice parameter was calculated assuming cubic symmetry by employing the relation

$$d_{h,k,l} = \frac{a}{\sqrt{h^2 + k^2 + l^2}} \dots\dots\dots(3.8)$$

The average particle size was determined from the measured width of their diffraction curves by using Debye Scherrer formula (39,49)

$$D = \frac{0.9\lambda}{\beta \cos \theta} \dots\dots\dots(3.9)$$

Here λ is the wavelength of Cu K_{α} radiation ($\lambda = 1.5405 \text{ \AA}$), β is the angular width which is equal to the full width half maximum.

The X-ray density of the prepared ceramic samples were calculated using the relation

$$\rho_x = \frac{nM}{a^3 N} \dots\dots\dots(3.10)$$

where n is the no. of molecules/unit cell, M is the molecular weight, a is the lattice parameters and N is the Avogadro number(39,77).

The apparent density is calculated by considering the cylindrical shape of the pellets and by using the relation

$$\rho_a = \frac{m}{V} = \frac{m}{\pi r^2 h} \dots\dots\dots(3.11)$$

where m is the mass of the corresponding pellets, r is the radius of the pellet and h is the thickness of the pellet.

From the calculated values of the apparent density(ρ_a) and X-ray density(ρ_x), porosity P of the ceramic nickel zinc ferrites were calculated by using the relation

$$P = \frac{\rho_x - \rho_a}{\rho_x} \dots\dots\dots(3.12)$$

The surface area in m^2/g was evaluated from these data using the relation

$$S = \frac{6000}{D\rho} \dots\dots\dots(3.13)$$

where 'D' is the diameter of the particle in nm and ' ρ ' is the density of the particle in g/cc. (79).

3.10 Incorporation of $\text{Ni}_{1-x}\text{Zn}_x\text{Fe}_2\text{O}_4$ in natural rubber matrix.

Pre-characterised ceramic nickel zinc ferrite samples were then incorporated into a natural rubber matrix. For this an appropriate recipe is chosen and the mixing of ferrite with the matrix is done using a Brabender plasticorder. (The Brabender plasticorder is an instrument for measuring processability of polymers and for blending of polymers. It is also called the torque meter.) The temperature of the mixing chamber is controlled by circulating oil and can be varied up to 300°C . The

mixing was done at around 70°C and this was carried out for a period of 7minutes. A constant torque of 450Nm and frequency of rotation 50rpm was maintained. The samples containing NZF at various loading namely 30, 60, 90 and 120 phr in NR are prepared. (phr-parts per hundred rubber by weight). The recipe for compounding is given in the form of a table below.

Ingredients	Blank	30phr	60phr	90phr	120phr
NR(natural rubber)	100.0	100.0	100.0	100.0	100.0
Zinc Oxide	5.0	5.0	5.0	5.0	5.0
Stearic acid	3.0	3.0	3.0	3.0	3.0
Sulphur	2.5	2.5	2.5	2.5	2.5
MBTS	0.8	0.8	0.8	0.8	0.8
TMTD	0.2	0.2	0.2	0.2	0.2
Ni _{1-x} Zn _x Fe ₂ O ₄	0.0	30.0	60.0	90.0	120.0

Table :3.1 Recipe for mixing

Here Sulphur acts as the vulcanising agent. It brings about cross linking and converts rubber to form bound structure. Usually 0.5 to 5 phr sulphur is added. Saturated polymers cannot be crosslinked with sulphur and organic peroxide is needed for crosslinking. Vulcanisation with sulphur is very slow and can be accelerated with the addition of organic and inorganic compounds known as accelerators. 0.5 to 2 phr of accelerators are usually used. In the present case the accelerators used are MBTS (mercapto benzothiazole disulphide) and TMTD(tetra methyl thiuran disulphide). These accelerators have the advantage of safe processing and are less scorchy and inexpensive. ZnO (3 – 5phr) along with fatty acids such as stearic acid (1-3 phr) is the most commonly used activator/coactivator. These ingredients activate the accelerators to work more effectively and increase the cure rate.

After mixing in the Brabender plasticorder these compounds are further homogenized using a two roll mill. Then it is moulded into thin rectangular shaped sheets at 150⁰ C at their respective cure time in accordance with ASTM D 3188 using an electrically heated hydraulic press. The moulding is to be done at a temperature of

150°C at their respective cure time. Hence prior to moulding the cure time or the cure characteristics are to be evaluated (78-83).

3.11 Cure characteristics

After the compounding of the elastomer with the magnetic filler according to the recipe, the resulting blend is to be vulcanised. For this cure characteristics of the vulcanisable rubber compounds is to be understood. Knowledge of these cure characteristics also throws light on the processability of composites (75). Parameters like maximum and minimum torque, cure time and cure temperature were evaluated by determining the cure characteristics of compounds on a Gottfert Elastograph (model: 67.85). Maximum torque is a measure of the stiffness or shear modulus of fully vulcanised test specimen at the vulcanisation temperature. Minimum torque is the stiffness of the unvulcanised test specimen at the lowest point of the cure curve. Cure time is the time required for 90% curing of the test specimen. The cure test is done as explained in the next paragraph(78-83). .

A test specimen of the vulcanisable rubber compound is inserted into the curometer test cavity and after a closure action it is contained in a sealed cavity under positive pressure. The cavity is maintained at some elevated vulcanisation temperature. In the present case the temperature is maintained at 150°C. The rubber totally surrounds the biconnical disc after the dies are closed. The disc is oscillated through a small amplitude (1 or 3°) and this action exerts a shear strain on the test specimen. The force required to oscillate or rotate the disc to the maximum amplitude is continuously recorded as a function of time, with the force being proportional to the shear modulus or stiffness of the test specimen at the test temperature. This stiffness first decreases as it warms up and it increases as a result of vulcanisation. The test is completed when recorded torque either reaches an equilibrium or when predetermined time is elapsed. The time required to obtain the cure curve is a function of characteristics of the rubber compound and of the test temperature. Thus from the cure curve obtained the cure parameters are extracted. Using these parameters the compounds are then vulcanized at 150°C on an electrically heated laboratory hydraulic press up to the respective cure time to make sheets of the sample. The entire test is carried out according to the ASTM standards.(ASTM D2084-95)

3.12 Evaluation of hardness of the prepared RFCs

Hardness is defined as the resistance of a material to deformation, particularly permanent deformation, indentation or scratching. It is purely a relative term and in any study of hardness a relative account of the hardness of different grades of the material can be obtained. Durometer hardness tester is used for measuring the relative hardness of soft materials. It is based on the penetration of specified indenter forced onto the material under specified conditions. It consists of a pressure foot, an indenter and an indicating device. The indenter is spring loaded and the point of the indenter protrudes through the hole in the base. The most commonly used instrument is Durometer, made by Shore Instrument Company. There are several shore instruments namely A,B,C,D and O, designed to give different readings from soft sponge upto ebonite type material. Shore A durometer readings are most common. On shore A scale 0 would be soft and 100 hard. As a comparison, rubber band is 35 in Shore A and rubber tyre tread is 70. Ebonite is much more hard/solid and is read about 60 shore D and a bowling ball is 90 shore D(79-85).

The hardness measured using Type A Durometer is expressed in a unit called 'Shore A' and that measured using Type B is called 'Shore B' and so on. In the present set of experiments Type A Durometer is used. The hardness (Shore A) of the moulded samples were tested by using Zwick 3114 hardness tester in accordance with ASTM D 2240 – 86. The tests were carried out on a mechanically unstressed sample of 12 mm diameter and minimum 6 mm thickness. The test is carried out by first placing the specimen on a hard, flat surface. The pressure foot of the instrument is pressed onto the specimen. A load of 12.5 N was applied and after ensuring firm contact with the specimen, the readings were taken after 10 seconds of indentation.

3.13 Evaluation of Mechanical properties

Tensile strength, modulus and elongation are some of the most important indications of the strength of the material(79-85). A tensile test is a measure of the ability of a material to withstand the forces that tend to pull it apart and to determine to what extent the material stretches before breaking. A tensile testing machine has a fixed or essentially stationary part carrying one grip and a movable part carrying a second grip. Self aligning grips which are employed for holding the test specimen

between the fixed and movable parts prevent alignment problem of the specimen. The test specimen is cut from the moulded sheets according to ASTM standards.

Fig 3.7 shows a representative shape of the tensile testing specimen used in the present study.

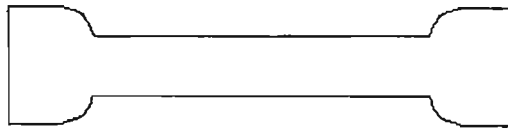


Fig3.7 Test Specimen for tensile measurements

Mechanical properties of the representative samples of the RFCs were determined using the universal testing machine (UTM) model Instron 4500. Dumb-bell shaped samples were cut from the prepared RFCs containing $Ni_{1-x}Zn_xFe_2O_4$ ($x=0.2, 0.6$ and 1.0) at various loadings of 30,60,90 and 120phr. Parameters namely tensile strength, 100% modulus and elongation at break were determined for the samples containing NZF at different loadings.

3.14 Dielectric measurements

The investigation of dielectric properties helps us in understanding the structure of materials. The accurate knowledge of dielectric properties of a material is a prerequisite for many technological applications. Dielectric information is also useful for improving ferrite microwave absorbers. The dielectric constant or permittivity is defined as the ratio of the field strength in vacuum to that in the material for same distribution of charges. Dielectric constant is dependent on parameters like frequency, temperature, orientation, mixture, pressure and molecule structure of the material.

An electrical conductor charged with a quantity of electricity q at a potential V is said to have a capacity $C=q/V$. The capacity of a simple parallel plate capacitor is given by

$$C = \frac{\epsilon A}{d} \dots\dots\dots(3.14)$$

where A is the area of the parallel plates, d is the separation between the plates and ϵ is the ratio of dielectric constant of the medium between the plates to that of free space.

This equation is exploited in evaluating the dielectric constant of the ceramic nickel zinc ferrites and Rubber ferrite composites containing NZF in NR.

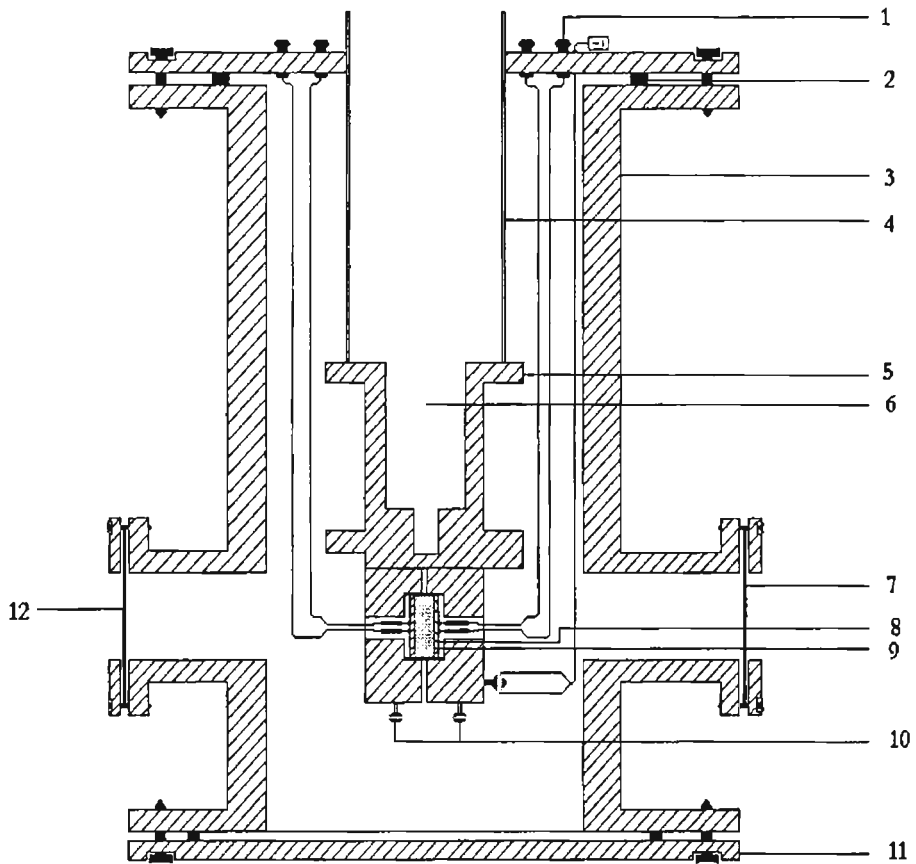
The dielectric properties of $Ni_{1-x}Zn_xFe_2O_4$ were studied by using a dielectric cell and an impedance analyser (Model: HP 4285A) in the frequency range 100KHz to 8 MHz. A dielectric cell was fabricated for this purpose. Fig 3.8 shows a schematic form of the fabricated dielectric cell.

Pellet samples of $Ni_{1-x}Zn_xFe_2O_4$ having a diameter of 12mm were loaded onto the spring loaded sample holder assembly. The capacitance values at different frequencies ranging from 5Hz to 13Mhz was noted. The dielectric constant was calculated using the formula

$$C = \frac{\epsilon_0 \cdot \epsilon_r \cdot A}{d} \dots\dots\dots(3.15)$$

where A is the area of the sample pieces used and d their thickness. ϵ_0 and ϵ_r are the dielectric constant of the air and medium respectively and C is the capacitance value (78).

The dielectric constants were evaluated for different compositions and different loadings of the nickel zinc ferrites in NR matrix. The dielectric cell is provided with provisions for heating and the measurements were carried out from room temperature to 120⁰C for all samples.



- | | |
|-------------------------|----------------------|
| 1. BNC | 7. Glass Window |
| 2. Neoprine O Ring | 8. Copper Electrodes |
| 3. MS Chamber | 9. Sample |
| 4. SS Pipe | 10. Fixing Screws |
| 5. Sample Holder | 11. MS Flange |
| 6. Liq. Nitrogen Cavity | 12. To Vacuum pump |

Figure 3.8 Schematic representation of dielectric cell

The entire data acquisition and evaluation of the dielectric constant were automated by using a package called LabVIEW which in turn is based on G programming. LabVIEW is a programming language for data acquisition, analysis, simulation or

computer control of instruments, techniques or processes. LabVIEW is an acronym for Laboratory Virtual Instrument Engineering Workbench and is a proprietary item owned by National Instruments. LabVIEW is an object oriented language and its style, syntax and data flow is different from conventional linear programming languages. Appropriate modifications were incorporated in the software so as to enable the data acquisition automatic and visual observation of the graphs on the computer screen. It has been possible to acquire 20,000 data points or more in a matter of 5 to 10 minutes by using the modified package.

3.15 AC conductivity measurements

The ac electrical conductivity of both the ceramic and rubber ferrite composites were calculated by utilizing the dielectric parameters. The dielectric studies of both ceramic and rubber ferrite composites were carried out by using a dielectric cell and a HP 4285A impedance analyzer. The details of these measurements are given in the previous section (3.14).

The theory (86) involved in the evaluation of ac conductivity from dielectric constant may be briefed as follows. Any capacitor when charged under an ac voltage suffers a loss current due to ohmic resistance or impedance by heat absorption. For a parallel plate capacitor of area A and separation d , the ac conductivity is given by the relation

$$\sigma_{ac} = \frac{J}{E} \dots\dots\dots(3.16)$$

Here J is the current density and E is the field density.

J and E are given by the relations

$$E = \frac{D}{\epsilon} = \frac{q}{\epsilon} = \frac{V}{d} \dots\dots\dots(3.17)$$

D is the displacement vector of the dipole charges. ε is the complex permittivity of the material, V is the potential difference between the plates of the capacitor and d is the inter plate distance.

$$J = \frac{dq}{dt} \text{ and } q \text{ is given by } \frac{Q}{A} = \frac{V\varepsilon}{d}$$

$$J = \frac{\varepsilon}{d} \frac{dV}{dt} = \frac{\varepsilon}{d} Vj\omega \quad \dots\dots\dots(3.18)$$

Substituting for J and E from the relations 3.17 and 3.18 we get

$$\sigma_{ac} = \frac{J}{E} = \varepsilon j \omega, \text{ considering } \varepsilon \text{ as a complex entity of the form}$$

$\varepsilon^* = (\varepsilon^1 - j\varepsilon^{11})$ and neglecting the imaginary term in the conductivity we can write

$$\sigma_{ac} = \omega \varepsilon^{11} \quad \dots\dots\dots(3.19)$$

But the loss factor or dissipation factor in any dielectric is given by the relation

$$\tan\delta = \frac{\varepsilon^{11}(\omega)}{\varepsilon^1(\omega)} \quad \dots\dots\dots(3.20)$$

Hence from the dielectric loss and dielectric constant AC conductivity of these samples can be evaluated using the relation

$$\sigma_{ac} = 2\pi f \tan\delta \varepsilon_0 \varepsilon_r \quad \dots\dots\dots(3.21)$$

f is the frequency of the applied field ε_0 is the absolute permittivity, ε_r is the relative permittivity and $\tan\delta$ is the loss factor.

CHAPTER 4

EFFECT OF CYCLING ON THE MAGNETIZATION OF MAGNETIC NANOCOMPOSITES AND DECOMPOSITION STUDIES ON THE COMPOSITES

4.1. Introduction

Particles possessing nanometric dimensions lying in the range 1-10nm are found to be exhibiting superior properties compared to their bulk counterparts. It is also reported that for small particles the energy level spacing of quantised electronic states is comparable to kT at temperatures of 1K and so it is possible to observe quantum size effects at finite temperatures in such small particles (87). Also, the large reduction in linear dimensions and the boundary and surface conditions play an important role in moulding the physical properties of small particles. Magnetic properties of small particles are of immense importance because of their potential applications. Magnetic nanocomposites and magnetic nanomaterials have an important place among nanomaterials and they have the potential to replace many of the conventional magnetic materials.

Nanocomposites with magnetic nanoparticles dispersed in polymer matrices have gained considerable attention because of their wide ranging applications. Below a critical size they become single domain as against the multidomain in bulk. These composites exhibit remarkable properties like superparamagnetism, quantum tunneling of magnetization and magnetocaloric effect. They also exhibit large coercivity values. Such changes in physical properties, brought about by the dimensional changes, make these materials attractive for many applications including magnetic recording, ceramics, catalysts, colour imaging and magnetic refrigeration. (21-23, 87-91)

Studies carried out on nanometric magnetic particles include ultrafine metallic iron and iron alloy particles as well as nanometer sized iron oxide particles embedded in Al_2O_3 , SiO_2 , porous glass and nonmagnetic polymer matrices (91-96).

Attempts are made to prepare nanostructured materials and gain control over physical properties, so as to tailor materials for potential applications. Synthesizing magnetic nanocomposites based on $\gamma\text{-Fe}_2\text{O}_3$ gives scope for the development of newer materials with improved magnetic and electrical properties. There are different methods like sol gel, gas phase condensation, high energy ball milling and ion exchange followed by reduction, for the preparation of magnetic nanocomposites. Some of these techniques are listed in Chapter 3.

In this chapter the preparation of magnetic nanocomposites containing $\gamma\text{-Fe}_2\text{O}_3$ embedded in a polymer matrix of sulphonated polystyrene by the method of ion exchange is explained. Samples have been prepared using both weak and strong ion exchange resins. Different preparative conditions have also been tried. The prepared samples have been characterized by techniques like X-ray powder diffraction (XRD), Vibrating Sample Magnetometry (VSM), Differential Scanning Calorimetry (DSC) and chemical analysis. Optimization of preparative conditions and influence of various parameters on the magnetization of these samples are also studied. Decomposition studies on these prepared samples were also carried out to study the effect of temperature on the particle size and also to confirm the formation of magnetic iron oxide ($\gamma\text{-Fe}_2\text{O}_3$) in the matrix.

4.2. Optimization of the preparation conditions

Nanometer sized $\gamma\text{-Fe}_2\text{O}_3$ particles were embedded in a polymer matrix by the method of ion exchange followed by reduction. The method adopted here is a modification of the preparation scheme reported by Ziolo et al (21,96). The polymer matrix employed is a cross linked polymer of sulphonated polystyrene and divinyl benzene, which have exchangeable H^+ ion containing SO_3H^+ groups. The schematic of a polystyrene structure is given in Chapter 2. For the sake of continuity it is reproduced in figure 4.1.

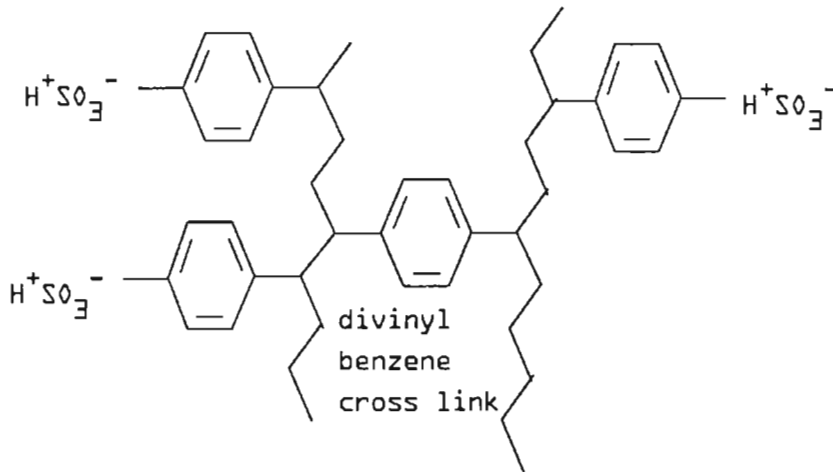


Figure 4.1 schematic of sulphonated polystyrene

The ion exchange resin was exchanged with Fe ions from an aqueous solution of ferrous sulphate and these exchanged Fe ions were then converted into $\text{Fe}(\text{OH})_2$. This was then oxidized to yield, presumably, $\gamma\text{-Fe}_2\text{O}_3$. Drop wise addition of dilute aqueous solution of hydrogen peroxide (H_2O_2) accelerated the conversion to oxide. The resin was then washed with water and then dried. Instead of adding H_2O_2 , the addition of hydrazine hydrate solution was also tried for the conversion of hydroxide into oxide. Both weak as well as strong ion exchange resins were used for the preparation of nanocomposites. The preparation scheme can be depicted as shown in Figure 4.2.

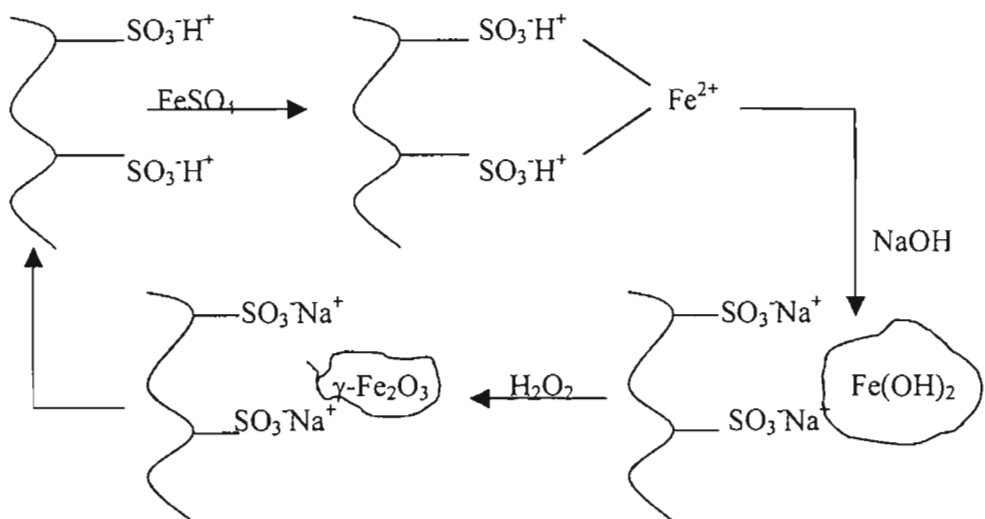


Figure 4.2 Scheme of preparation of nanocomposites

The preparative conditions were optimized by trial and error method. The maximum value of the saturation magnetization obtained is taken as the optimum condition. The table 4.1 gives the details of different samples prepared and their magnetization values. Weak resin samples were prepared with the addition of both hydrazine hydrate and hydrogen peroxide. They are labeled as WRC1 and WRC2. Their magnetization values were compared and it was observed that both reactants produced magnetic component in the matrix but the addition of H₂O₂ produced more yield. The next attempt was to change the ion exchange matrix. Instead of weak ion exchange resin strong resin was used for the preparation. Here also hydrazine hydrate and H₂O₂ were tried and the samples are labeled as SRC1 and SRC2. Comparison of the magnetization values indicated that strong resin without hydrazine hydrate and with H₂O₂ produced more yield as far as the magnetic component is considered.

Sample ID	Saturation Magnetization (M _s) Am ² /kg
WRC1	0.48
WRC2	0.78
SRC1	1.47
SRC2	1.99
SRC4	3.10
SA1	4.55
SA8	8.50
SA12	9.18

Table 4.1 Details of Samples prepared and Magnetisation values

The effect of concentration of FeSO₄ solution on the amount of incorporated iron oxide in the matrix was also studied. For this another sample with the strong resin

as the base matrix was prepared with the addition of more concentrated solution of FeSO_4 . This sample is labeled as SRC4. It was observed that as the concentration of FeSO_4 increases the magnetization also increases. Hence a saturated solution of FeSO_4 is selected as the optimum concentration of FeSO_4 .

Cycling of the preparation procedures was also done on one sample of strong ion exchange resin. The samples after first, eighth and twelfth cycles were taken. These cycled samples are labeled as SA1, SA8 and SA12 for 1st, 8th and 12th cycled samples respectively. It is found that by cycling the preparation steps more and more sites are exchanged by Fe ions and hence the possibility of incorporating more Fe_2O_3 in the matrix.

Thus the strong ion exchange resin, saturated solution of FeSO_4 , addition of H_2O_2 for conversion to oxide and cycling the preparation schemes are the optimum conditions for incorporation of iron oxide in polymer matrix.

4.3. XRD studies

XRD spectra of the samples were recorded using Rigaku Dmax XRD as explained in Chapter 3. The XRD spectrum of a representative sample is shown in Fig. 4.3. The XRD pattern exhibits a broad peak centered at around $2\theta = 35.5^\circ$ which corresponds to a d value of 0.253 nm which is characteristic of $\gamma\text{-Fe}_2\text{O}_3$. The reported d value for $\gamma\text{-Fe}_2\text{O}_3$ is 0.252 nm. As the particle size decreases the width of the diffraction peak increases and hence the broad peak is a characteristic of a nanoscopic material. (97-99)

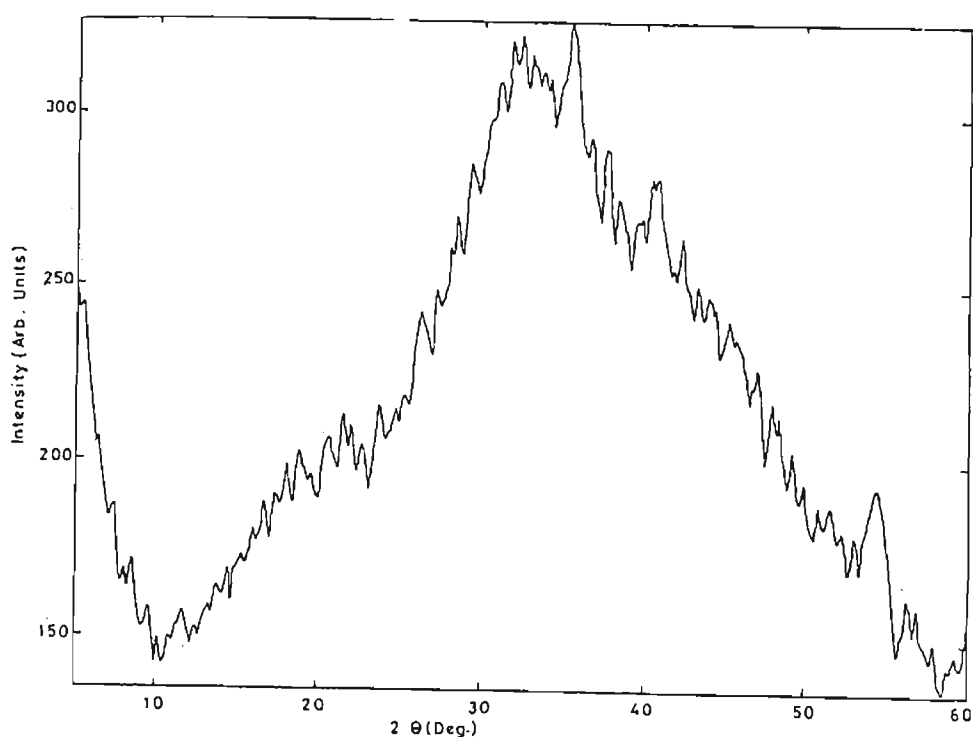


Fig.4.5 XRD Spectrum of a representative sample (SRC4).

To confirm the formation of gamma phase of iron oxide and to study the effect of heating/temperature on the sample, decomposition studies on these samples were carried out. Prior to undertaking the decomposition studies a representative sample was subjected to thermal studies by employing differential scanning calorimetry. A representative spectrum is shown in Fig 4.4. It can be seen that the onset of decomposition is at around 200°C and is completed at around 400°C . Based on the gathered information the samples were subjected to decomposition studies. For this the sample was heated at different temperatures in air at 200 , 250 and 400°C and the XRD spectra of the decomposed samples were recorded afterwards. The spectra recorded at different temperatures are shown in figures 4.5a to 4.5c. The details extracted from these XRD spectra are given in Table 4.2a to 4.2c.

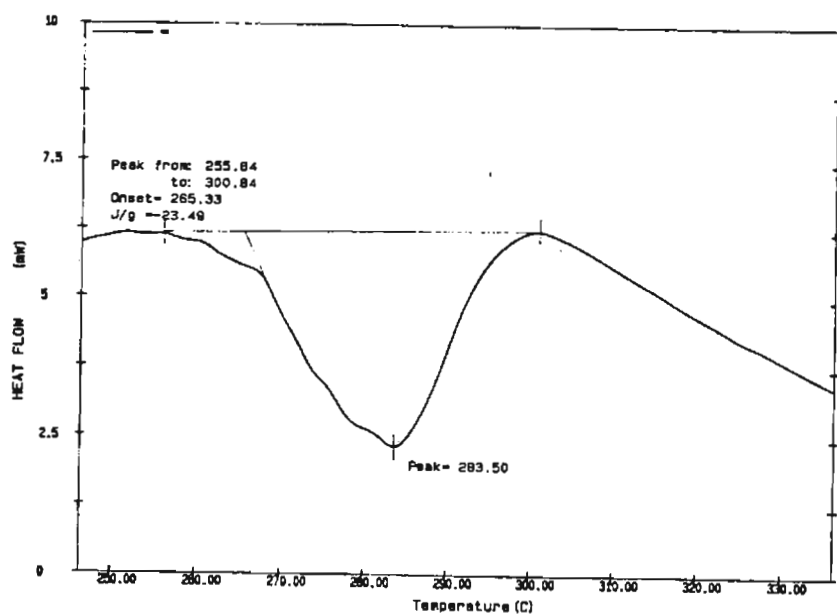


Fig 4.4 Representative DSC Spectrum of the sample SA12.

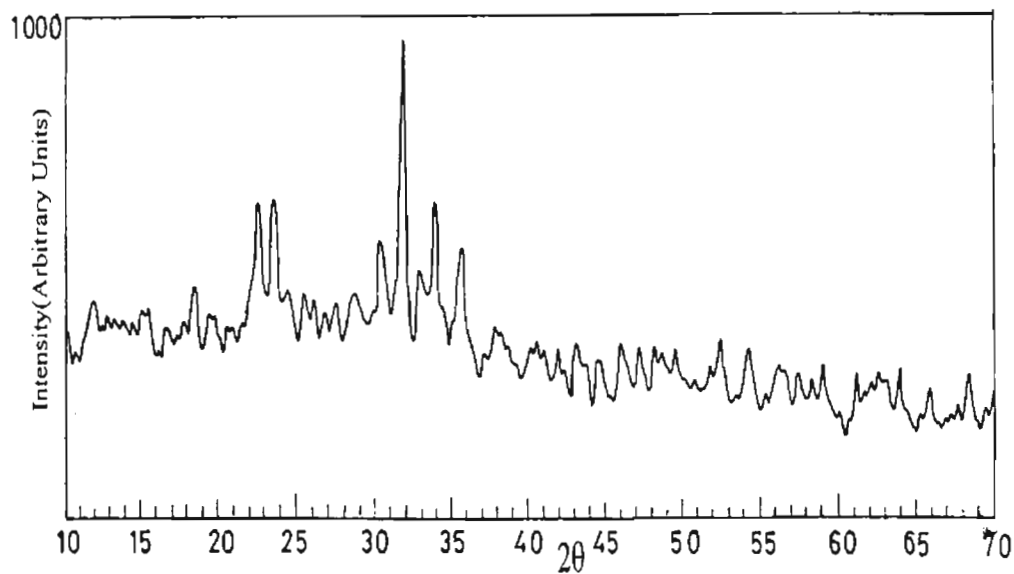


Fig. 4.5a. - XRD spectra of the sample decomposed at 200°C

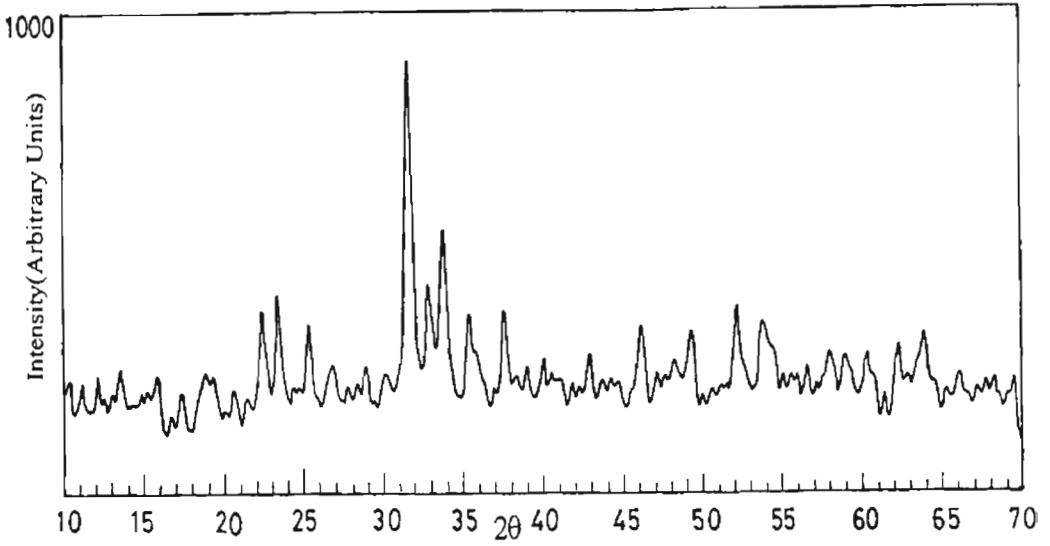


Fig.4.5b. XRD Spectra of the Sample decomposed at 250°C

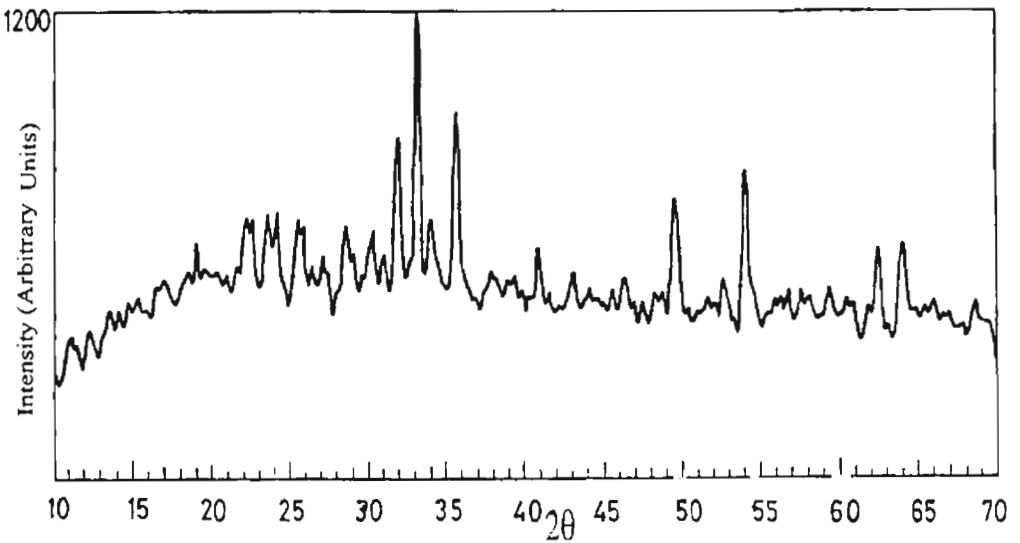


Fig.4.5c. XRD Spectra of the sample decomposed at 400°C

From these studies it is found that as the temperature of decomposition increases the particle size increases and hence more and more crystallinity is achieved which is evidenced from the appearance of peaks in the XRD spectra. Also from the table below it can be seen that as the temperature is increased the alpha phase of the iron oxide becomes predominant and the composite loses its magnetic characteristics. It is also observed that the gamma phase of iron oxide is becoming less and less intense as the temperature of decomposition increases.

The average particle size evaluated by employing Scherrer's formula indicates that the decomposed samples exhibit an average particle size lying in the range 30-50nm.

200°C				
2θ	Phase identified	Relative Intensity(%)	'd' values in Å ⁰	Particle size in Å ⁰
18.5	γFe ₂ O ₃ /Fe ₃ O ₄	36.3	4.795	330.64
22.5	αFe ₂ O ₃	58	3.948	
23.5	γFe ₂ O ₃	58	3.748	
30	γFe ₂ O ₃ / Fe ₃ O ₄	47.8	2.98	
33.5	αFe ₂ O ₃	100	2.674	
35.5	γFe ₂ O ₃ / Fe ₃ O ₄	59.4	2.52	
36.5	αFe ₂ O ₃	44.9	2.459	

Table 4.2a.XRD parameters of the sample decomposed at 200°C

250°C				
2θ	Phase identified	Relative Intensity (%)	d values in Å ⁰	Particle size in Å ⁰
25	αFe ₂ O ₃	39.4	3.568	413.12
31.5	γFe ₂ O ₃ / Fe ₃ O ₄	73.2	2.838	
33	αFe ₂ O ₃	100	2.713	
34	αFe ₂ O ₃	40.8	2.635	
34.5	γFe ₂ O ₃	54.9	2.57	
36	γFe ₂ O ₃ / Fe ₃ O ₄	32.3	2.493	
50	αFe ₂ O ₃	28.2	1.822	
53	αFe ₂ O ₃ / Fe ₃ O ₄	35.2	1.726	
54	αFe ₂ O ₃ / Fe ₃ O ₄	29.6	1.484	

Table 4.2b XRD parameters of the sample decomposed at 250°C

400°C				
2θ	Phase identified	Relative Intensity(%)	d values in Å ⁰	Particle size in Å ⁰
25.5	γFe ₂ O ₃	46.5	3.492	473.94
33	αFe ₂ O ₃	100	2.714	
35.75	γFe ₂ O ₃ /αFe ₂ O ₃	73.2	2.511	
41	αFe ₂ O ₃	35.4	2.201	
49.7	αFe ₂ O ₃	49.3	1.834	
52.5	αFe ₂ O ₃	26.8	1.741	
54	αFe ₂ O ₃	56.33	1.697	
62.5	αFe ₂ O ₃	35.2	1.484	
64	αFe ₂ O ₃	35.2	1.4536	

Table 4.2c XRD parameters of the sample decomposed at 400°C

4.4. Magnetic studies.

Magnetisation measurements on weak and strong ion exchange resins were carried out by using VSM and a representative hysteresis loop is shown in Fig.4.6. The results are given in table 4.3. The results reveal that strong resins can exchange more Fe ions than weak resins and hence yield more magnetic component in the matrix. This may be attributed to the existence of more ion exchange sites available in the strong ion exchange resin matrix. Magnetisation results on samples prepared with and without hydrogen peroxide show that addition of H₂O₂ increases the oxidation of Fe(OH)₂ to γ-Fe₂O₃ and hence creates more magnetic particles in the matrix. Cycled samples show more magnetization compared to the uncycled ones and the saturation magnetization is found to increase with the increase in number of cycles. Thus cycling induces more magnetic component in the matrix as more sites are exchanged and the content of Fe₂O₃ is increased which is evidenced by the increase of Fe concentration in the nanocomposite. However, there exists a maximum value of the saturation

magnetization (M_s) that could be obtained for the composite. This has been theoretically calculated to be around $16\text{Am}^2/\text{kg}$. It is to be noted that in our set of experiments a maximum of about $9\text{Am}^2/\text{kg}$ was obtained for the composite corresponding to 12 cycles.

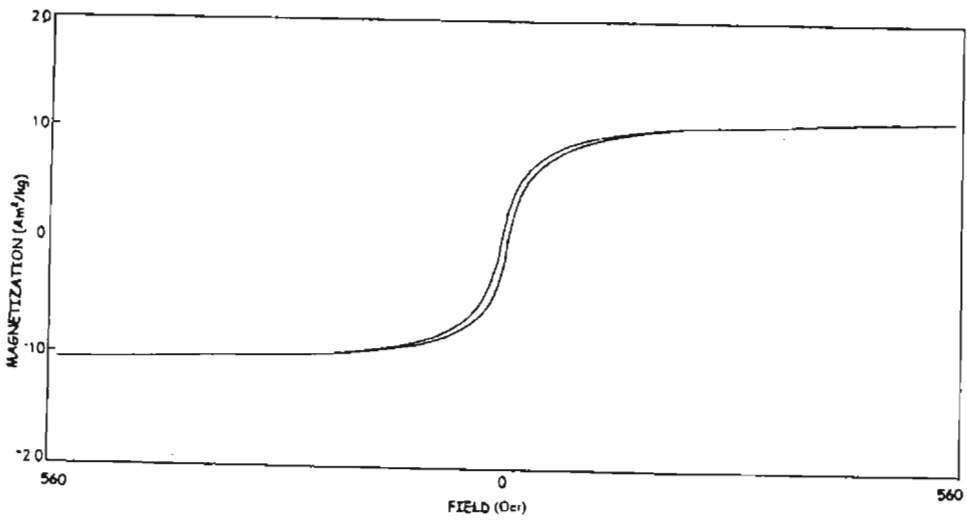


Fig.4.6. Hysteresis loop of a representative sample.

Sample ID	Saturation Magnetization (M_s) Am^2/kg	Coercivity (H_c) A/m	Remanent Magnetization (M_r) Am^2/kg
WRC1	0.48	8974	0.066
WRC2	0.78	10270	0.066
SRC1	1.47	7165	0.14
SRC2	1.99	7165	0.15
SRC4	3.10	3888	0.40
SA1	4.55	4219	0.39
SA8	8.50	5254	1.10
SA12	9.18	4936	1.39

Table 4.3 Magnetisation Parameters of nanocomposites samples.

4.5. Fe content Estimation

The Fe contents on cycled samples were also estimated. Fe content and saturation magnetization versus number of cycles were also plotted for SA1, SA8 and SA12 and is shown in Fig.4.7. The results indicate an increase in Fe content with the increase in number of cycles. It can be noticed that as cycling increases the iron content also increases which in turn increases the saturation magnetization. This is evident from the graph showing Ms/Fe content versus number of cycles. Differentiation between $\text{Fe}^{2+}/\text{Fe}^{3+}$ is not possible by these techniques and only the total amount of Fe present in the composite is evaluated. Moreover it cannot be said for sure whether these reactions have resulted in Fe_3O_4 or $\gamma\text{-Fe}_2\text{O}_3$ in the matrix. However, XRD studies point to the formation of gamma iron oxide in the matrix.

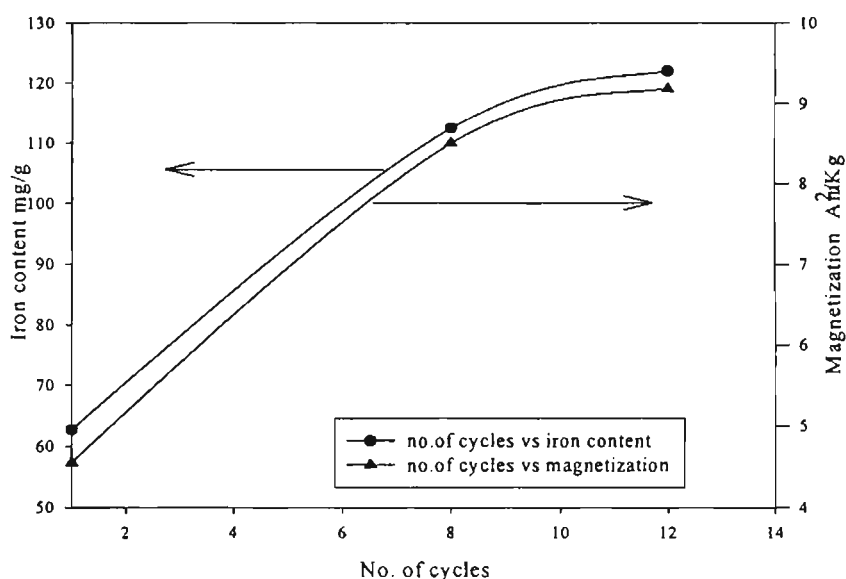


Fig. 4.7. Fe content and Saturation Magnetization Vs no. of cycles for SA1, SA8, SA12

4.6. Mössbauer Studies.

The room temperature Mössbauer studies were carried out on these samples. The Fe^{57} Mössbauer spectrum of a representative sample (SRC4) recorded at room temperature is shown in Fig.4.8. The Mössbauer spectrum could satisfactorily be fitted, based on a computer program code developed by Bent et al (100), with two doublets corresponding to Fe^{3+} in A and B sites. The relative

intensities of the A and B site spectra are in the ratio 85:15. The Mössbauer parameters from the fittings are shown in table 4.4. The values reported here are in agreement with the values reported by Shull et al. The room temperature Mössbauer spectrum for $\gamma\text{-Fe}_2\text{O}_3$ /polymer nanocomposite reported by Shull et.al and others (95,98,101) corresponds to a central doublet with an isomer shift of 0.3mm/s and a quadrupole splitting of 0.6mm/s.

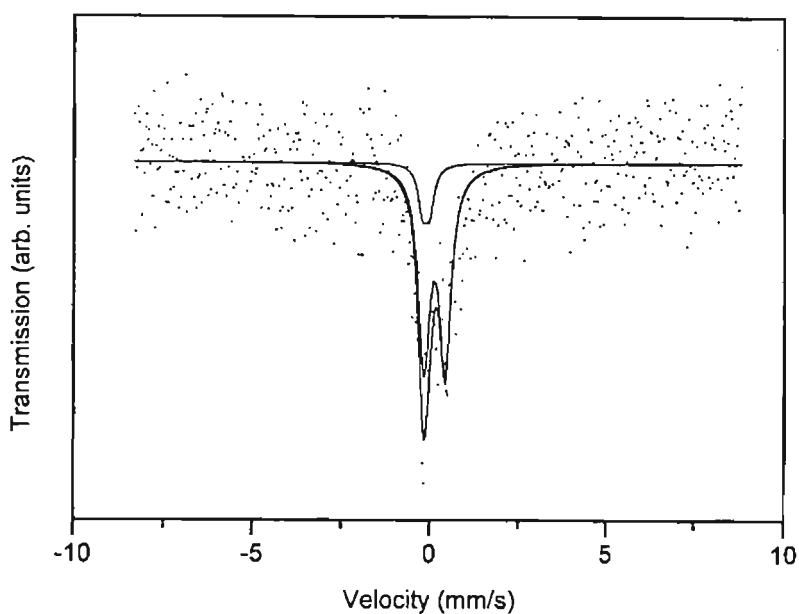


Fig.4.8 Room Temperature Mössbauer Spectra of uncycled sample

Doublet	C.S. mm/s ⁺	Q.S. mm/s	Linewidth mm/s	Relative intensity
I	0.26	0.60	0.40	85
II	0.02	0.20	0.30	15

Table 4.4. Mössbauer Results on uncycled sample

The low temperature measurements on the SA12 sample were made and figure 4.9 shows the variation of magnetisation with temperature. The low temperature behavior of the cycled sample has been further investigated by different studies like Mössbauer and ESR. The room temperature and low

temperature Mössbauer Spectra of the cycled samples were recorded. The results are explained in detail in chapter 5.

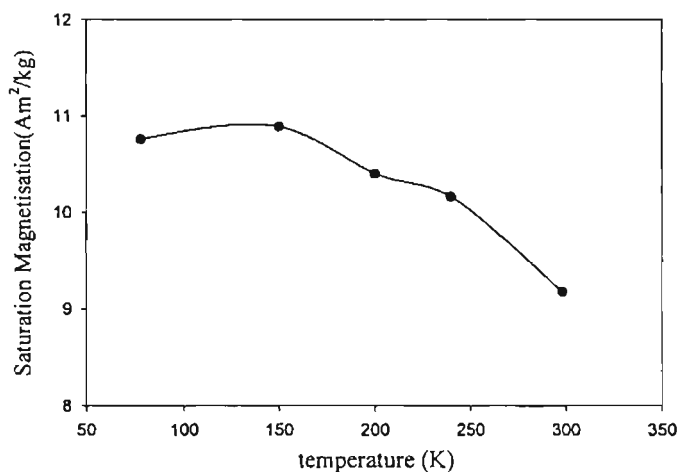


Fig.4.9 Variation of Saturation magnetisation with temperature

4.7. Conclusion

Magnetic nanocomposites containing γ -Fe₂O₃ nanocrystals embedded in a polymer matrix have been synthesized by ion exchange by using both weak and strong resins and precipitation reaction. The conditions has been standardized and optimized. The polymer matrix provides localized nucleation sites and imposes an upper limit to the particle size, thereby minimizing the degree of aggregation. These studies indicate that by cycling the preparation steps and by the addition of dilute hydrogen peroxide one can achieve good yield as far as the magnetic component is considered. It is the strong ion exchange resin which give maximum yield when compared to week resins. Fe content enhancement with cycling tallies well with the magnetization measurements. Decomposition studies on the sample confirm the presence of gamma iron oxide in the matrix. The particle size estimation of the decomposed samples indicate that the particle size increases as the decomposition temperature increases. But even for the highest decomposition temperature, in the present study (400⁰C), the particle size was found to be less than 50nm. Low temperature studies were carried out on these samples. Further investigations were carried out using ESR and Mössbauer spectroscopy and this will be discussed in detail in the next chapter.

CHAPTER 5

LOW TEMPERATURE STUDIES ON MAGNETIC NANOCOMPOSITES

5.1 Introduction

The particle size effects dominate the magnetic properties of magnetic nanocomposites and the effect becomes more prominent as the particle size decreases. Nanophase materials and nano composites, characterised by an ultra fine grain size (< 50 nm) have created a great deal of interest in recent years by virtue of their unusual mechanical, electrical, optical and magnetic properties. The magnetic nanocomposites in which the magnetic nanoparticles are dispersed in nonmagnetic matrices have been found to possess entirely different magnetic characteristics with respect to their bulk counter parts(20,21). The reduction in size modifies the magnetic order in these materials. The magnetic nanocomposites can be prepared by isolating the magnetic regions in nonmagnetic matrices by precipitating from some solid solutions. The gross magnetic behaviour of a magnetic nanocomposite will be either paramagnetic or superparamagnetic. Because of the ease in controlling the magnetic behaviour by adjusting the processing parameters, such materials present a greater possibility for designing materials with specific properties. They find potential applications in recording industry for achieving high density information storage and in the refrigeration industry.

Magnetic nanocomposite containing $\gamma\text{-Fe}_2\text{O}_3$ have been prepared by the ion exchange method and the effect of cycling of the preparation procedure on the magnetic properties of these nanocomposites have been studied. The results have already been discussed in Chapter 4. In this chapter the investigations carried out on the low temperature magnetic behaviour of this composite samples are explained. These studies have been conducted to investigate the low temperature behaviour of these samples with a view to understanding the

superparamagnetic/single domain characteristics of the magnetic component on the matrix.

According to Bean et al (43) there are three kinds of magnetic structures for small particles namely multidomain, single domain and quasidomain. A superparamagnetic particle is a single domain particle whose direction of magnetization fluctuates by thermal activation and attains thermal equilibrium with the applied field. Superparamagnetism is analogous to paramagnetism with the only difference is that the magnetic moment involved is not that of a single atom but of a single domain which may contain 10^5 or more atoms ferromagnetically coupled with exchange forces. Thus in superparamagnetism the behaviour of single domain particles in thermodynamic equilibrium is identical to atomic paramagnetism except that the moments involved are very large(43,44). Thermal fluctuations will cause the direction of magnetization to undergo random reorientation. For non-interacting particles the magnetic susceptibility of the assembly of particles is the same as that of a classical Langevin paramagnetism with the magnetic moment of each particle equal to that of large a number of atoms. If the particles are fixed in space thermal activation is the mechanism for achieving thermodynamic equilibrium. The relaxation time τ required for the assembly to achieve equilibrium increases exponentially with KV/kT This is of the form

$$\tau = \tau_0 \exp(KV/kT) \dots \dots \dots (5.1)$$

where K is the anisotropy constant, T is the temperature and k is the Boltzman constant(46). In an assembly of particles the relaxation time of particles with smaller volume is short and their response is fast under the influence of an external magnetic field. Larger particles are magnetically frozen.

For particles of volume V there is a critical temperature called blocking temperature(T_B) below which the magnetic moments are fixed that is their approach to thermodynamic equilibrium is blocked.

If the time of the experiment is around 100s then the blocking temperature is $T_B = KV/25k_B$ and the critical volume is $V_c = 25k_B T/K$. Only particles with volume less than V_c will respond superparamagnetically to an external field at temperature T .

Most of the reported literature indicates that magnetic nanocomposites do not show hysteresis at room temperature and hysteresis is observed only below the blocking temperature which is normally well below room temperature(95-99). But there also exist reports on nanocomposites with blocking temperature much above room temperature. T.Ambrose et. al (102) have reported T_B to be much above room temperature in Fe- Al_2O_3 systems. Roy et al have also reported T_B to be above room temperature in Fe/ SiO_2 system(103). However, the reports on blocking temperature by R.D.Shull, Ziolo and others are contradictory and they have reported T_B to be well below room temperature(95-99).

In the earlier chapter (Chapter 4) preparation of nanocomposite have been explained in detail. The conditions for the preparation of these composites have been optimized and samples were prepared under these optimized conditions. Magnetic measurements on these prepared samples were carried out by using VSM PAR 4500. Both room temperature and low temperature magnetic measurements on the sample SA12 (prepared after 12 cycles of the procedures given in fig.4.1) were carried out. The magnetic parameters namely saturation magnetization and coercivity were obtained. The thermomagnetisation curve of one representative sample was also recorded. From the magnetic measurements on the cycled and uncycled samples, it was observed that the cycling increases the amount of magnetic component incorporated.

^{57}Fe Mössbauer spectra of the sample were recorded at room temperature using a constant acceleration Mössbauer spectrometer and the spectrum was fitted to obtain the quadrupole splitting and isomer shift. The spectra were recorded at RT, 150K and at 100K. The ESR spectra of selected samples were also recorded both at room temperature and at 110K.

Low temperature magnetic measurements on one representative sample was carried out and it was observed that the magnetization increases with decrease in temperature. This is explained in chapter 4. It was found to be in accordance with the normal theoretical approach. That is as the temperature decreases more and more ordering of moments come in and hence magnetisation increases.

5.2 Low temperature magnetisation studies.

The temperature dependence of saturation magnetisation of the SA12 sample was studied. The saturation magnetisation values are plotted against $T^{3/2}$ and Fig. 5.1 shows the temperature dependence saturation magnetisation. The curve clearly indicates that the system obeys Bloch law given by $\sigma_s = \sigma_0(1-BT^{3/2})$ where B is called the Bloch constant or spin wave constant. The present system is found to be obeying the Bloch law above 120K and there is a deviation from Bloch law below 120K.

The $T^{3/2}$ dependence indicates that the spin wave excitations in the ultrafine particles. However the spin wave constant B evaluated is found to be of the order of 10^{-4} which is the typical order for nanosized samples as reported by Wang Jian Ping et al(104). For bulk iron this constant is reported to be of the order of 10^{-6} . Wang Jian Ping et al observed a B value of 10^{-5} for a system of Fe-SiO₂ prepared by sol-gel method. The increase in spin wave constant B is probably caused by both in the finite size effect which causes the softening and cutoff of some spin waves, and surface effects that have been confirmed in magnetic thin films(105).

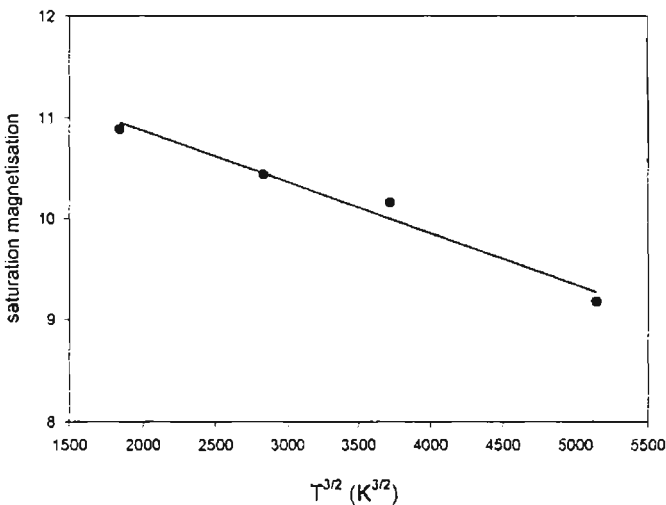


Fig.5.1 $T^{3/2}$ dependence of saturation magnetisation

The thermomagnetisation curve for on representative sample is given in Fig 5.2. This graph shows a sudden change in magnetization at around 120K. Inorder to probe into this particular behaviour, the Mossbauer studies and ESR studies were also carried out on these samples.

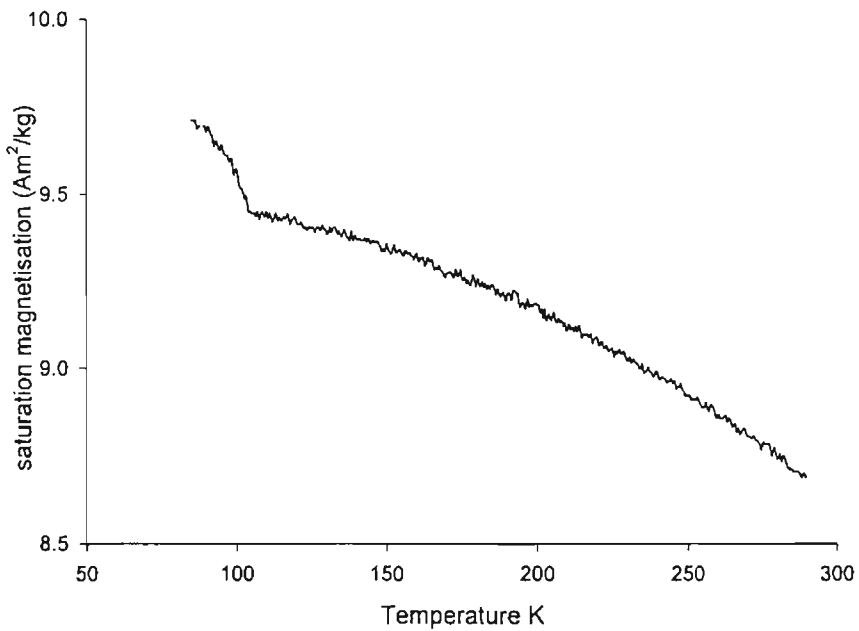


Fig 5.2 .Thermomagnetisation curve for SA12

5.3 Mossbauer Studies

The room temperature Mossbauer studies was carried out on some representative samples. These were done both on the cycled and uncycled samples. The low temperature Mossbauer spectra at 150K and at 100K were recorded for the cycled sample.

The Fe⁵⁷ Mössbauer spectrum of a representative uncycled sample (SRC4) recorded at room temperature is shown in Fig.4.8. For continuity this result is included in this chapter (cf. Fig.5.3).

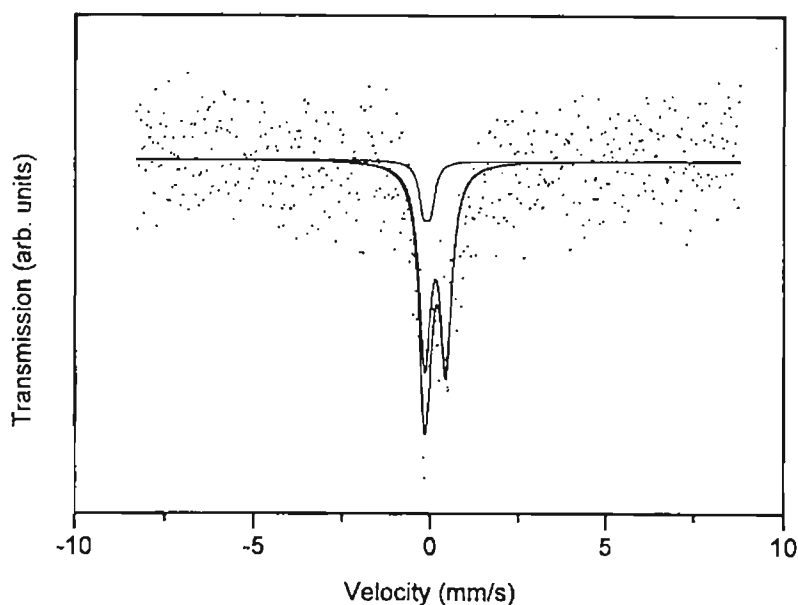


Fig.5.3 Room Temperature Mossbauer Spectra of uncycled sample

The Mössbauer spectrum could satisfactorily be fitted with two doublets corresponding to Fe^{3+} in A and B sites. The values of different parameters namely, Isomer shift and quadrupole splitting are in agreement with the values reported by Shull *et al*(95-99,101). The room temperature Mössbauer spectrum for $\gamma\text{-Fe}_2\text{O}_3$ polymer nanocomposite reported by Shull *et al* corresponds to a central doublet with an isomer shift of 0.3mm/s and a quadrupole splitting of 0.6mm/s.

The Mössbauer spectra of the cycled samples were also recorded at room temperature and at low temperatures. The low temperature measurements include that carried out at 150K and at 100K.

Generally a sample of superparamagnetic material will contain a range of particle size and hence a range of values for T_B . So the Mössbauer spectra of the sample will consist of a magnetically split sextet corresponding to large crystallites and a quadrupole split doublet corresponding to smaller crystallites (95-99,106). A clear indication in the Mössbauer for Superparamagnetic smaller particles is that the spectral area of the doublet increases at expense of the sextet. Also, reports indicate that if the isomer shift is in the range of 0.29-0.33mm/s, then they are typical of compounds containing Fe^{3+} in the octahedral co-

ordination and they are similar to those found in the nanocrystalline samples(106-114). If there are large quadrupole splitting that is greater than 0.7 they represent very small crystallites. This is because their large surface to volume ratio causes lattice strain and correspondingly large electric field gradient at the iron nuclei. It may also be noted that conventional large crystallites have a quadrupole splitting of 0.16 to 0.8 mm/s.

In the present system the room temperature as well as low temperature Mossbauer Spectra were recorded for the cycled sample. The general fit of room temperature Mossbauer spectra of SA12 is shown in Fig.5.4. The spectrum is satisfactorily fitted into a superposition of sharp central doublet and a broad sextet. The fitted doublet and sextet are shown in figures 5.5 and 5.6. The parameters like isomer shift, quadrupole splitting and hyperfine field were obtained from the spectra. They are listed in table 5.1. From these values it can be said that the sample consists of a mixture of superparamagnetic and ferromagnetic oxides of iron. The hyperfine field of 501KOe corresponds to gamma phase of iron oxide. This is in agreement with various reports (106-114)

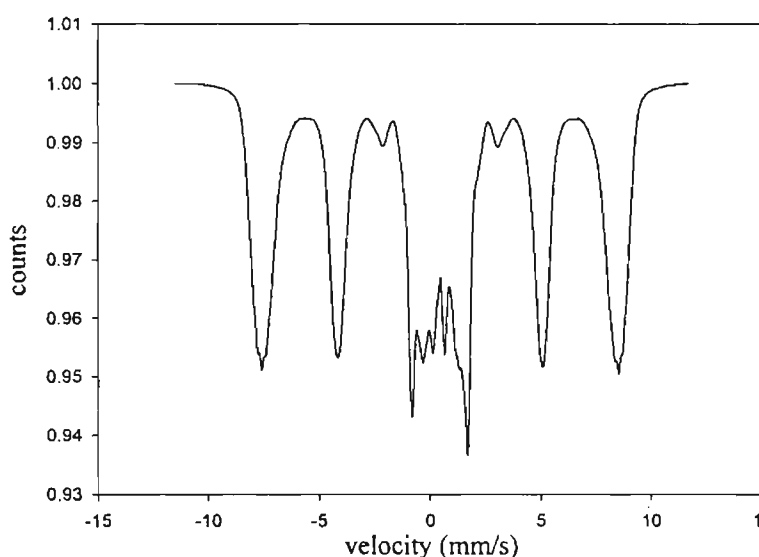


Fig 5.4 General fit of the room temperature Mossbauer spectra of SA12

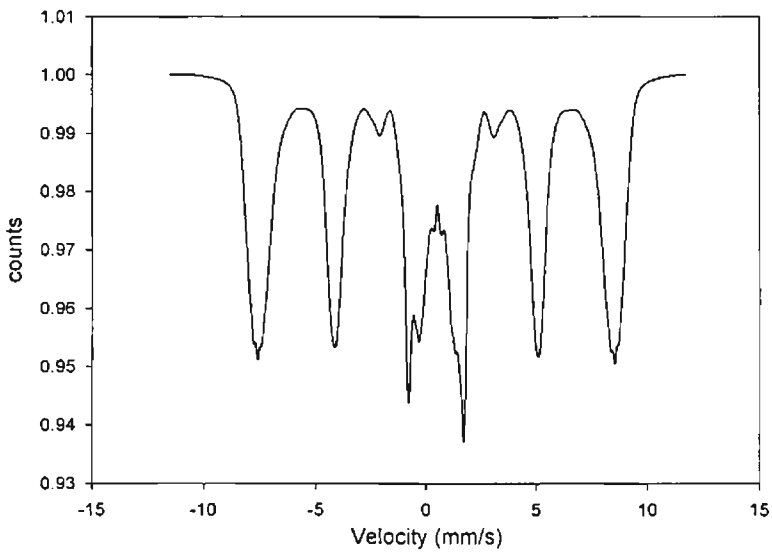


Fig. 5.5 Mossbauer spectrum of the ferrimagnetic component in SA12

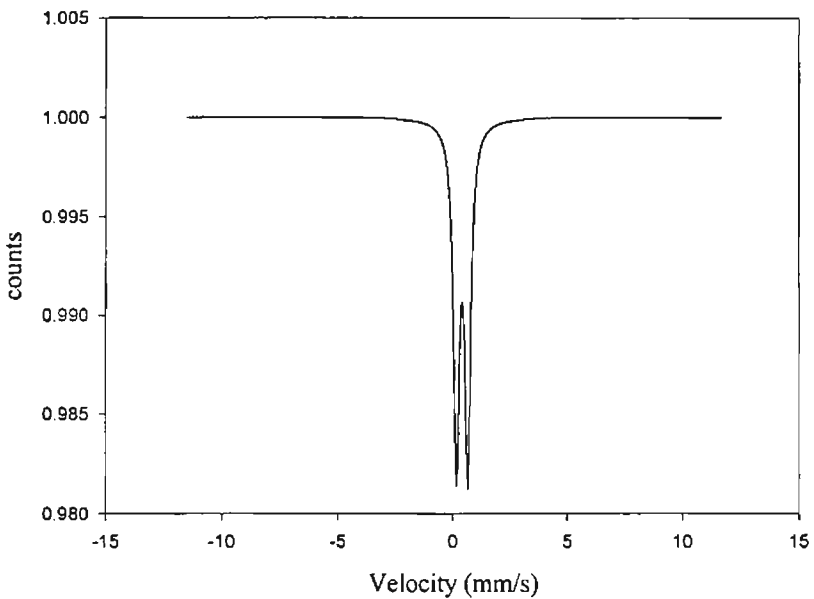


Fig.5.6 Mossbauer spectrum showing the superparamagnetic component in SA12

The hyperfine field distribution of room temperature spectra is shown in figure 5.7. It shows a broad hyperfine field with peaks around 47T and 33T. It also shows some minor peaks around low field values. From the broad hyperfine field distribution it can be concluded that the magnetic component in the matrix is either in the amorphous form or nanocrystalline form exhibiting superparamagnetic relaxation. The minor peaks in the hyperfine field distribution

indicate that some nonmagnetic Fe is present in the system. The quadrupole split spectrum of this nonmagnetic Fe will contribute peaks in the low field region.

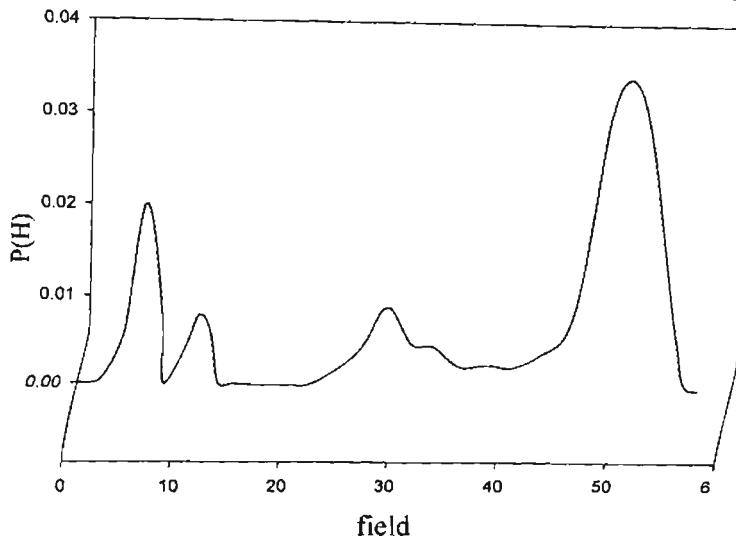


Fig.5.7 Hyperfine field distribution for SA12 at RT

The low temperature Mossbauer spectra were also recorded at 150K and 100K. These spectra were also fitted into superposition of a central doublet and a sextet extending to large velocities. The general fitted spectrum, the central doublet and separated sextet for 150K are shown in figures 5.8, 5.9 and 5.10 respectively. The Mossbauer parameters are shown in table 5.1.

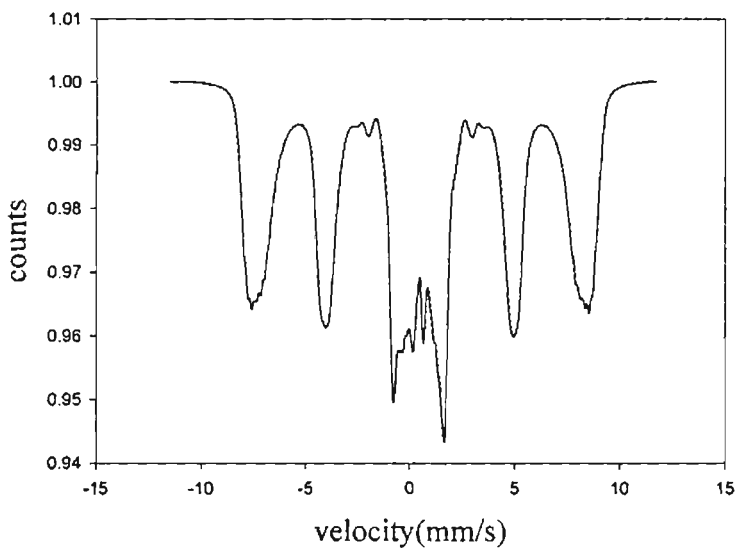


Fig.5.8 Total Spectrum of SA12 recorded at 150K

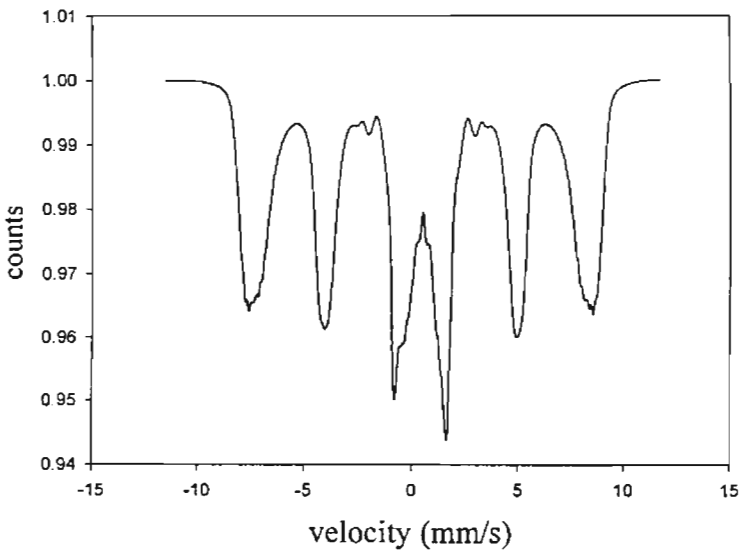


Fig 5.9 Ferrimagnetic component of SA12 at 150K

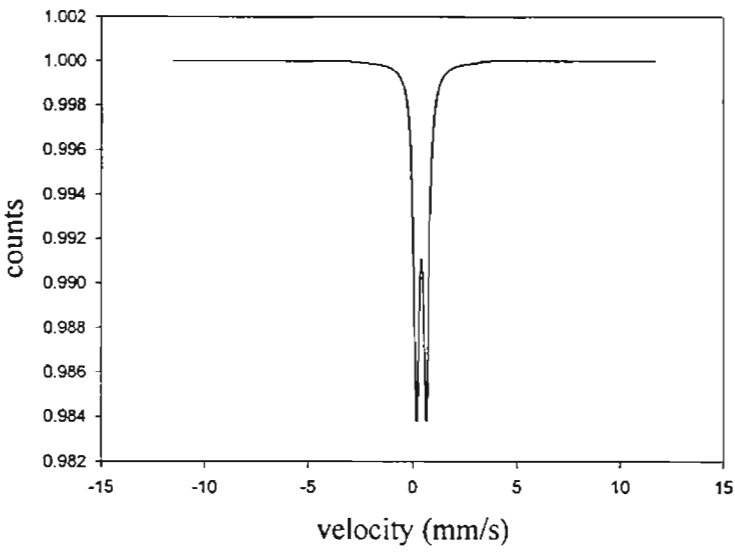


Fig.5.10 Sperparamagnetic component in SA12 at 150K

Hyperfine field distribution at 150 K is shown in figure 5.11

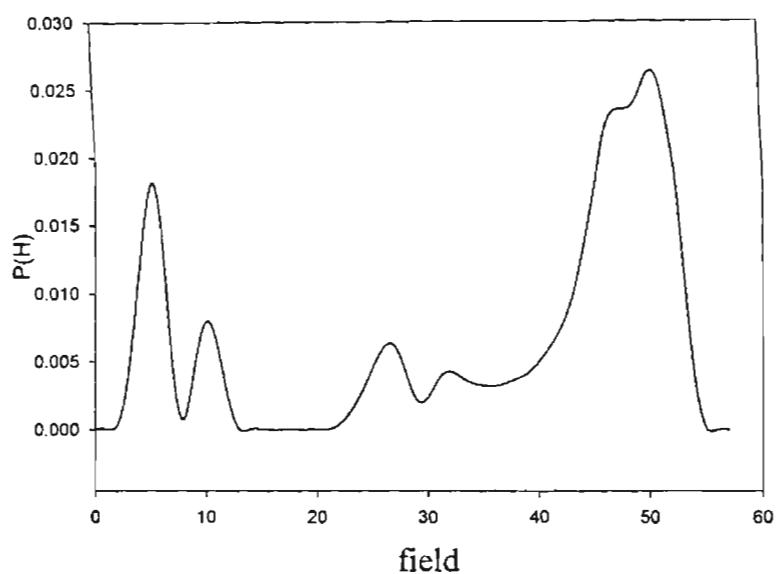


Fig 5.11 Hyperfine field distribution of SA12 at 150K

The total spectrum and the component spectra namely the sextet and doublet for SA12 at 100K are shown in figures 5.12, 5.13 and 5.14 respectively.

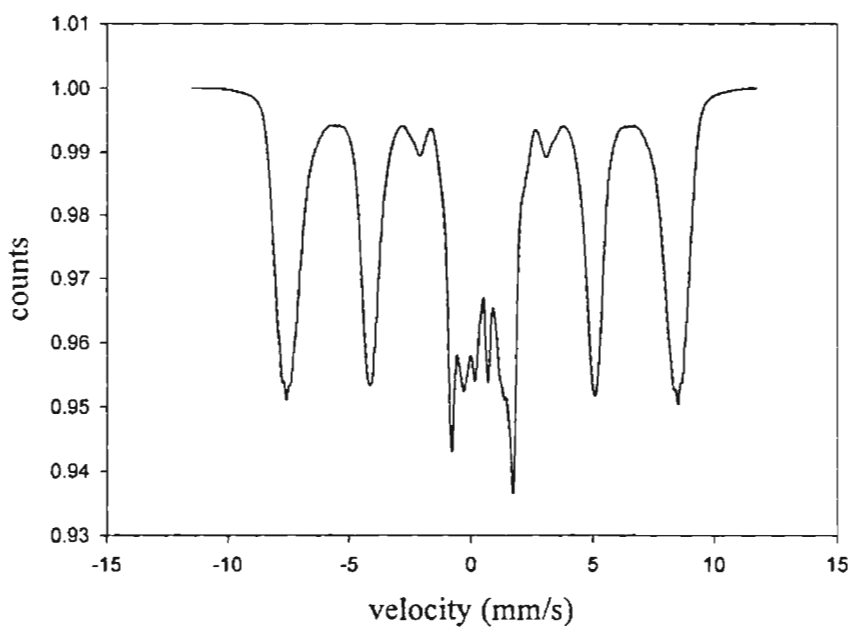


Fig.5.12 Total spectra of SA12 recorded at 100K

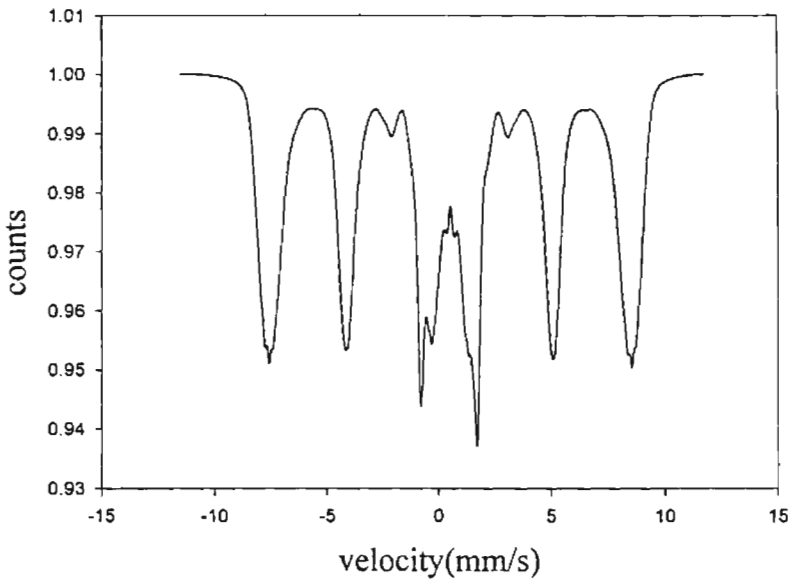


Fig.5.13 Spectra of ferrimagnetic component in SA12 at 100K

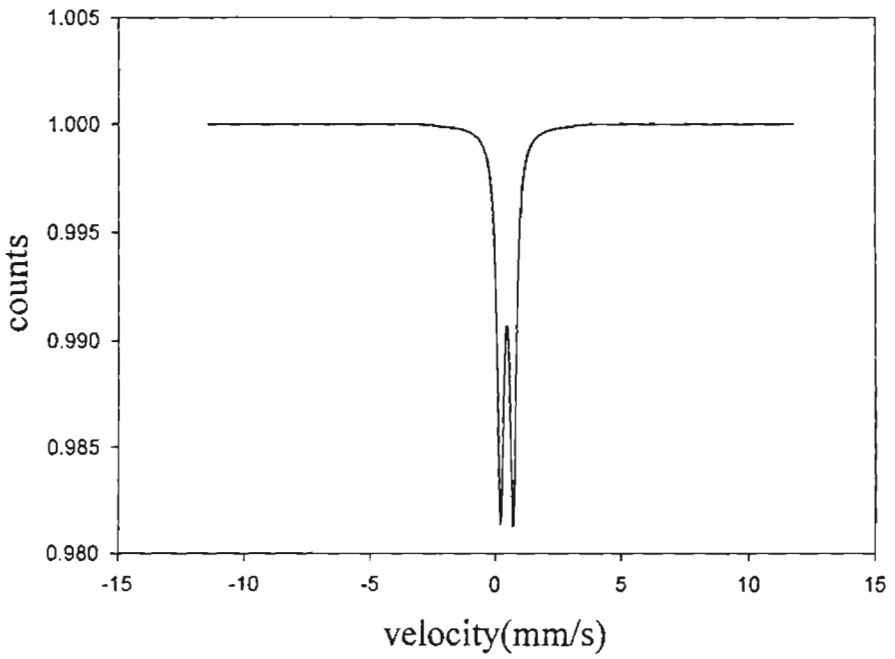


Fig.5.14 Superparamagnetic component in SA12 recorded at 100K

The hyperfine field distribution in SA12 sample at 100K is shown in figure 5.15

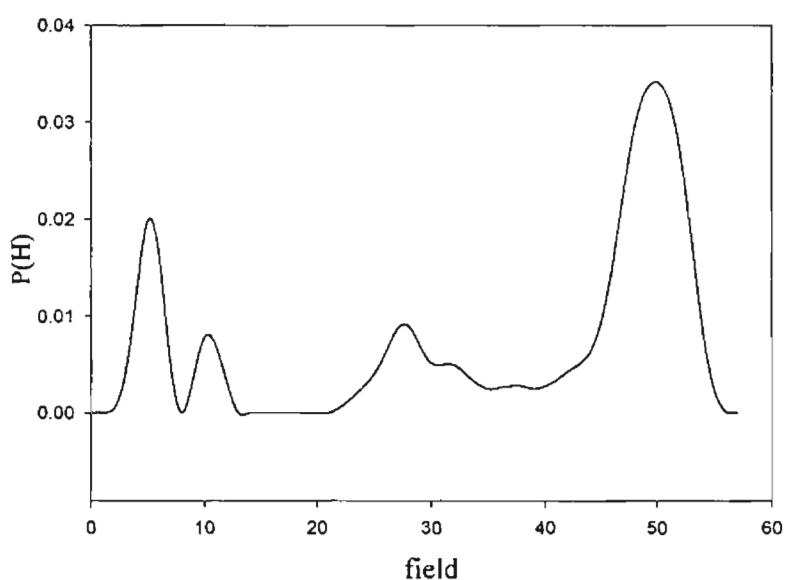


Fig 5.15 Hyperfine field distribution for SA12 at 100K

Temperature	Ferrimagnetic component			SP component	
	Isomer shift mm/s	Quadrupole Splitting mm/s	Hyperfine field kOe	Isomer shift mm/s	Quadrupole splitting mm/s
298K	0.47	1.2	500.8	0.43	0.55
150K	0.47	1.2	500.9	0.43	0.55
100K	0.47	1.2	500.8	0.43	0.55

Table. 5.1 The Mossbauer Parameters of the cycled sample.

From the table 5.1 it can be seen that the hyperfine field obtained for the samples at room temperature as well low temperatures is at around 501 KOe which is again characteristic of gamma iron oxide. The isomer shift and Quadrupole splitting for the SP component at all temperatures is around 0.43mm/s and 0.55mm/s respectively which are characteristic of nanosized iron oxide(95-99). Thus from the room temperature and low temperature Mössbauer spectra it

can be said that the magnetic component may be in the nanocrystalline form exhibiting superparamagnetic relaxation. At least some of the Fe atoms are nonmagnetic which may be due to Fe impurities which are also present in traces in the system. At low temperatures of 150K and 100K the hyperfine field considerably narrows down with only one peak around 50T. This also suggests that probably the broad hyperfine field distribution at room temperature is because of superparamagnetic relaxation of nanoparticles.

The mechanical coupling of small particles to its surrounding can also be studied by using Mossbauer since the thermal vibrations cause a lowering of the recoil free fraction(113). Temperature dependence of relative area of the Mossbauer spectra will give an idea about the same which will be undertaken later as a continuation of this work.

5.4 ESR studies on the nanocomposite samples.

The ESR spectra of the prepared samples were recorded at different temperatures and the parameters like line width (ΔH_{PP}) and splitting factor(g) were determined. The number of spins/g for the cycled samples were also calculated by comparing it with the standard spectra of DPPH recorded under identical conditions. The spectra were recorded at room temperature, 110K and liquid nitrogen temperature. Fig. 5.16 and fig 5.17 depicts a representative ESR spectra of a sample recorded at RT and 110K respectively. Figure 5.18 shows the ESR of WRC sample. A sharp kink at around a g value of 5 was observed for the samples at low temperature. This is in agreement with the reports of other researchers. This may be attributed to the presence of SP particles in the matrix. The broad spectra obtained is a characteristic of a ferrimagnetic system(116,117). It may also be noted that the weak sample showed only a small signal, which again may be due to the small amount of the magnetic component in it. Table 5.2 gives the various parameters obtained for different samples at different temperatures.

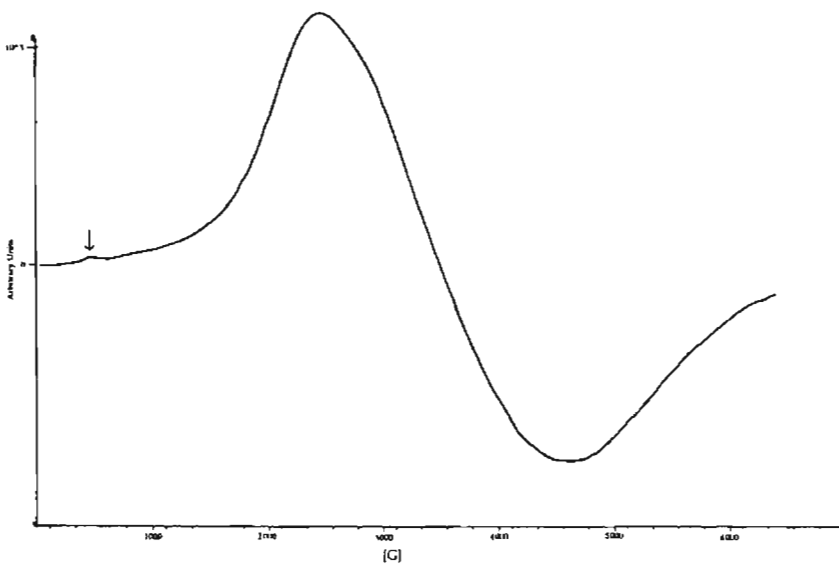


Fig. 5.16 Representative ESR spectrum of SA12 recorded at room temperature

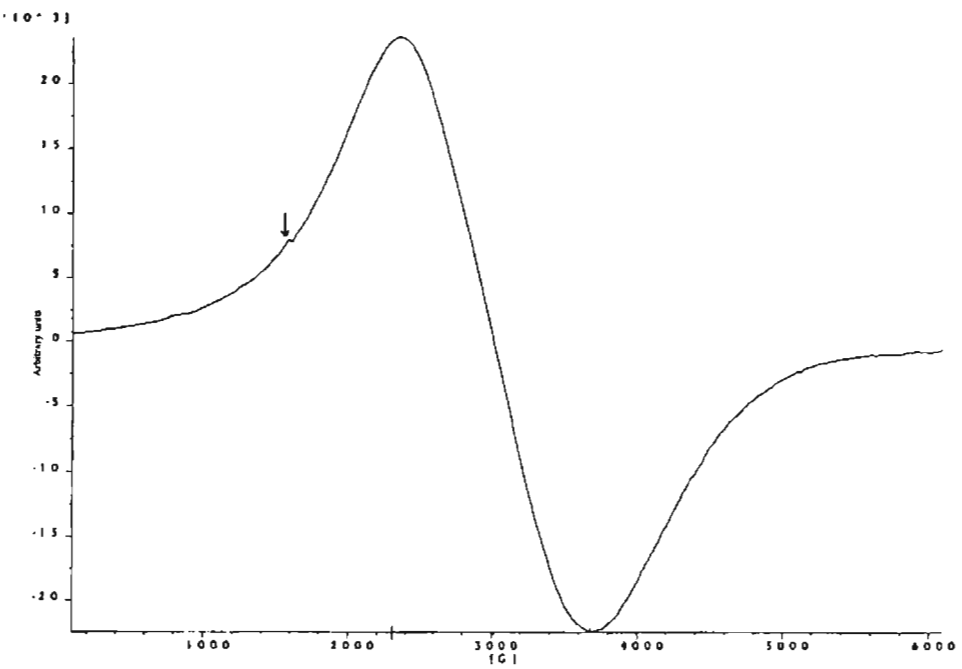


Fig.5.17 Representative ESR spectrum of SA1 recorded at 110K

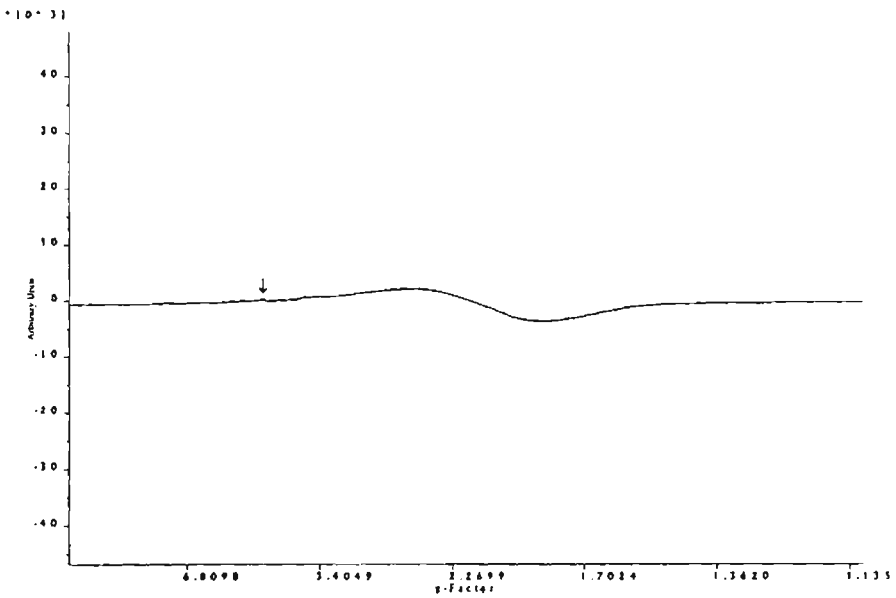


Figure 5.18 ESR spectrum of WRC recorded at 110K

From the table it can be noted that as the cycling increases the peak to peak width (ΔH_{pp}) also increases. This increase in linewidth may be due to increase in interparticle interaction. As the system becomes more and more concentrated with respect to the magnetic component and the interparticle field increases and thereby it increases the linewidth. This observation is in agreement with that reported by Upadhyay et al(117). This is also evidenced from the increase in number of spins with the increase in number of cycles. Thus it can be said that cycling increases the ferrimagnetic component in the matrix.

The increase in linewidth with decrease in temperature also points to the increased interparticle interaction(115-118). If regularly spaced magnetic centers dispersed in a nonmagnetic matrix are superparamagnetic then the net spin $\Delta n S \gg 0$, where Δn is the net population of spins aligned along the easy axis of magnetisation and S is the effective spin of the magnetic centers. Then the linewidth ΔH_{pp} is given by $\Delta H_{pp} = L \tanh [\Delta E / 2kT]$ and $L = 5g\beta S n / R^3$ where g -is the g -factor, β - is the Bohr magneton, n -total number of magnetic centers, R -distance between the adjacent particles and ΔE is the energy barrier which also explains the decrease in linewidth with increase in temperature. However Mossbauer studies indicate that SP phase is small in quantity in the present system under investigation

Sample	Temperature	ΔH_{PP} [G]	g-factor	No. of spins/gm
WRC	298K	1080	2.10	
	80K	1560	2.27	
SRC	110K	1420	2.267	
SA1	298K	1020	2.14	1.328E20
	110K	1400	2.266	
	80K	1420	2.30	
SA8	298K	1380	2.518	3.347E21
	110K	1550	2.719	
	80K	1900	2.953	
SA12	298K	1380	2.518	2.753E22
	110K	1850	2.719	
	80K	1860	2.753	

Table 5.2 ESR parameters of the Nanocomposite samples

5.5 Conclusion

Low temperature magnetisation studies, Mossbauer and ESR studies carried out on selected nanocomposites samples indicate that the composites consist of very fine particles of $\gamma\text{-Fe}_2\text{O}_3$. A definite amount of this iron oxide exists in the superparamagnetic phase. The evaluation of the Bloch constant and its numerical value suggest that the particles are definitely in the superparamagnetic state. However, deviations from Bloch equation at temperatures below 120K points to surface effects caused by finite sizes of the particle which causes the softening and cut off of the spin waves, this warrants further investigations.

Mossbauer spectroscopic studies gives conclusive evidence for the existence of $\gamma\text{-Fe}_2\text{O}_3$ phase in the nanocomposites. Cycling increases the amount of ferrimagnetic component in the nanocomposites. Some traces of nonmagnetic impurity, characteristic of Fe atom have been detected. The broad hyperfine field distribution noticed in the Mossbauer spectrum is indicative of superparamagnetic relaxation. But this is to be confirmed by other experiments. ESR studies provide complementary evidence to the presence of superparamagnetic particles. The increased ΔH_{pp} is an indirect evidence of increased interparticle interactions at low temperature. Since the thermal vibrations cause a lowering of the recoil free fraction. A plot of *ln area* vs temperature will generate information about the mechanical coupling of small particles with the surroundings. This is to be investigated further.

CHAPTER 6

MAGNETIC AND PROCESSABILITY STUDIES ON RUBBER FERRITE COMPOSITES

6.1. Introduction

Rubber ferrite composites are composite materials with ferrite fillers as one of the constituents and natural or synthetic rubber as the base matrix. In these magnetic polymers the magnetic powder as well as the polymer will affect the processibility and other physical properties of the final product. In tailoring composites for various applications it is necessary to select the proper filler and a matrix. The physical and chemical properties of the magnetic composites will possibly be influenced by the interactions with the filler and the matrix.

Incorporation of polycrystalline ferrites in elastomer matrixes will lead to rubber ferrite composites (RFC) (34-36). An appropriate selection of magnetic filler and matrix can result in RFCs with required properties for different applications. Rubber ferrite composites (RFCs) can be synthesized by the incorporation of ferrite powders in natural or synthetic rubber as matrixes. This can, not only bring in economy but also can produce flexible magnets. Factors like percolation limit or nature of the matrix, like saturated/ unsaturated / polar rubber all influences the final properties of the composites. A systematic study of these composites may be of help in tailoring materials for various applications.

The processibility of the polymer are important since the final vulcanized product is to be moulded. This necessitates the evaluation of cure parameters. The cure parameters namely the maximum torque, minimum torque and curetime were also evaluated. The variation in the cure parameters with loading is also studied. The evaluation of cure characteristics also throws light on the mechanical properties of the composites(119,120).

In applications involving RFCs at high frequencies it is necessary to modify the magnetic and dielectric properties. This is true for RFCs intended for

microwave applications where the composite material warrants an appropriate permeability and permittivity(121-125). Normally simple mixture equations relate the total magnetic property of the composite with the weight fraction of the filler loaded and magnetization of the magnetic component in the RFC. This has an inherent draw back especially, when systems of the type $Ni_{1-x}Zn_xFe_2O_4$ for various x is incorporated to make RFCs. The tailoring of magnetic properties of RFC necessitates the knowledge of the saturation magnetization (M_s) of the filler corresponding to that particular composition x . The variations of M_s with composition were studied for ceramic as well as RFC for various loadings and a general relation connecting the magnetic property of the filler and the composites will be formulated so as to predict the properties of the composites.

6.2. Structural evaluation.

$Ni_{1-x}Zn_xFe_2O_4$ for various x has prepared by ceramic techniques (73-76). The details are cited in Chapter 2. The XRD spectra of all the samples were recorded in a Rigaku Dmax C diffractometer. From the X ray powder diffractograms recorded for NZF series, parameters namely, inter atomic spacing 'd', relative intensity ($I/I_0 \times 100$), lattice constant 'a' and particle size 'D' were determined. The evaluation of the structural parameters indicates that the compounds are monophasic without any detectable impurities and are crystalline in nature(126). The XRD spectra of these ferrites are shown in figures 6.1a to 6.1f. The lattice parameters for different compositions were calculated from the x-ray spectra using the Bragg relation(39,77). The details are cited in Chapter 3. It was observed that the lattice parameter corresponding to NZF series lies in the range 8.3 to 8.4 \AA and the variation of lattice parameter with composition is in accordance with Vegards law(127,128). The results are depicted in figure6.2.

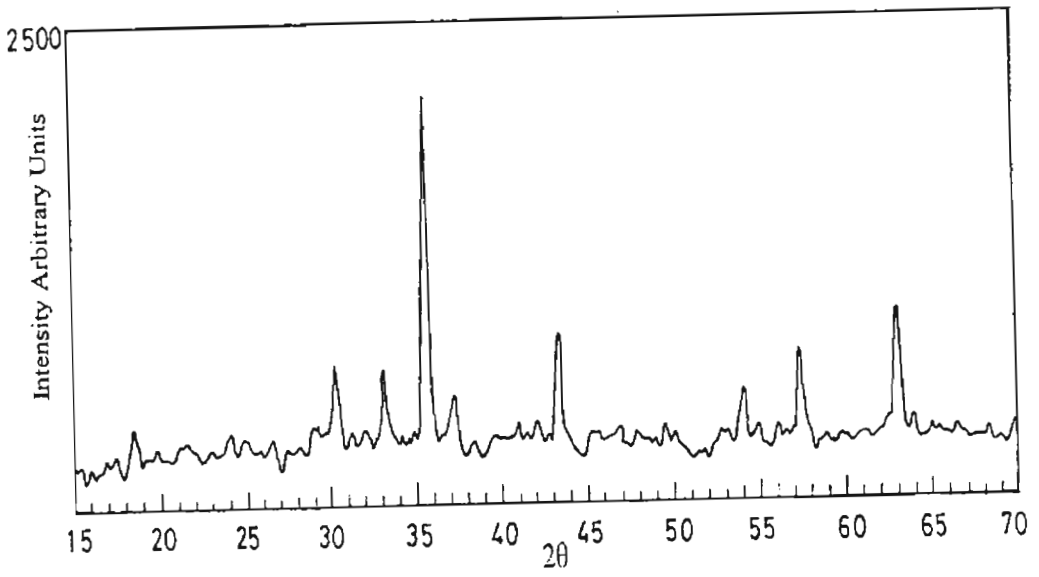


Fig.6.1a.XRD spectra of Nickel Ferrite (NiFe_2O_4)

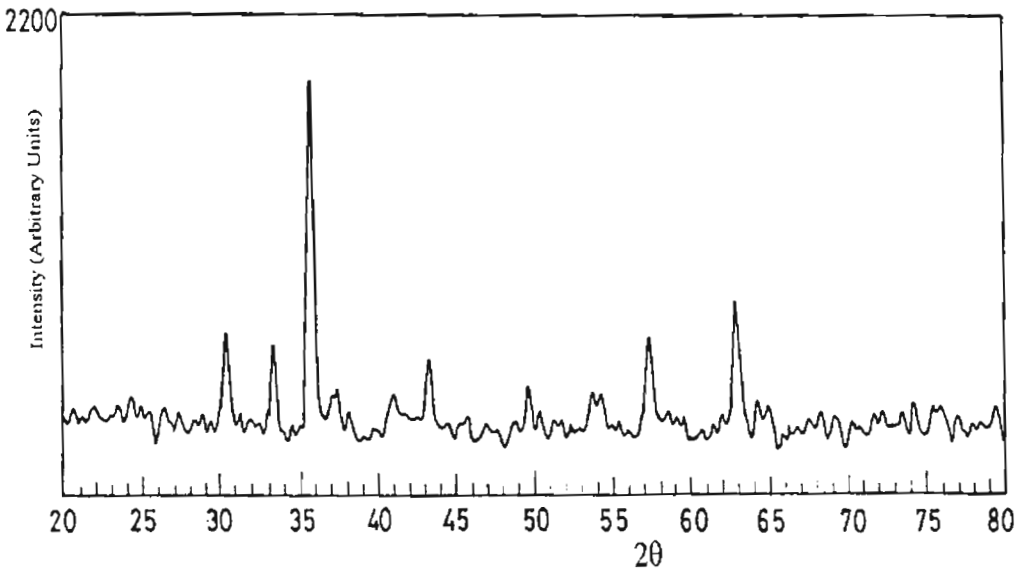


Fig.6.1b.XRD spectra of Nickel Zinc Ferrite ($\text{Ni}_{0.8}\text{Zn}_{0.2}\text{Fe}_2\text{O}_4$)

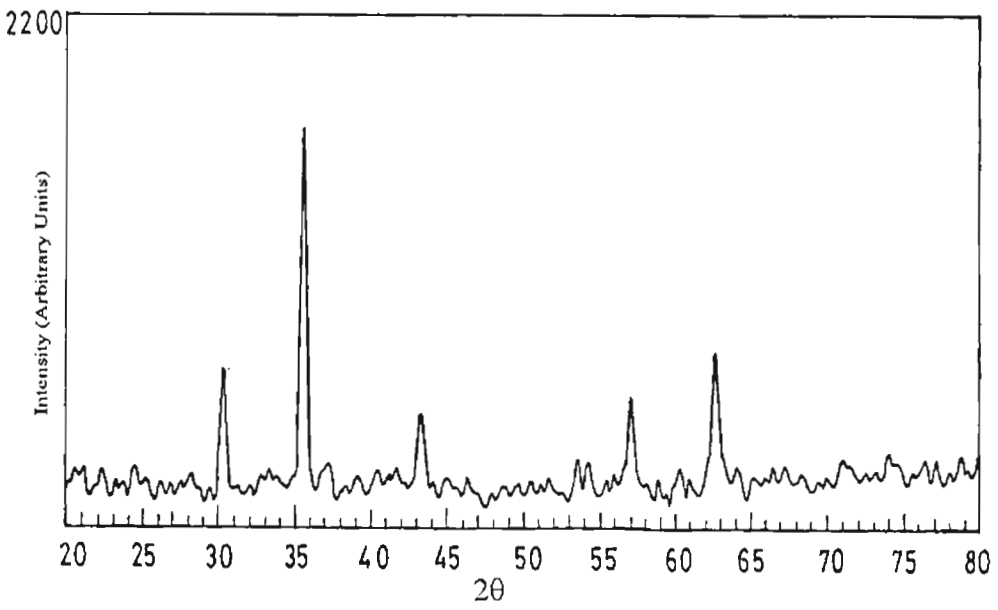


Fig.6.1c.XRD spectra of Nickel Zinc Ferrite ($\text{Ni}_{0.6}\text{Zn}_{0.4}\text{Fe}_2\text{O}_4$)

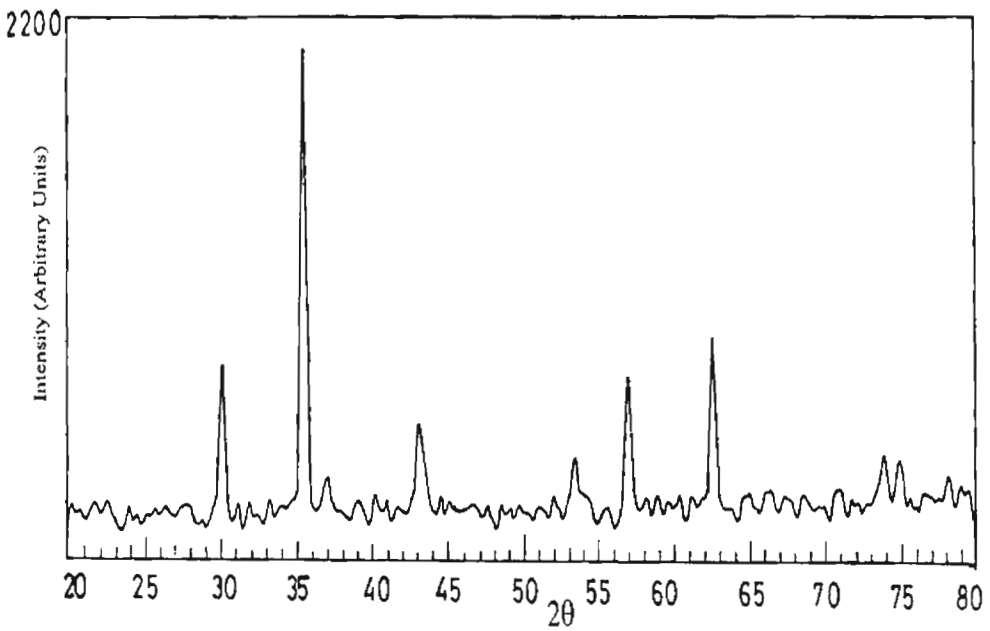


Fig.6.1d.XRD spectra of Nickel Zinc Ferrite ($\text{Ni}_{0.4}\text{Zn}_{0.6}\text{Fe}_2\text{O}_4$)

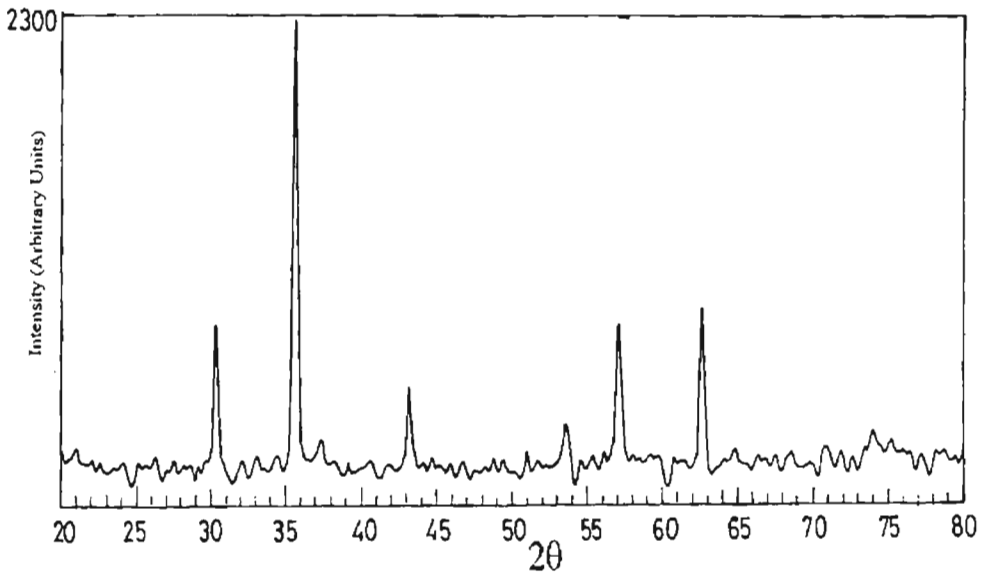


Fig.6.1e.XRD spectra of Nickel Zinc Ferrite ($\text{Ni}_{0.2}\text{Zn}_{0.8}\text{Fe}_2\text{O}_4$)

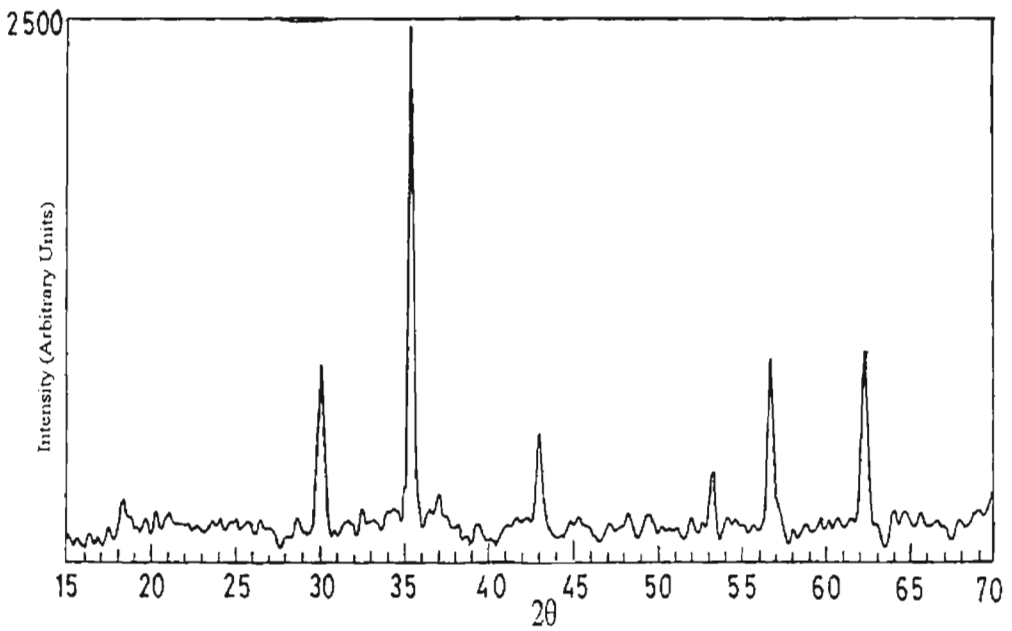


Fig.6.1f.XRD spectra of Zinc Ferrite (ZnFe_2O_4)

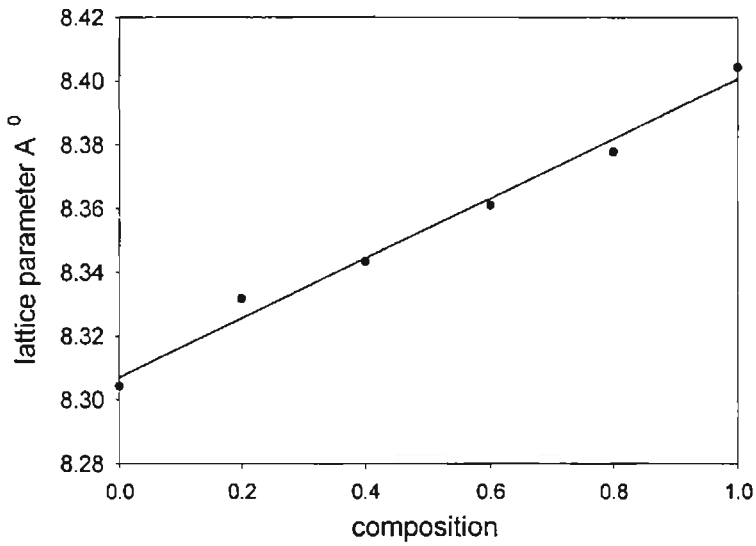


Figure 6.2 Variation of lattice parameter with composition

The average particle size was calculated from the x-ray spectra using the Debye Scherrer formula (cf Chapter 3). This was calculated for all compositions of Nickel zinc ferrites. The variation in particle size with composition is shown in Figure 6.3.

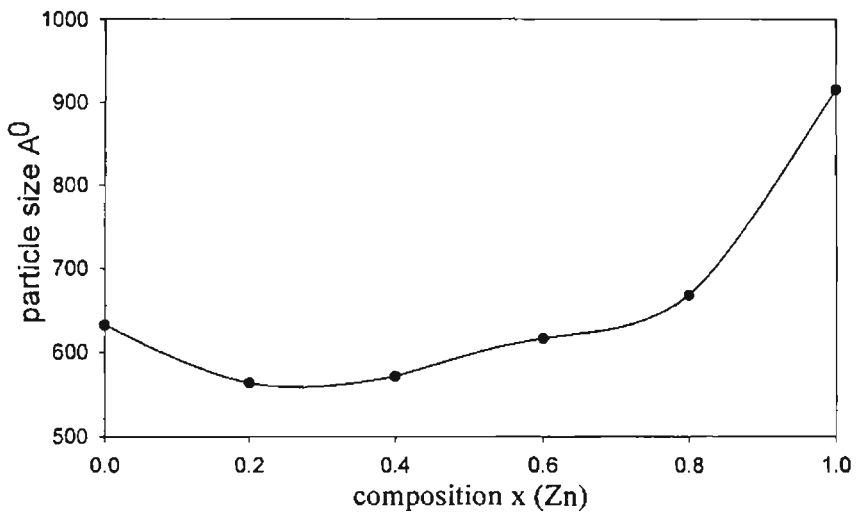


Figure 6.3 Variation of particle size with composition

The surface area for these powders were also evaluated using the relation $S = \frac{6000}{D\rho}$, where S is the surface area ρ is the density and D is the particle size. The variation of surface area with increasing zinc content is plotted and is shown in figure 6.4.

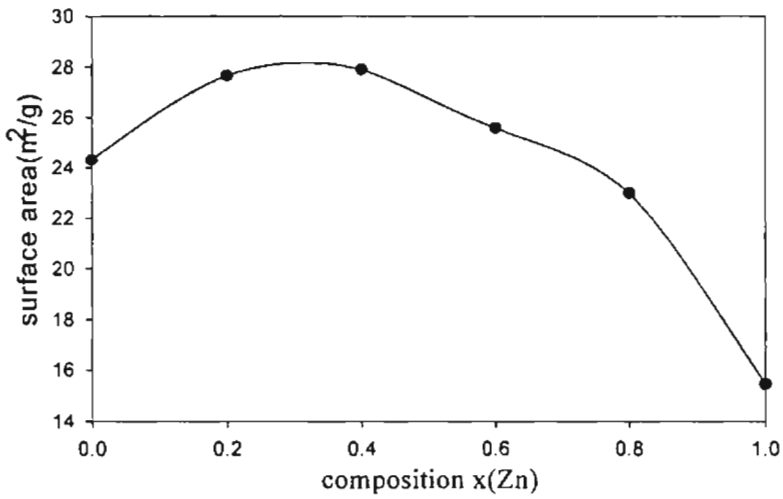


Figure 6.4. Variation of surface area with composition

The porosity of the ceramic samples were also calculated using the calculated values of apparent density and x-ray density values. The results are depicted in Figure 6.5

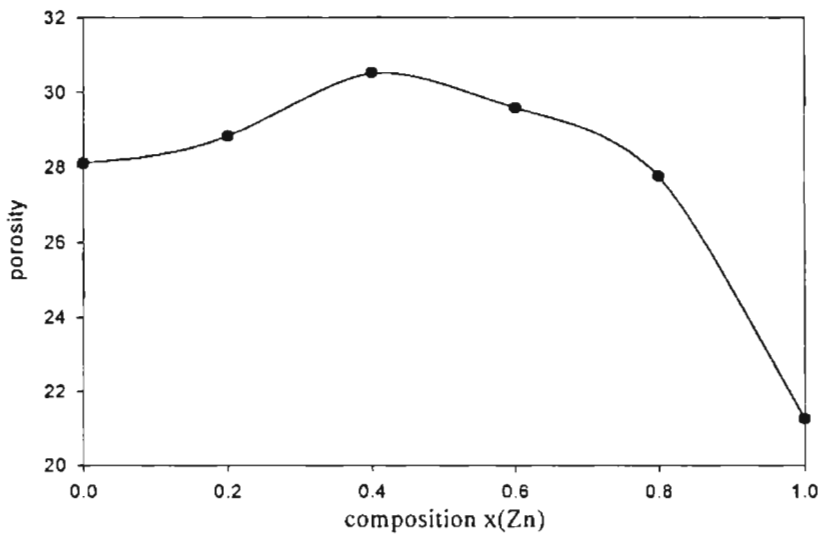


Fig.6.5 Variation of porosity with composition

The particle size (cf Fig.6.3) of the prepared ceramic sample is very much dependent on the preparative conditions namely the sintering temperature and other sintering conditions. The particle size first decreases for $x=0.2$ and thereafter it shows an increasing trend with increase in Zn content. As the particle size and surface area are inversely proportional as the particle size increase naturally surface area will decrease and vice-versa. This is evident from Fig. 6.4. Porosity of the ceramic samples increases first with the increase in zinc content reaches a maximum at $x=0.4$ and then it decreases with increase in zinc content.

6.3. Cure characteristics

The vulcanization characteristics of the prepared rubber compounds were determined by using the Gottfert elastograph as explained in chapter 3. Cure characteristics were plotted for all composites and from the cure characteristics parameters namely maximum torque, minimum torque, cure time etc were evaluated. A representative cure characteristic curve is shown in Fig. 6.6. For a typical rubber compound, characteristics namely scorch time and time for different percentages of cure are also available from this study. However for the present study we will concentrate on the cure parameters which have a bearing on the mechanical properties of the vulcanized compounds(129,130).

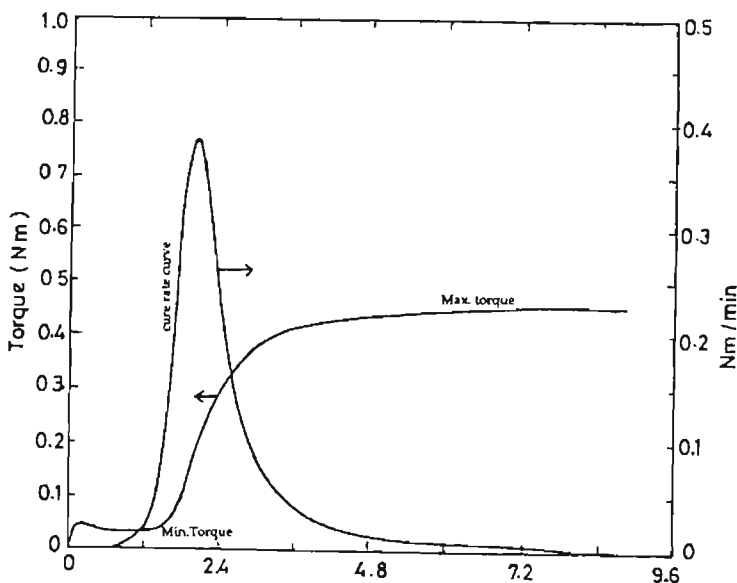


Fig6.6 Representative Cure Characteristic curve for RFC.

Graphs showing the variation of maximum torque and minimum torque with filler loading are also plotted and are shown in Fig 6.7 and Fig.6.8. It is seen that the maximum torque increases with loading for almost all compositions. Maximum torque gives an idea about the shear modulus of the fully vulcanized compound at the vulcanization temperature. It is evident from the graph (Fig 6.7) that the maximum torque increases with loading for all compositions of zinc in the NZF series.

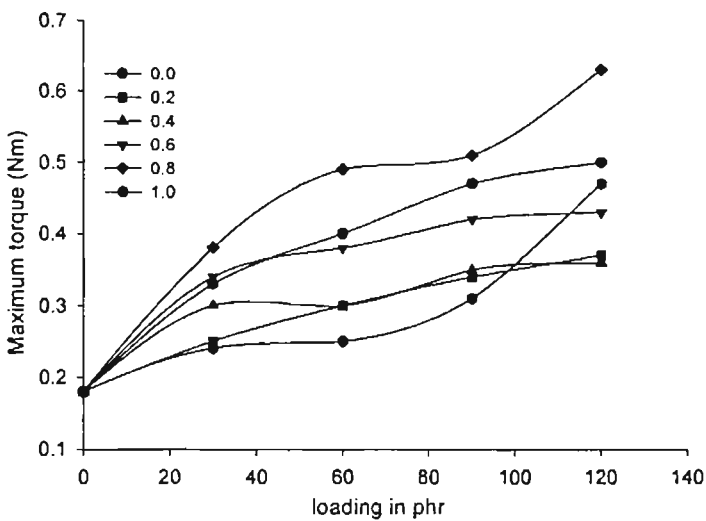


Fig. 6.7 Variation of maximum torque with loading

Minimum torque is an indirect measure of the viscosity of the compound. Or it can be generally treated as the measure of the stiffness of the unvulcanised test specimen taken at the lowest point of the curve. Minimum torque also shows an increasing trend for lower loading and saturates at higher loadings. The variation pattern is by and large the same for $x = 0.8$ and 0.2 . It may also be noted that the minimum torque values for $x = 0.0, 0.2$ and 1.0 coincides.

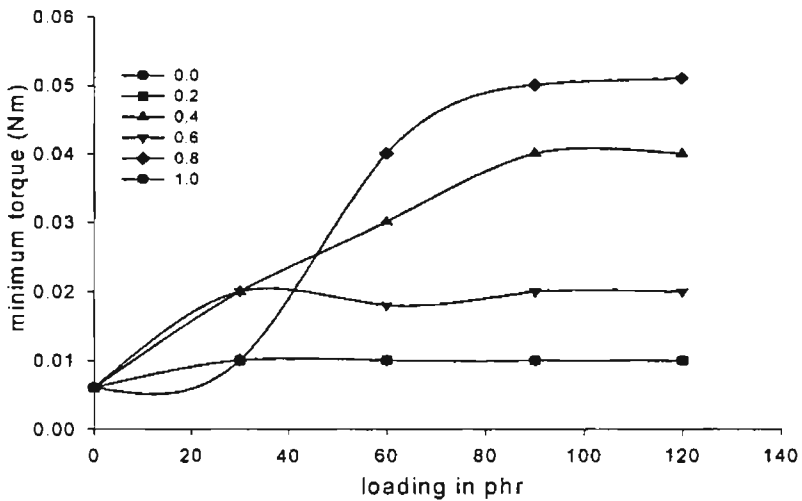


Fig 6.8 Variation of minimum torque with loading

Cure time is defined as the time required for optimum vulcanization of the samples. This is an important parameter as far as the vulcanization is concerned. Evaluation of cure time is a prerequisite for moulding the compounds. The variations in cure time for different loadings were studied for RFCs containing NZF in natural rubber matrix. The variations are shown in Fig 6.9.

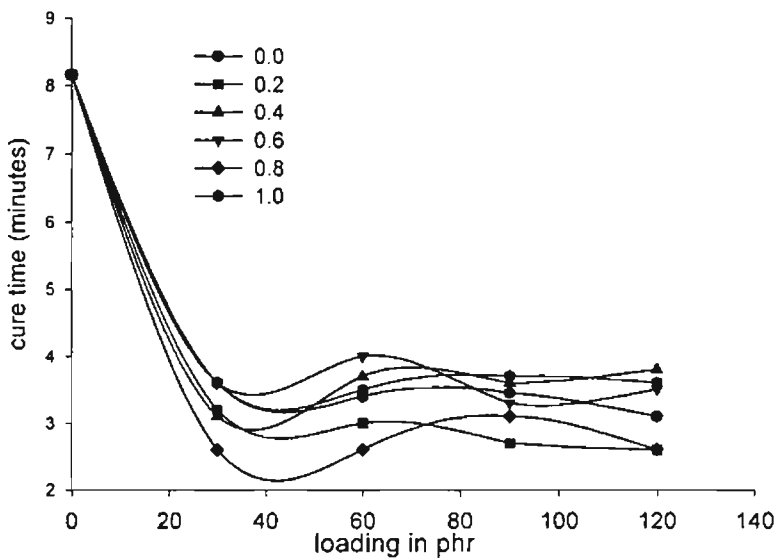


Fig.6.9 Variation of cure time with loading

From Fig. 6.9 it is seen that cure time sharply decreases for initial filler loadings (30 phr) and the change in cure time is only marginal for additional loadings of the filler. The above observations confirm that the filler addition does not affect the processability of the composites considerably. It is known from literature that the physico-chemical changes that occur during vulcanization is due to two factors namely, the specific surface activity and surface area(51,79).

Surface area variation with x (Fig. 6.4) does not resemble the variation pattern observed for cure time versus x for the corresponding composites. This means that there is an interplay of surface activity and surface area which acts in tandem to nullify the effect mutually. However earlier experiments conducted on RFCs containing hexagonal ferrites with and without carbon black indicates that the cure properties are dependent on particle size or surface area. That was for a different compound containing barium ferrite.

6.4. Magnetic measurements

6.4.1. Ceramic samples.

Magnetic measurements on the ceramic nickel zinc ferrites were carried out by using VSM as explained in the experimental chapter and the loop parameters namely saturation magnetisation (M_s) and coercivity (H_c) were evaluated. Fig 6.10 shows a representative hysteresis loop of the ceramic nickel zinc ferrite.

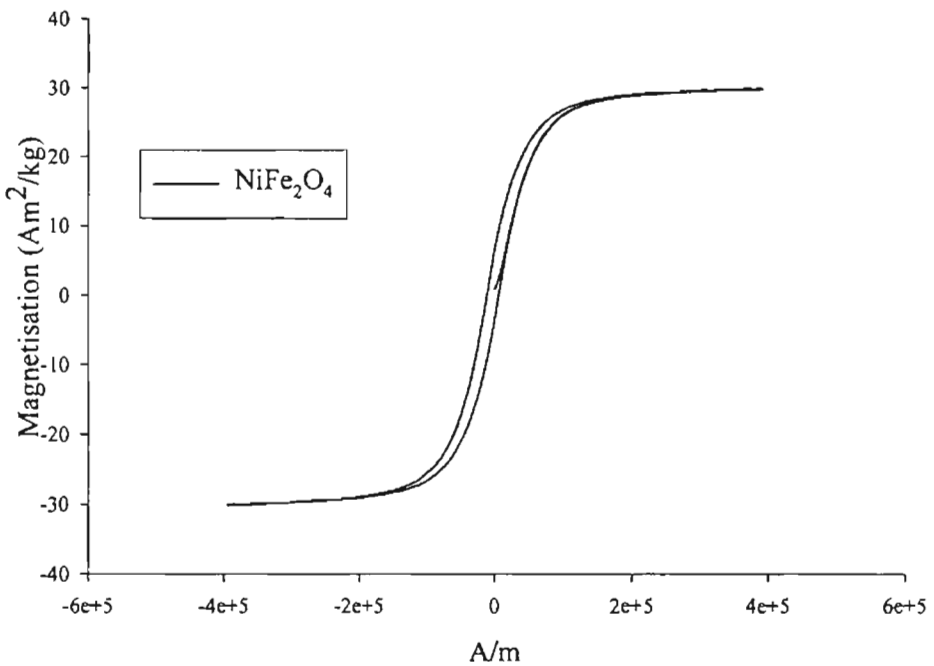


Fig-6.10 Representative hysteresis loop for ceramic NZF

The variation of M_s with composition are plotted and is shown in Fig.6.11.

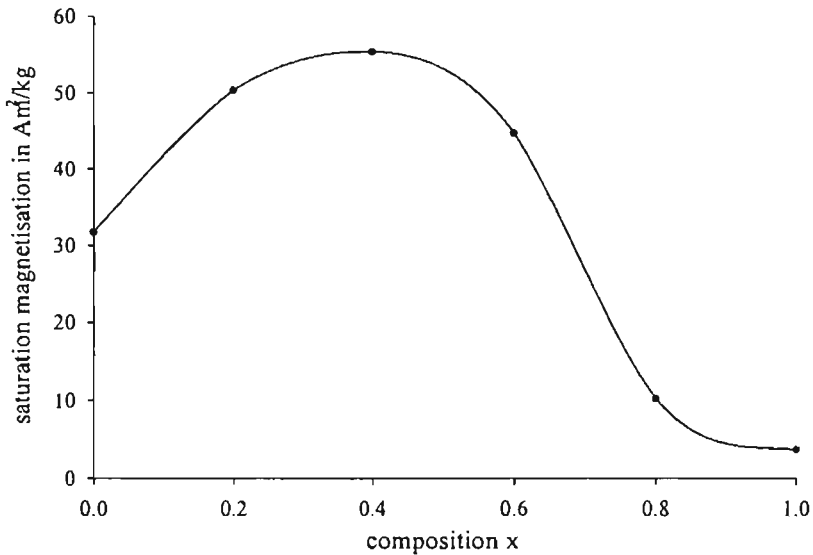


Fig 6.11. Variation of saturation magnetisation with composition for ceramic NZF

The variation of magnetisation (M_s) with composition is in accordance with those reported already by various researchers(1,10,73,131). The saturation magnetisation increases first with increase in zinc content and reaches a maximum at $x=0.4$ and then it decreases with increase in zinc content. This can be explained on the assumption that as the zinc content increases the relative number of ferric ions on the B site decreases and this will cause a reduction in A-B interaction. This increase of zinc concentration makes A-B interaction weaker and this makes B-B interactions to dominate. The ionic moments on the B site are no longer parallel to one another. This is called canting of spins and angles between them determine the moment of the B sublattice. This causes a reduction in B sublattice moment. The average canting angle among the B site spins were found out by various researchers by neutron diffraction studies(73,131-135). The strength and sign of the B-B exchange interactions relative to the A-B exchange interactions determine the canting angle.

This explanation is valid for systems conforming to the particles in the coarser regime. However recent experiments carried out by various researchers in the fine particle regime point to another possibility(136-139). Earlier it has been

assumed that zinc and nickel have definite site preferences depending on their site preference energies. Accordingly they occupy A and B sites respectively and that too exclusively. Experiments conducted on zinc ferrite have revealed that Zn occupies A sites instead of their exclusive preference for B sites. Experiments were conducted in the laboratory by Sindhu et al (78) on fine particle Nickel zinc series and initial indications are that the possibility of Ni occupying A site cannot be ruled out. However confirmatory evidence has to be sought by neutron scattering experiments. This is to be carried out later.

The variation of coercivity is also plotted Fig 6.12 for ceramic nickel zinc ferrites. It is well known that the coercivity is dependent on different parameters namely sintering conditions and particle size (1,8). From the figure it may be noted that the as the zinc content increases the coercivity decreases and for $x=1.0$ it increases sharply.

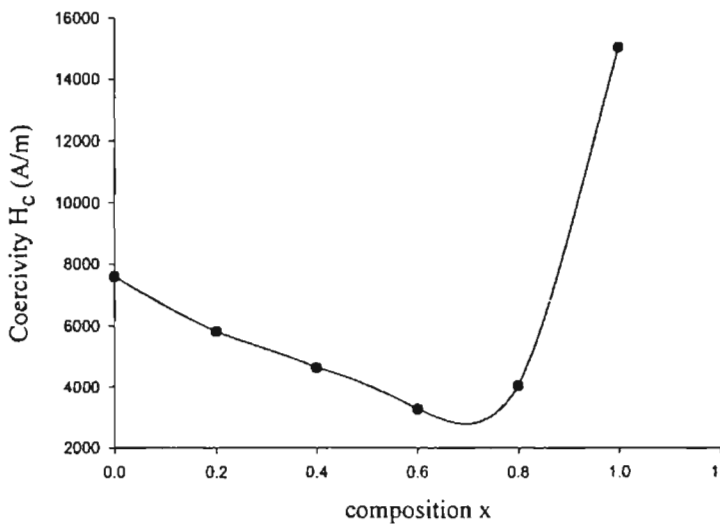


Fig.6.12 Variation of coercivity with composition for ceramic NZF

6.4.2. Composite Samples

The hysteresis loops for composite samples were also recorded. Fig. 6.13 shows the representative hysteresis loops for RFC.

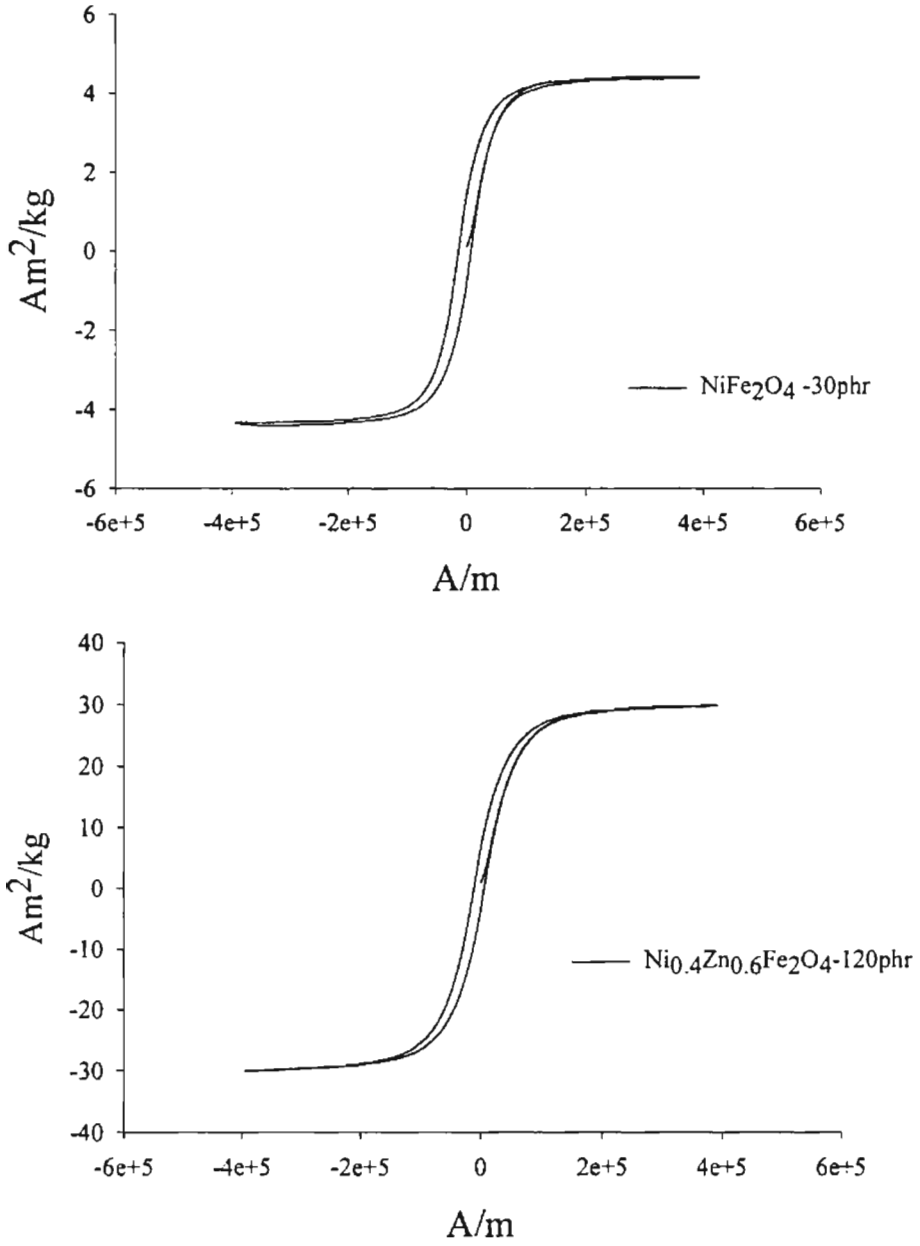


Fig.6.13 Representative hysteresis loops for RFC

The variation of saturation magnetisation with composition for the rubber ferrite composite is given in Fig. 6.14.

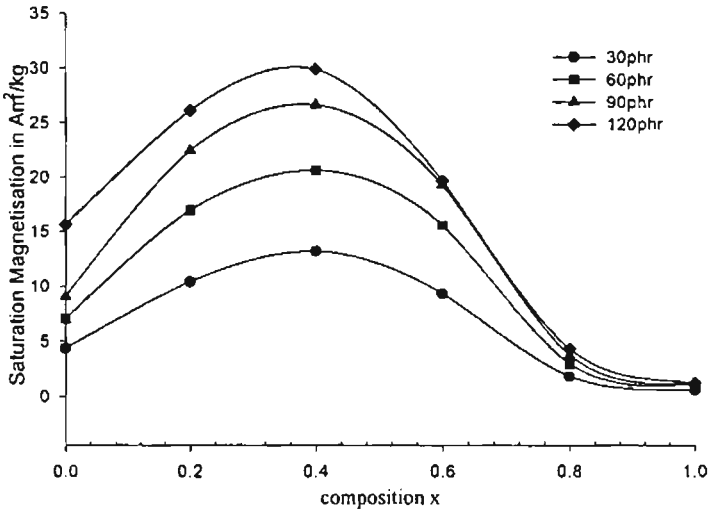


Fig.6.14 variation of saturation magnetisation with composition for RFC

From the figures 6.11 and 6.14, it can be seen that the behaviour is same for both ceramic and RFC.

The variation of saturation magnetization of the composites with the loading of the filler is also studied. Fig 6.15 shows the variation of magnetization with loading. The magnetization shows a steady increase with loading.

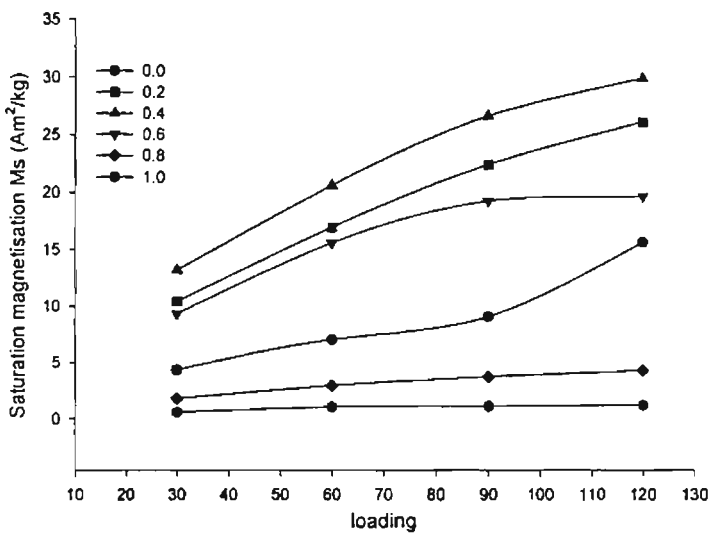


Fig 6.15. Variation of saturation magnetisation with loading

The variation of coercivity with composition for RFCs are shown in Fig. 6.16. It shows almost similar behaviour as that of the ceramic component. The slight variations in coercivity of ceramic and composites may be attributed to the small particle size changes that can occur during compounding/milling. However this variation is negligible.

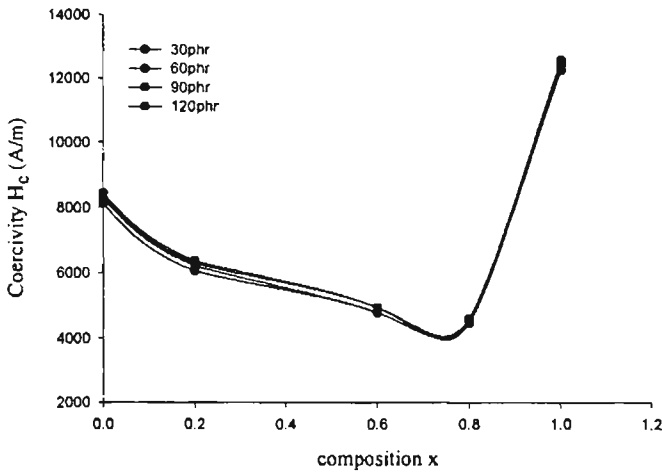


Fig.6.16 Variation of Coercivity with composition for RFC

The similarity between the ceramic and composite samples rules out the possibility of any filler matrix interaction at least at the macroscopic level.

6.4.3. Tailoring magnetic properties(saturation magnetisation-Ms)

Attempts are also made to tailor the magnetic properties of the composites from the known values of the saturation magnetisation (Ms) of the ceramic fillers. If the Ms values of the ceramic fillers are known a simple mixture equation of the general form (equation 6.1) involving the weight fractions of the filler can be employed to estimate the Ms of the composite samples.

$$M_{rfc} = W_1M_1 + W_2M_2 \quad \dots\dots\dots (6.1)$$

where **W₁** is the weight fraction of filler, **M₁** is the magnetisation of the filler, **W₂** is the weight fraction of matrix, **M₂** is the magnetisation of the matrix.

Since the matrix namely NR is nonmagnetic this equation can be reduced to the following form

$$M_{rfc} = W_1 M_1 \dots\dots\dots (6.2)$$

The Ms values were calculated using equation 6.2 and the measured and calculated values of Ms are shown in Fig. 6.17.

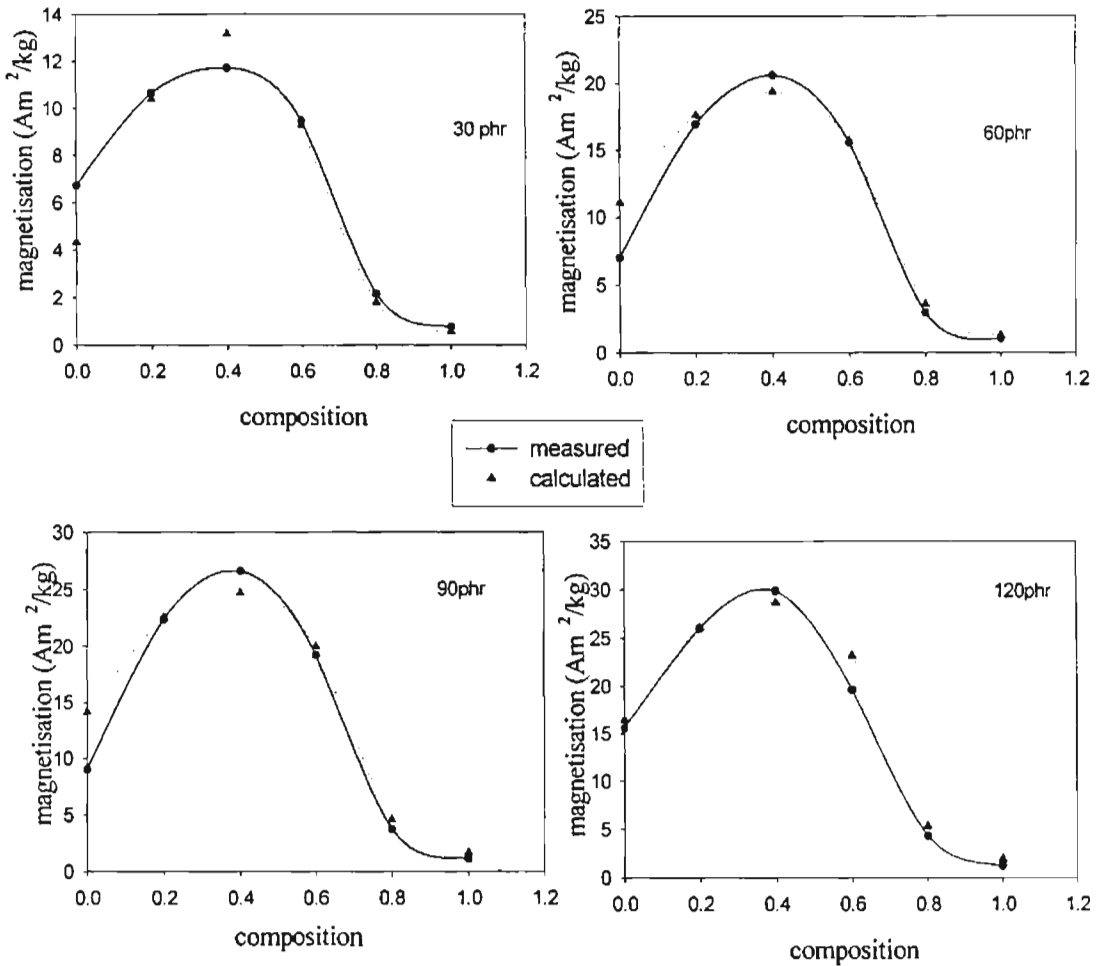


Fig 6.17. Measured and Calculated values of Ms (equation 6.2)

This mixture equation requires the magnetization corresponding to all x values of the filler in order to predetermine the saturation magnetization (Ms) of the corresponding composites. This is one of the drawbacks of the simple mixture equation. Here one needs to know the Ms of the ceramic component of the particular 'x' to be loaded into the filler.

However, an inspection of the behaviour of Ms vs x reveals that it follows a Gaussian profile and can be represented by a general formula

$$M = A \exp\left(-0.5\left(\frac{x-x_0}{b}\right)^2\right) \dots\dots\dots(6.3)$$

This was first formulated by fitting the experimental data of Ms for different x and for different loadings. This was then modified to the final form (equation 6.4) by giving appropriate meanings to the coefficients obtained. The final equation is of the form

$$M_{rfc} = (1 + 0.2x)M_{cermax}W_2 \exp\left(-0.5\left(\frac{x-x_0}{0.26}\right)^2\right) \dots\dots\dots(6.4)$$

where M_{cermax} is the magnetisation corresponding to maximum Ms of the ceramic filler.

x is the composition

x_0 is the composition corresponding to the maximum Ms of the filler.

The validity of the modified equation (ie, equation 6.4) was checked by comparing the calculated and measured values of Ms for different loading and compositions in RFC. The variation of calculated and measured values of Ms with composition is shown in Fig.6.18. From the graph it can be seen that they are in excellent agreement. The formulated equation can also be applied to other systems with different matrix and fillers. This equation requires only the maximum Ms value of the filler and the corresponding composition. As far as a series belonging to a filler representing a series similar to $Ni_{1-x}Zn_xFe_2O_4$ or $Mn_{1-x}Zn_xFe_2O_4$ is concerned the saturation magnetisation Ms is generally determined by the Neels two sublattice model and it is given by the difference between M_B and M_A where M_A and M_B are the total magnetic moment of the A (tetrahedral) sublattice and B (octahedral) sublattice respectively. The total magnetisation (Ms) of the compound

is determined by the formula $Ms = \frac{\mu \times mol.wt.}{5585}$. Generally M_B and M_A are the

total spin only magnetic moment of the cations, It is easier to predict the Ms of the filler theoretically too. This is one of the advantage of choosing the nickel zinc ferrite series as the filler in making RFCs apart from their superior dielectric properties. It may also be noted that this equation can be modified for predicting

the saturation magnetization of ceramic samples in systems showing similar behaviour with composition as well. Since the general equation

$$M = A \exp\left(-0.5\left(\frac{x-x_0}{b}\right)^2\right)$$
 is valid for the ceramic filler series $\text{Ni}_{1-x}\text{Zn}_x\text{Fe}_2\text{O}_4$, if x_0 is known or can be calculated say by employing Neels tow sublattice model, the predetermination of M_s is made much simpler.

The formulated equation requires only the magnetisation M_s of that particular x which shows maximum magnetisation. Thus it is clear that RFCs with appropriate M_s and H_c can be tailored by a judicious choice of the filler belonging to a particular series. The weight fraction can be increased to acquire the required M_s . For applications where H_c is a determining factor, mixed ferrites containing cobalt or surface modified with Co is an excellent filler candidate for making RFCs with large coercivity. Appropriate heat-treated magnetic fillers also enhance the coercivity of fillers.

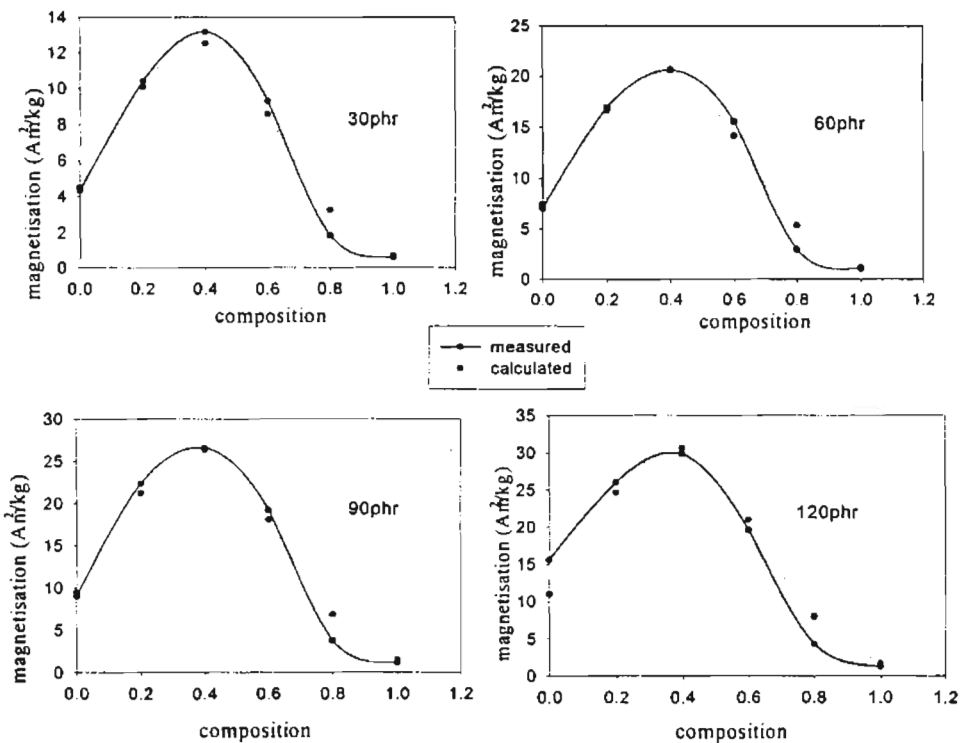


Fig.6.18 Measured and calculated values of magnetisation (equation 6.4)

By synthesizing RFC, we have the unique advantage of modifying M_s and H_c according to the requirement. It may also be noted that the desired M_s can be imparted by appropriate choice of composition and loading. The H_c of the composite will be that of the ceramic component without much change. However, it is to be noted that the H_c is dependent on various parameters like particle size and heat treatment. These results indicate that the magnetic property can be suitably modified by the appropriate loading of the filler with a particular composition. The calculated values tally well with the measured values of the saturation magnetization which indicate that it is possible to tailor materials with a definite magnetization value by appropriate loading of the proper filler with an appropriate composition(x) in a NR matrix.

This formulated equation is also found to be valid for similar systems. Anantharaman et al (140) have confirmed this finding on RFCs prepared with nickel zinc ferrite in a butyl rubber matrix and manganese zinc ferrite in natural rubber matrix. These investigations reveal that the required magnetic properties to these matrices can be imparted to the matrix without compromising on the processability, flexibility and mechanical properties.

6.5. Conclusion

Rubber ferrite composites (RFCs) containing $Ni_{1-x}Zn_xFe_2O_4$ in natural rubber matrix have been prepared. The cure characteristics reveal that the processability and flexibility of the matrix is not much affected even upto a maximum loading of 120 phr of the filler in our set of experiments. It also indicate that the percolation threshold is not yet reached for a maximum loading of 120phr of the filler in the present study. Magnetic parameters of the ceramic as well as RFCs were studied. The anomalous magnetic behaviour of nickel zinc ferrite in the fine particle regime points to the fact that the assumed cation distribution is quite different in the fine particle regime and nickel could be occupying A site too rather than the exclusive B site. This observation warrants further advanced studies by neutron scattering. Also studies pertaining to the occurrence of surface spins in NZF series also needs additional experiments by other techniques. A general equation for predicting the saturation magnetization (M_s) of the ceramic

as well as the composite samples is formulated. As far as the prediction of σ_s of RFCs is concerned the general equation of the form

$$\sigma_{rfc} = (1 + 0.2x) \sigma_{cer. max.} \cdot W_2 \cdot \exp\left[-0.5\left(\frac{x - x_0}{b}\right)^2\right] \text{ where } b \approx 0.26 \text{ is suitable.}$$

It is to be noted that the calculation requires only the maximum magnetisation value corresponding to the composition x_0 . It is found that the measured and calculated values are in very good agreement. The coercivity variation with loading is found to be minimal. This indirectly shows that there is not much matrix filler interaction atleast at the macroscopic level. The formulated equation will aid in predicting the properties and tailoring materials for various applications. This method of preparation can be adopted for preparing RFCs for microwave applications.

CHAPTER 7

DIELECTRIC AND MECHANICAL PROPERTIES OF RUBBER FERRITE COMPOSITES

7.1. Introduction.

Composite magnetic materials have the unique advantage of being modified and tailored for various applications. Rubber ferrite composites prepared by incorporating ferrites in rubber matrixes have the advantage of easy mouldability and flexibility. Generally composites are designed to exploit the best properties of the constituents to produce a material that surpasses the performance of the individual components. The uses to which composites can be put are as limitless as the types of composites themselves. The chemical and physical properties of composites can be tailored to meet the needs of each individual application. RFCs give advantage of making use of the best of the filler and the matrix and thus enables to have RFCs with predetermined dielectric properties with the required mechanical properties. Dielectric measurements on materials provide initial design parameters for many electronic applications (141-148).

Dielectric properties in polycrystalline materials are influenced by factors like preparative conditions, cation distribution, grain size, the ratio of $\text{Fe}^{3+}/\text{Fe}^{2+}$ ions, ac conductivity and sintering temperature(148,149). The dependence of these factors on the dielectric properties of ceramic fillers will also have a profound influence on the overall physical properties of the composites incorporated with the filler (36). The evaluation of dielectric properties of the filler as well as the composites assumes significance in understanding the physical properties of these composites. RFCs containing Nickel Zinc ferrite ($\text{Ni}_{1-x}\text{Zn}_x\text{Fe}_2\text{O}_4$) in a natural rubber matrix have been prepared and their mechanical and dielectric properties have been evaluated. The ceramic ferrite samples were prepared by conventional solid state reactions. Their incorporation in natural rubber matrix is achieved according to a specific recipe. The

preparation details are cited in Chapter 3. The variation of dielectric constant of the ceramic as well as RFCs with frequency, composition, loading and temperature were studied and the results are correlated. These studies are carried out for different temperatures from room temperature to 120⁰C for all samples. Appropriate mixture equations are also formulated to predict the dielectric constant of the composites from the available dielectric constant of its constituents. The validity of these equations have been checked with the observed values of the dielectric constants.

The mechanical properties are one of the most important properties of plastic materials because all applications involve some degree of mechanical loading. A tensile test is a measurement of the ability of a material to withstand the forces that tend to pull it apart and to determine to what extent the material stretches before breaking. Different types of plastic materials are often compared on the basis of their tensile strength, elongation and modulus. Hence the evaluation of these properties also assumes significance in making devices based on RFCs. The mechanical properties namely tensile strength, elongation at break and 100% modulus of the prepared samples are also evaluated. Hardness of the prepared composite samples are also evaluated using a Shore A hardness tester.(79-85) The findings of the dielectric measurements and the mechanical properties on RFCs are explained in this chapter.

7.2. Dielectric Measurements

7.2.1. Ceramic samples

a) Frequency dependence

In ferrites, very high dielectric constant, at very low frequencies, have been reported by various researchers(50,149-153). The reported values for dielectric constant of nickel zinc ferrites show that the dielectric constant fall from a DC value of several thousands to the normal values of the order of tens for a frequency of around 100kHz. These results have been explained by Koops phenomenological theory and Maxwell-Wagner interfacial polarisation(50,154). These theories give phenomenological picture of the dispersion process in ferrites. It is assumed that the dielectric structure of ferrites is formed of two layers, namely, the well conducting

grains and poorly conducting grain boundaries. At very low frequencies the oxidic grain boundaries are more active and this contributes to the very high dielectric constant at low frequencies. In our set of experiments, the measurements were carried out in the range 100kHz to 8MHz and only very low values for the dielectric constant were observed. Frequency dependence of the dielectric constant for all ceramic samples ($x=0$ to 1 in step of 0.2) are shown in Fig.7.1. A decrease in dielectric constant with increase of frequency is observed in our case also. This decrease is nominal at lower frequencies of the present measurement (ie upto 2MHz) and larger at higher frequencies. The dielectric constant measurements are made upto a maximum frequency of 8 MHz. The variation pattern remains the same for all compositions.

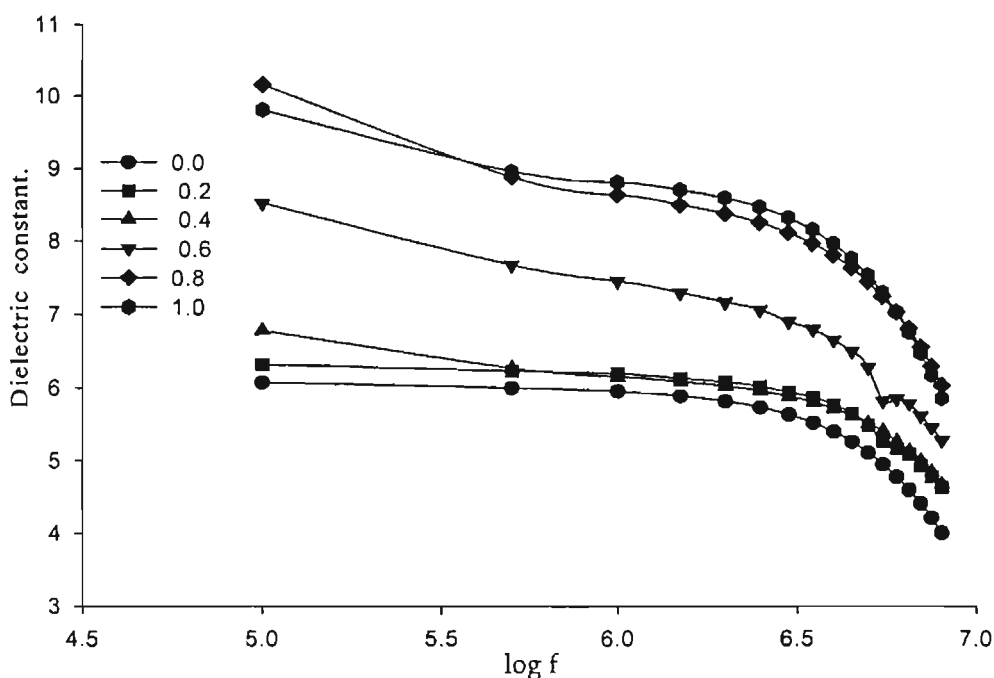


Fig.7.1 Variation of Dielectric Constant with frequency (ceramic NZF)

This frequency dependence of dielectric constant can also be explained in accordance with the Maxwell-Wagner model. It is reported that the time required for electronic or ionic polarization to set in is very small (10^{-12} to 10^{-15} s), compared with the time of the voltage sign change even for the highest frequency of the signal(155). Thus it can be said that the contribution of ionic and electronic polarization to the

dielectric dispersion is small and at lower frequencies the decrease in dielectric constant is nominal. But in the case of dipole polarization, as the frequency of the applied voltage changes the value of the dielectric constant at first remains unaltered and there after shows a decrease with increase in frequency. This is because at higher frequencies the polarization fails to settle itself completely in one half period, resulting in a decreased dielectric constant. It can be said that the polarization lags behind the applied voltage there by decreasing the dielectric constant.

Saxena et al(156) have studied the frequency dispersion of dielectric constant for lithium titanium ferrites, both experimentally and theoretically using the relation given by Habery and Wijn(157). They have employed a relation of the form

$$\varepsilon(\omega, T) = \left[(1+x) \frac{(\varepsilon_{hf} x(x\sigma_{lf}^2 + \sigma_{hf}^2) + \omega^2 \varepsilon_0^2 \varepsilon_{hf}^3 (1+x))}{(x^2(\sigma_{lf} + \sigma_{hf})^2 + \omega^2 \varepsilon_0^2 \varepsilon_{hf}^2 (1+x)^2)} \right] \dots\dots\dots(7.1)$$

where $x=d_1/d$. d_1 and d are the thickness of the surrounding layer and bulk ferrite grain respectively.

This equation involves the thickness of the grains and the grain boundaries. However no morphological studies were carried out in the present system and hence it is impossible to calculate the dielectric constant using this relation. It was observed that the variation pattern of dielectric constant with frequency in all our compositions resembles the theoretical predictions of saxena et al. The dielectric dispersion was fitted in to a general equation of the form

$$\varepsilon = \frac{\varepsilon_{lf} - b \log f}{1 - c \log f} \dots\dots\dots(7.2)$$

and it was found that the equation fits very well with the observed values. Also it was observed that the constant “ ε_{lf} ” corresponds to the low frequency value of the dielectric constant. This general fit was found to be true for all systems under the present study. The constants b and c are related to the grain size or grain boundary of the ferrite sample. This needs to be confirmed by further investigations. Figure 7.2 shows the representative graph showing the fitted curve and experimental curve for the dielectric dispersion.

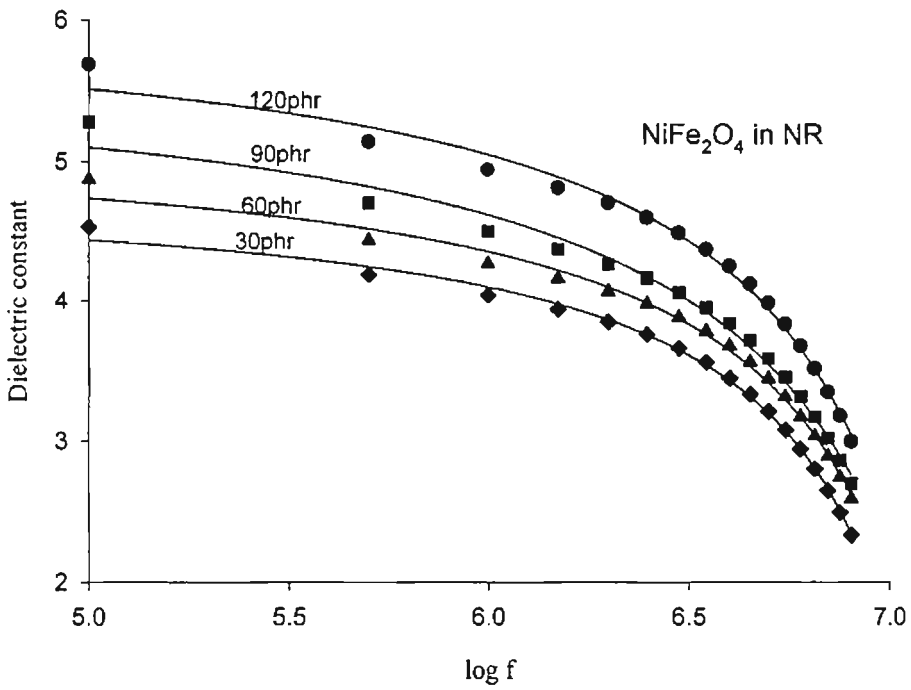
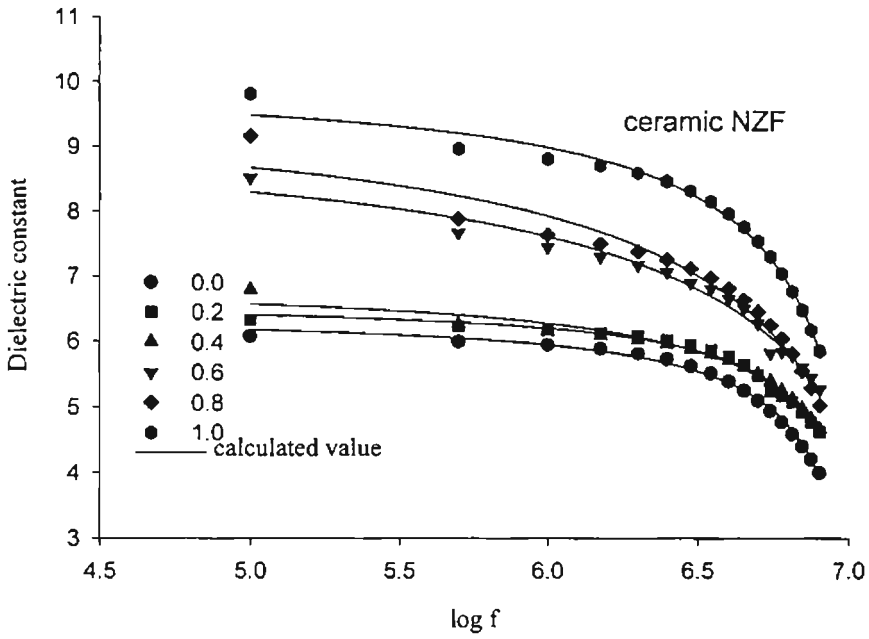


Fig.7.2 Fitted curves for the variation of dielectric constant with log f

b) Compositional dependence:

The variation of dielectric constant with composition (zinc content) is shown in Fig.7.3. It can be seen that the dielectric constant increases with increase of composition. The variation pattern remains the same for all frequencies. It is well known that the mechanism of dielectric polarisation in ferrites is analogous to the conduction mechanism. The conduction mechanism in ferrites can be expressed in terms of electron hopping between ferrous and ferric ions on the octahedral site for n-type semiconductor ferrites and in terms of hole hopping for p-type ferrites (Verwey type of conduction)(50,158). The extra electron on a ferrous ion requires little energy to move to a similarly situated adjacent ferric ion. The valence states of the ions are interchanged. Under the influence of an electric field these electrons can be considered to constitute the conduction current, jumping or hopping from one iron ion to the next. Similarly there is hole hopping or jumping in Nickel ions. Various researchers have reported that the hole hopping between Ni^{2+} and Ni^{3+} on B site is another possibility. This can also contribute to the electric conduction in ferrites. In $\text{Ni}_{1-x}\text{Zn}_x\text{Fe}_2\text{O}_4$ at $x=0.0$ the hole hopping ($\text{Ni}^{2+} \leftrightarrow \text{Ni}^{3+}$) at B site is the prominent mechanism. When ferrites containing Ni is cooled from an elevated temperature to room temperature Ni^{3+} ions are produced which together with the Ni^{2+} ions constitutes a hopping pair (159). As the zinc content increases Ni content at the B site decreases and hence hole hopping decreases. But at the same time the Fe content at the B site increases which inturn will increase the conductivity due to electron hopping ($\text{Fe}^{3+} \leftrightarrow \text{Fe}^{2+}$). It is also a known fact that in NZF systems the ($\text{Fe}^{3+} \leftrightarrow \text{Fe}^{2+}$) conversion is relatively less upto 0.4 and hence a slight decrease in dielectric constant at $x=0.4$ is observed. Beyond $x=0.4$ the electron hopping is more prominent and as zinc content increases electron hopping increases due to increased number of Fe^{3+} and Fe^{2+} ions on B site. At higher sintering temperatures the evaporation of zinc will contribute some Fe^{2+} ions to the B site and this will localize the hopping electrons and will decrease the $\text{Fe}^{3+}/\text{Fe}^{2+}$ ratio which inturn will result in a decrease in dielectric constant. (159-165).

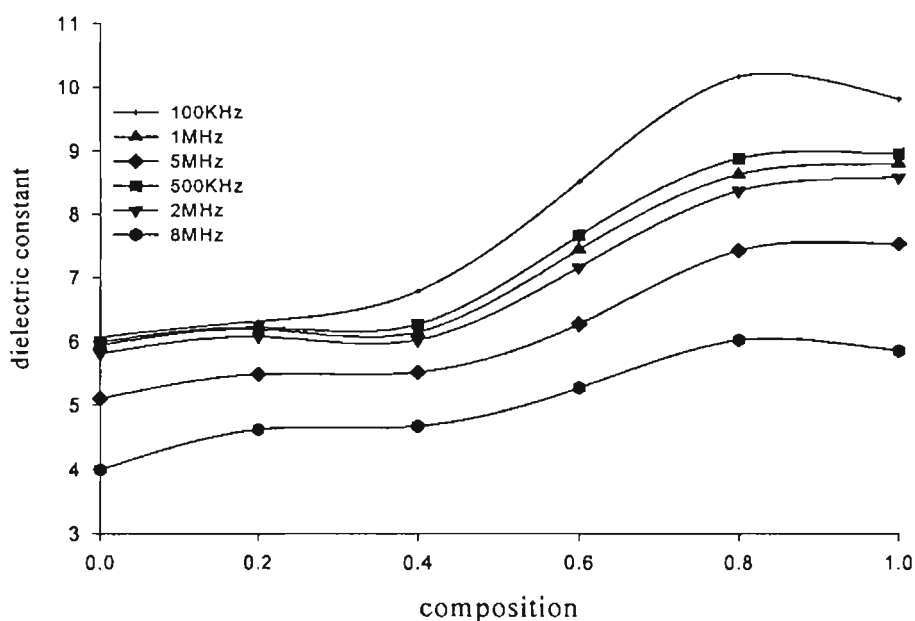


Fig.7.3 Variation of Dielectric constant with composition (ceramic NZF)

c) Temperature dependence:

The temperature dependence of the dielectric constant for the ceramic samples were also studied. Variations of relative permittivity in the temperature range 303K – 393K were noted. The behaviour of dielectric constant with temperature for ceramic NZF is shown in Fig.7.4. It was observed that the dielectric constant of ceramic samples increases with increase of temperature. The high dielectric constants at low frequencies found at high temperature may be explained by the presence of permanent dipole moments indicating a small effective charge separation. Such a small separation must be due to asymmetry in the fields experienced by either oxygen or metallic ions. In most cases, the atoms or molecules in the samples cannot orient themselves at low temperature region. When temperature rises the orientation of these dipoles is facilitated and this increases the dielectric polarization. But at very high temperature the chaotic thermal oscillations of molecules are intensified and the degree of orderliness of their orientation is diminished and thus the permittivity passes through a maximum value. In the present study the maximum temperature of measurement was only 393K and hence no decrease in dielectric constant was observed. Transitions are observed in NZF above 400°C and the here in these set of

experiments the temperature was not raised because NR degrades at higher temperatures. The variation of dielectric constant with temperature at low frequencies (100kHz) is much more pronounced than at higher frequencies. Variation pattern at all frequencies seems to be obeying the relation $y = y_0 + A \exp(BT)$ where A and B are two constants. For all compositions the same behaviour is observed. At higher frequencies temperature has little effect on the dielectric constant. (50,155,166)

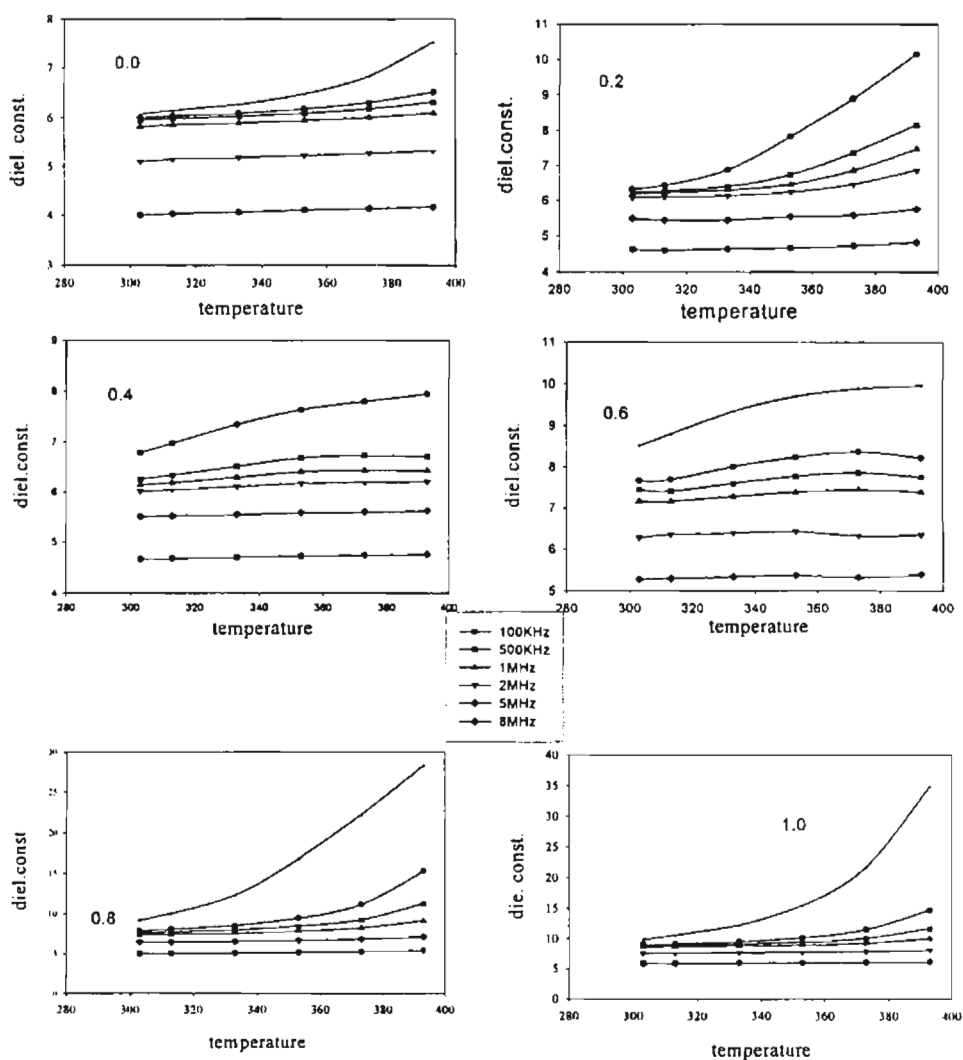


Fig.7.4 Variation of dielectric constant with temperature (ceramic NZF)

7.2.2. Dielectric properties of Blank Natural rubber

The dielectric constant at different temperatures for blank NR was also evaluated. The dielectric constant of unvulcanised natural rubber is reported to be in the range 2.6 to 3.0. A dielectric constant of 3.04 was obtained for blank NR. A decrease in dielectric constant with increase in temperature was observed for natural rubber. The variation pattern is shown in Fig.7.5. This is because as the temperature increases the polymer density will be reduced which in turn will cause a decrease in dielectric constant(166). In non-polar dielectrics due to thermal expansion of matter the ratio of number of molecules to the effective length of the dielectric diminishes with increase of temperature.

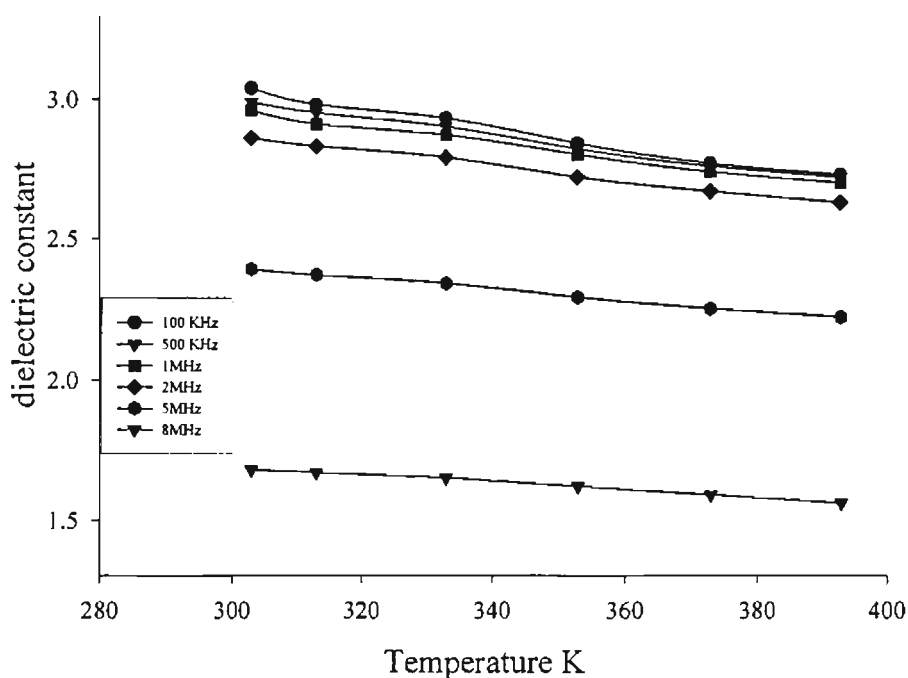


Fig 7.5. Variation of dielectric constant with temperature for Blank NR

7.2.3. Dielectric properties of Rubber ferrite composites

a) Frequency dependence of dielectric constant of RFC

The dielectric behaviour of RFC containing NR with change in frequency is depicted in Fig.7.6. This shows almost similar behaviour as that of the ceramic component in the matrix. The absolute values of the dielectric constant of the composites are found to be greater than that of the blank NR, but less than that of the ceramic component. Maximum dielectric constant is observed for the maximum loading of 120phr.

Thus it is clear that the dielectric properties are getting modified by addition of the filler and the required dielectric constant can be achieved by varying the loading of the filler.

b) Compositional dependence of dielectric constant of RFC

The variation pattern of dielectric constant with composition for rubber ferrite samples is shown in Fig.7.7. It was found that the variation is almost the same as that of the ceramic samples, the pattern remains the same for all loadings. From the graph it may be noted that the dielectric constant increases with increase in zinc content except for a small decrease at $x=0.4$. At lower loadings of the filler the behaviour resembles that of the matrix and at higher loadings it is predominantly dictated by the filler dielectric properties. These results suggest that the dielectric properties of the rubber matrix can be suitably modified by an appropriate choice of the composition and with the required loading of the filler.

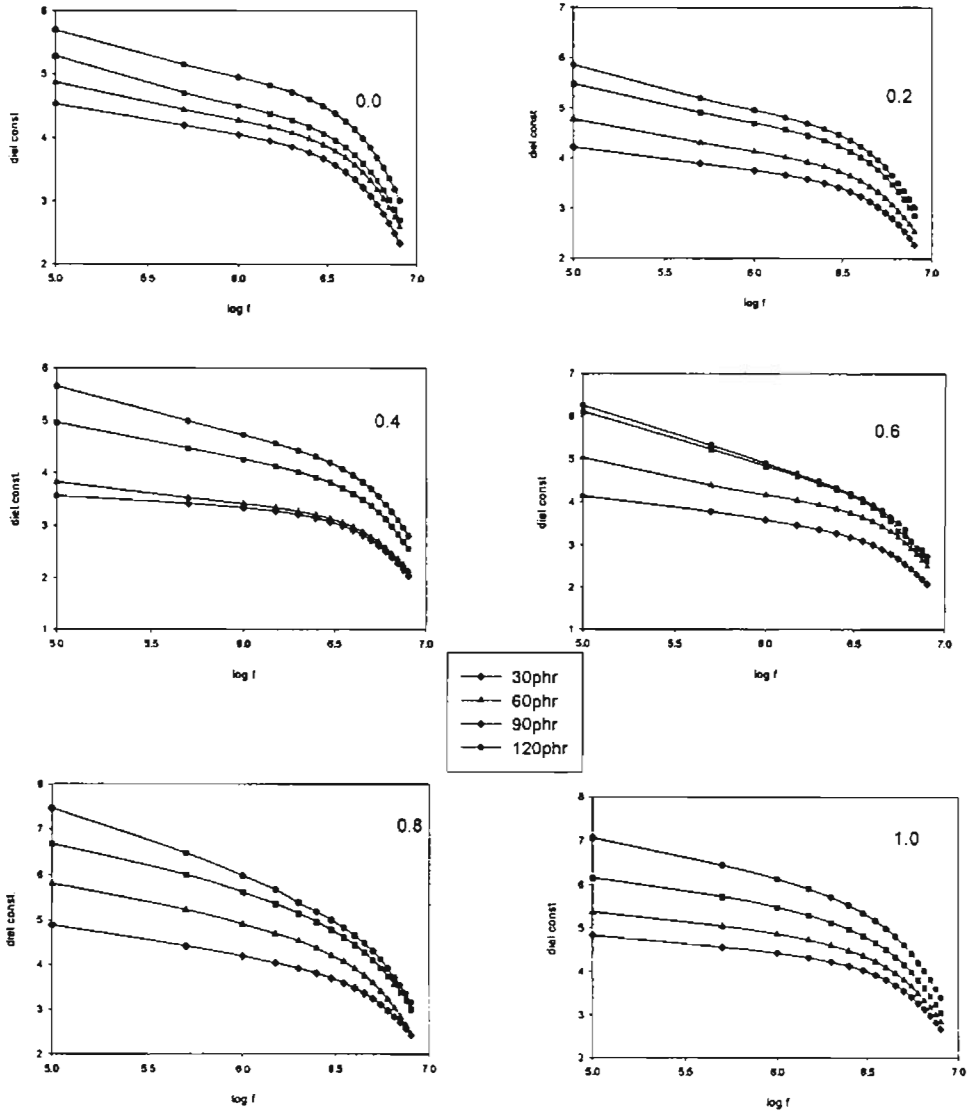


Fig. 7.6 Variation of dielectric constant with $\log f$ for RFC

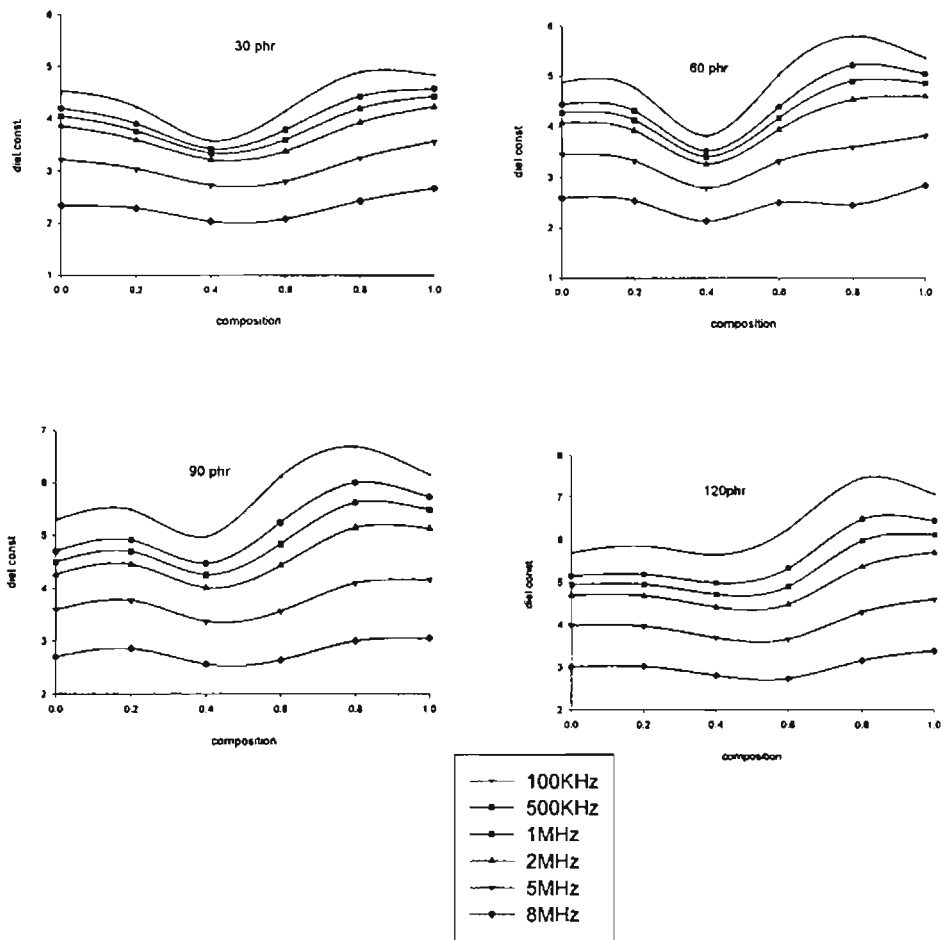


Fig. 7.7 Variation of dielectric constant with composition for RFC

c) Temperature dependence

The dielectric constant of rubber ferrite composites increases with increase of temperature. The variation is depicted graphically in Fig.7.8 (representative graphs). The increase in dielectric constant with increase in temperature is not so prominent as in the case of ceramic samples. It is also observed that the variation of dielectric constant with temperature is more at higher loadings of the filler.

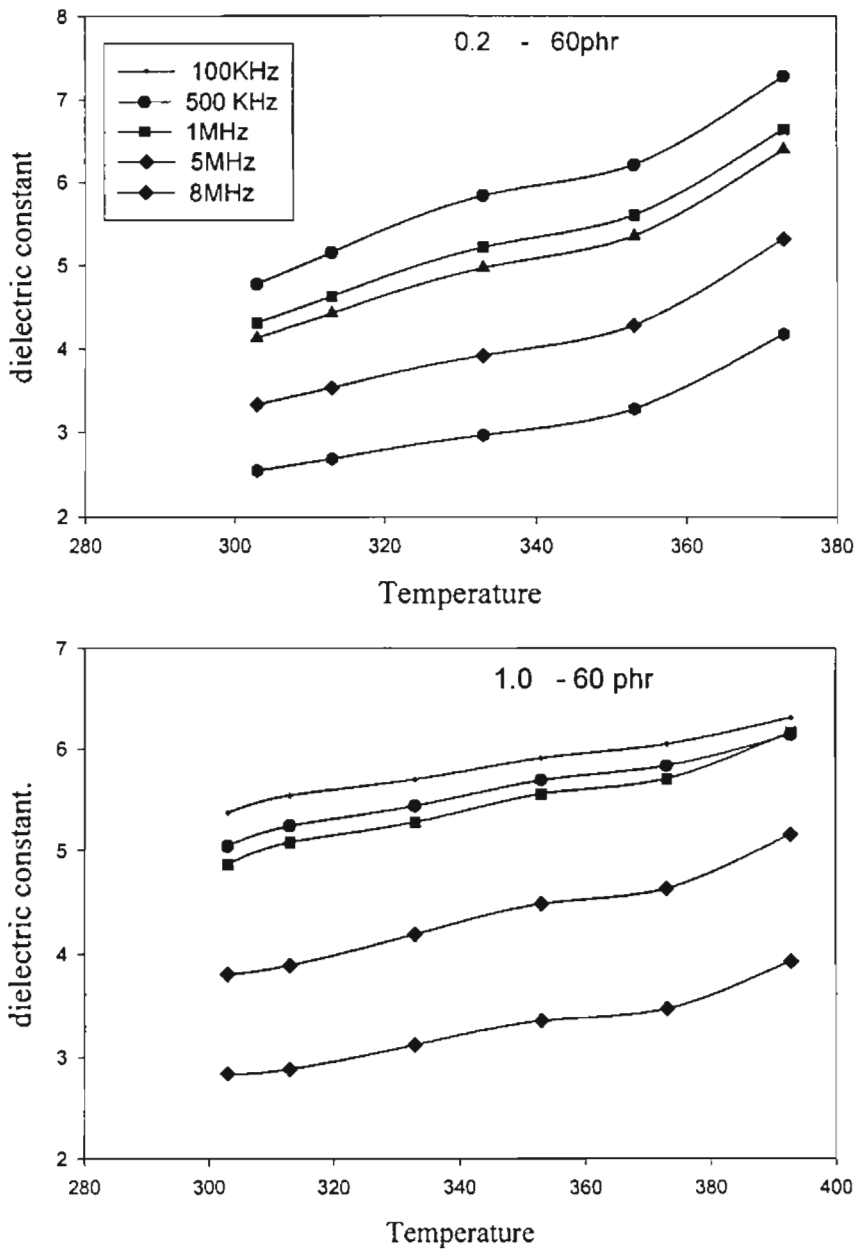


Fig.7.8 Variation of dielectric constant with temperature

d) Loading dependence:

Variations of dielectric constant with the loading of magnetic filler were also studied. Fig7.9 shows the variation in dielectric constant with loading. The dielectric constant was found to increase with increase in weight fraction of the ferrite material. Maximum values of dielectric constants for all compositions were observed for

loading corresponding to 120phr of each composition in NR. The variation is same for all compositions at different frequencies.

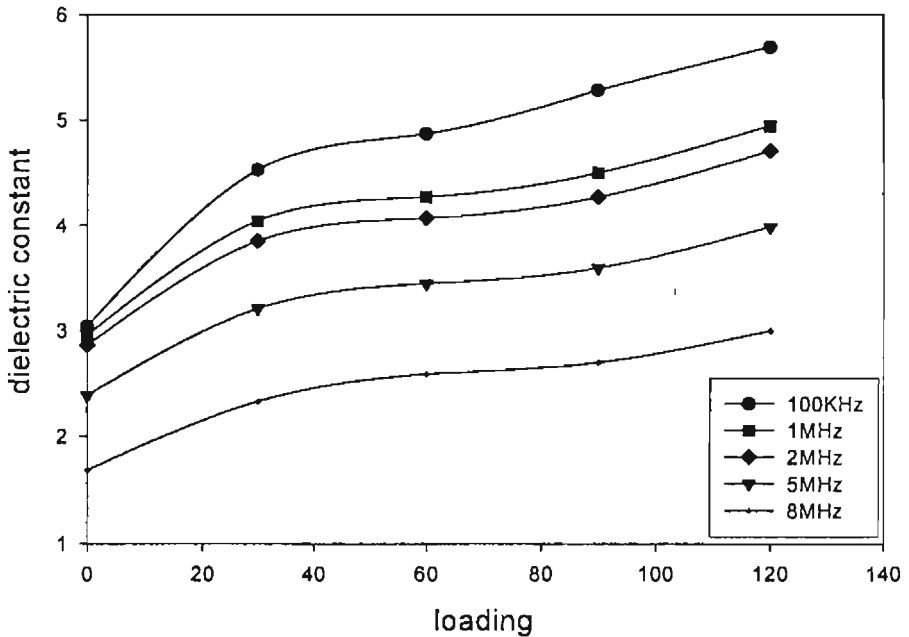


Fig.7.9 Variation of Dielectric constant with loading (nzf0.0)

Efforts were also made to correlate the dielectric constant of the composite samples with those of the ceramic filler and the blank matrix NR. Several mixture equations exists and can be employed to predetermine the dielectric constant of the composites correctly(155,168). For this, the Composite dielectric has to be considered as a mixture of several components.

For example, for a mixture of m component the dielectric constant ϵ^* is connected by a relation, where $\text{Log } \epsilon^*$ is given by

$$\sum_{i=1}^m y_i \log \epsilon_i \dots\dots\dots(7.3)$$

Where ϵ^* is the dielectric constant of the mixture and y is the weight fraction of the component. For a two component system the relationship can be written as

$$\log \epsilon^* = y_1 \log \epsilon_1 + y_2 \log \epsilon_2 \dots\dots\dots(7.4)$$

where ϵ^* is the dielectric constant of the composite, ϵ_1, y_1 and ϵ_2, y_2 are the dielectric constant and weight fractions of the matrix and the filler component respectively. The measured and calculated values (by employing equation 7.4) of dielectric constant is shown in Fig.7.10.

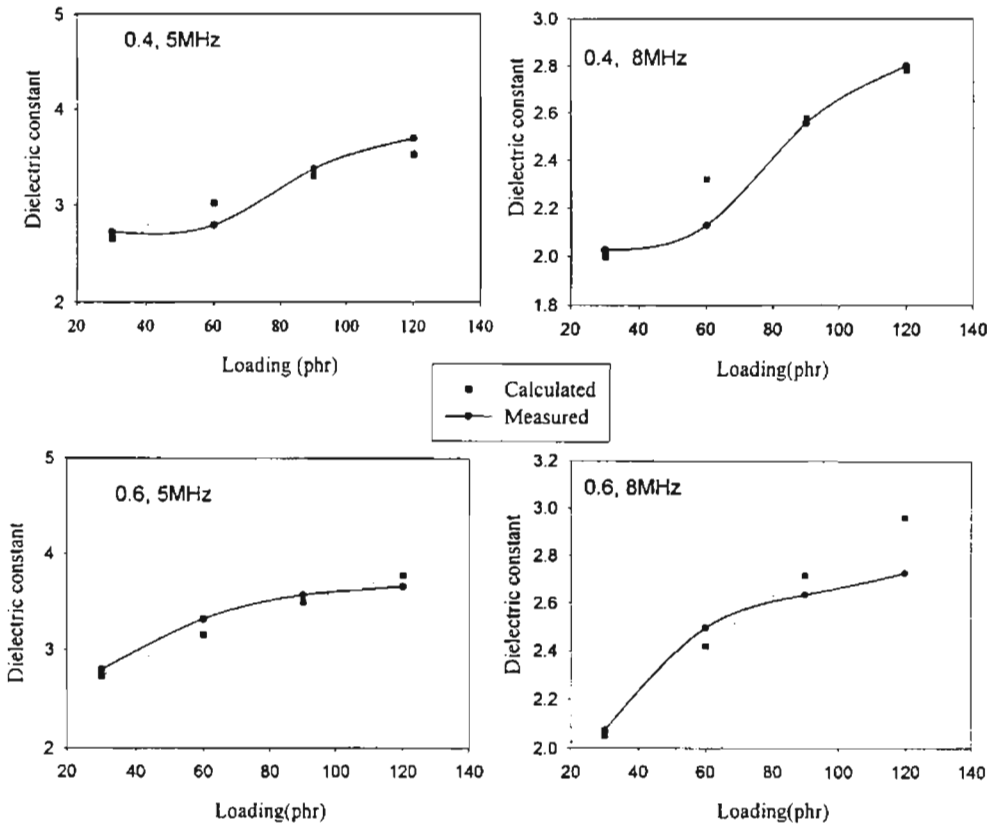


Fig.7.10 Measured and calculated values of dielectric constant

Another mixture equation of the form

$$\epsilon^* = \frac{\epsilon_1 \epsilon_2}{\epsilon_1 y_2 + \epsilon_2 y_1} \dots\dots\dots (7.5)$$

is also found to be useful for predicting the loading dependence of dielectric constant of the RFC. The dielectric constant of the composite were calculated using the equation 7.5 from the observed values of ϵ of the components and with the known value of the filler loading. These values were compared with the measured value of ϵ for the composites. Representative graphs showing the calculated (using equation7.5) and measured values of the dielectric constant are given in Fig.7.11.

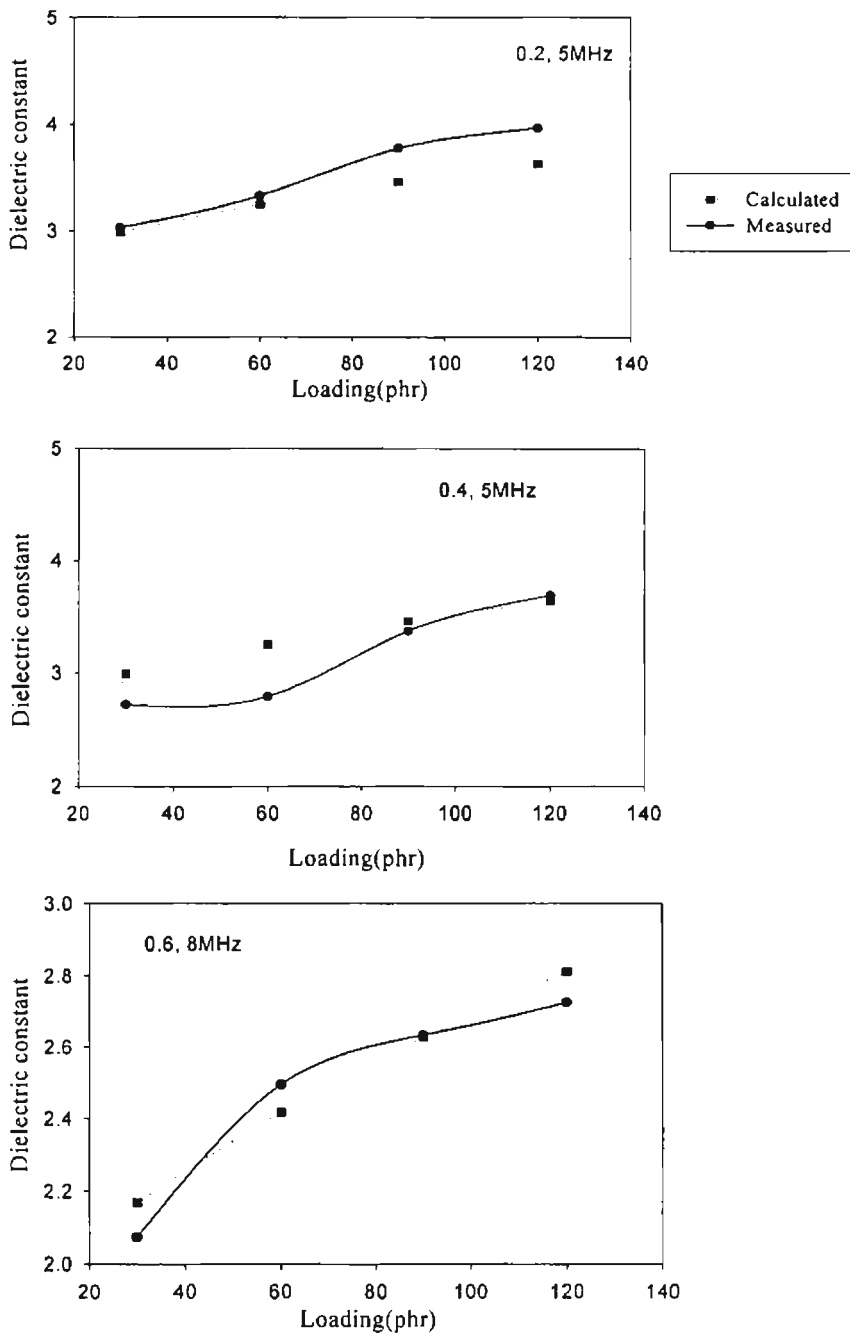


Fig.7.11 Measured and calculated values of dielectric constant

Comparison of the measured and calculated values of the dielectric constant by the above mentioned equations for various loadings and frequencies were made for all compositions. It indicates that equation 1 is suited for all frequencies, but at higher loadings equation 2 is better placed with respect to equation 1. It was also observed that equation 2 is not suited for the evaluation of ϵ at lower frequencies.

7.3. Mechanical Properties

The mechanical properties namely the tensile strength, elongation at break and 100% modulus were determined and their variation with loading was also studied. The variation of tensile strength with loading is shown in Fig.7.12. It shows that the tensile strength first decreases with initial loading upto 30phr and thereafter it increases with loading. It is known that stress induced crystallization will increase the tensile strength and hence blank NR has got a higher tensile strength(53-55,79) But the addition of filler will inhibit the stress induced crystallization which inturn will result in a decreased tensile strength for the initial filler loading of 30phr. For further loadings of the filler the tensile strength shows an increasing trend. This means that the filler NZF is acting as a semi reinforcing filler.

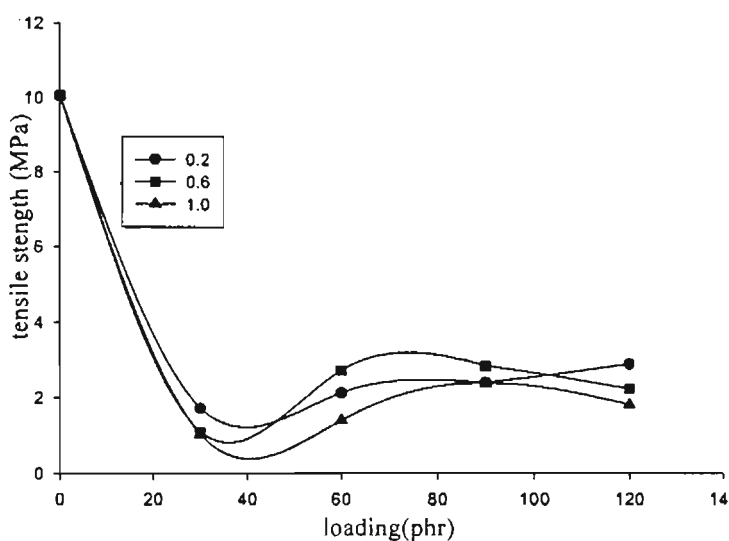


Fig7.12. Variation of tensile strength with loading

Here it may be noted that the variation pattern for tensile strength with loading and cure time vs loading (refer fig. 6.9) almost resembles. It has been studied and observed by many researchers that cross-linking between polymer molecules reduces their mobility and thus increases the modulus and strength(79,168-169). Cross linking generally affects the properties such as the tensile strength and elongation which are determined by large molecular deformations. But greater interaction between other effects makes the ultimate property unpredictable. So as the cure time increases cross-

linking also increases which in turn increases the tensile properties. Thus the cure time variation with loading indirectly gives an idea about the tensile strength variation with loading.

Elongation at break also shows a similar decrease for the initial loading and it remains by and large the same for higher loadings (Fig 7.13). This can also be explained as due to the decrease in stress induced crystallization. During elongation rearrangement or orientation occur to form crystallites, and this stress induced crystallization gives NR high strength in the blank form. But the addition of filler will inhibit this rearrangement or orientation there by reducing the elongation at break as well as tensile strength.

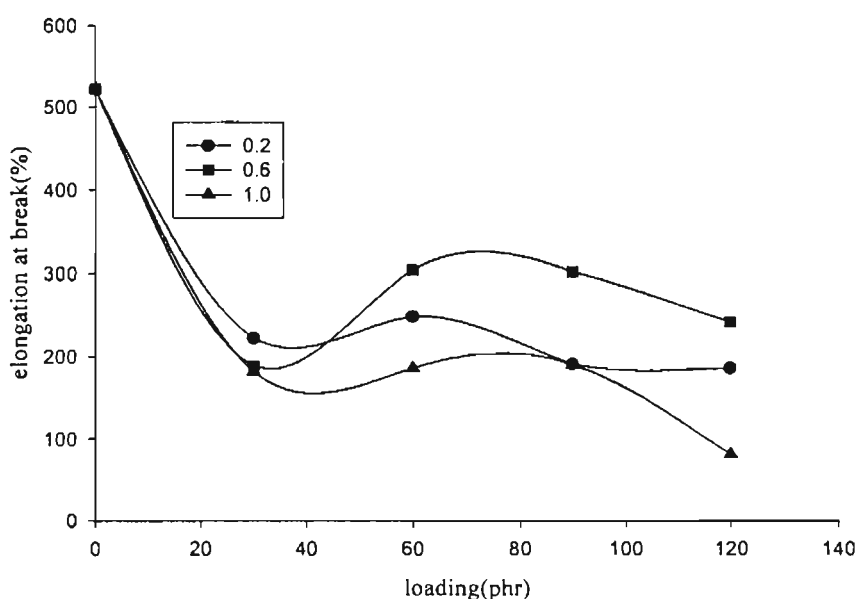


Fig.7.13 Variation of elongation at break with loading

100% modulus shows an increasing trend with increase in loading (Fig.7.14). This is evident from the cure characteristics too²⁸. It may also be noted that the filler addition will decrease the polymer molecular weight slightly and this will also cause a small decrease in the tensile as well as the modulus values.

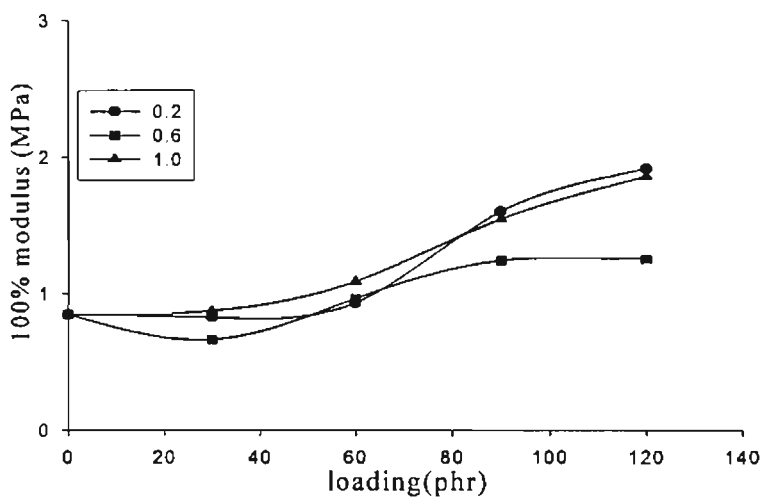


Fig.7.14 Variation of 100% modulus with loading

7.4 Hardness measurements

The hardness of these samples were also studied for different loadings of the filler and the results are shown in Fig.7.15. From the graph of hardness versus 'x', for all loadings of filler, the hardness shows a minimum either at $x=0.6$ or at $x=0.4$. But the maximum hardness for both the samples are much below the maximum permitted limit for the elastomer even for 120 phr loading of the filler. It is also to be noted that the reported value of hardness for natural rubber compounds lie in the range 30-100 in the shore A Durometer.(81).

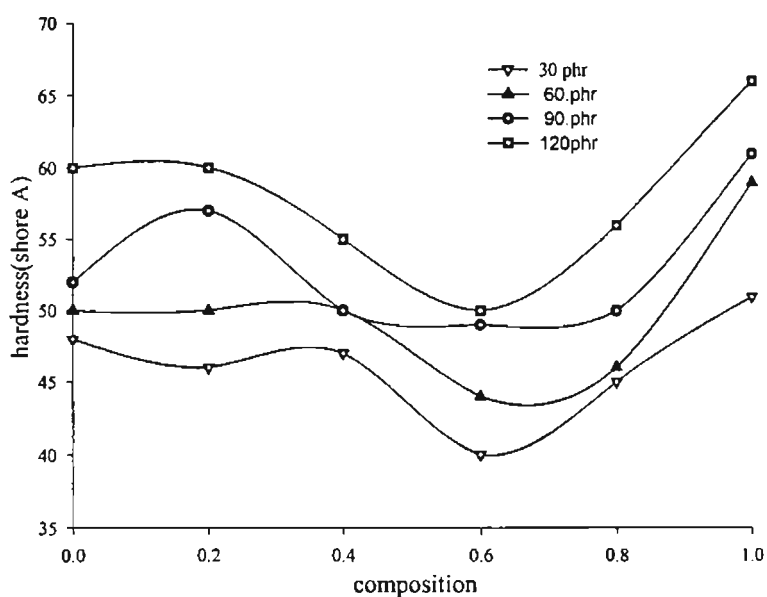


Fig.7.15 variation of hardness with composition for NZF

7.5. Conclusion

RFC containing NZF in NR matrix have been prepared at various loadings. Their dielectric properties were evaluated. Dependence of dielectric constant with temperature, loading, frequency and composition are studied and correlated. Mixture equation for predicting the dielectric constant at various loadings were also formulated and validity of these mixture equations were checked and found to be in good agreement with the observed values. Two mixture equations were tried and logarithmic equation of the form $\log \varepsilon^* = y_1 \log \varepsilon_1 + y_2 \log \varepsilon_2$ is found to be useful in the entire frequency range for higher loadings and equation of the form

$$\varepsilon^* = \frac{\varepsilon_1 \varepsilon_2}{\varepsilon_1 y_2 + \varepsilon_2 y_1} \quad \text{is useful for the entire loadings but for higher frequencies.}$$

These results suggest that appropriate loading and a judicious choice of the filler can manipulate dielectric properties of rubber ferrite composites. The mechanical properties of representative samples were studied and it was found that the filler modifies the mechanical properties. The hardness of the composites also increased with loading of the filler. It is also found that the curetime is also a determining factor as far as the tensile properties are concerned. It is also to be noted that the compositions corresponding to $x=0.4$ and 0.6 gives optimum strength and magnetisation and minimum hardness. The modification of these properties will aid in the design of composite materials for possible applications.

CHAPTER 8

AC CONDUCTIVITY STUDIES ON RUBBER FERRITE COMPOSITES

8.1 Introduction

All materials conduct electricity to a greater or lesser extent. Mixed ferrites like nickel zinc ferrites have low eddy current loss and high resistivity and hence they are important commercially. The electrical properties are most important for ferrites and composites containing ferrites used for various applications. The study of ac electrical conductivity gives an idea about the behaviour of charge carriers under an ac field, their mobility and the mechanism of conduction(170-179).

Rubber ferrite composites(RFC) which are composite materials made of ferrite filler and natural rubber have the advantages of being light in weight, soft, elastic, stable, flexible, processible and energy-saving. Their applications range from electronic & electric industry, motor stators and rotors, information technology, printing and decoration. The size, shape and magnetization pattern can be manufactured according to user's need. So RFCs are essentially dielectric materials and their electrical properties are very important from the application point of view. Hence the study of these materials, particularly in an ac field assumes significance.

Extensive studies on electrical properties of ferrites particularly of nickel zinc ferrites can be found in the literature(173-205). They have successfully explained the mechanism of conduction in ferrites as the Verwey type hopping conduction.

Rubber ferrite composite samples containing $Ni_{1-x}Zn_xFe_2O_4$ (x varying from 0 to 1) in natural rubber were prepared for different loading. Their dielectric constant and loss were evaluated by parallel plate capacitor method by using a dielectric cell and an Impedance analyzer (HP 4285A).

The theory involved in the evaluation of ac conductivity from dielectric constant is discussed in detail in Chapter 3. The conductivity cell for the

determination of $\tan\delta$ and ϵ was interfaced with a computer and the acquisition of data was automated. The details are given in chapter 3.

From the dielectric loss and dielectric constant AC conductivity of these samples can be evaluated using the relation

$$\sigma_{ac} = 2\pi f \tan\delta \epsilon_0 \epsilon_r$$

f is the frequency of the applied field ϵ_0 is the absolute permittivity, ϵ_r is the relative permittivity and $\tan\delta$ is the loss factor.

AC conductivity for all compositions of the ceramic samples were evaluated for the frequency range from 100kHz to 8MHz. The measurements were done at different temperatures of 30, 40, 60, 80, 100, 120°C. The AC conductivity of the composite samples were also evaluated under similar conditions.

8.2 Frequency dependence of AC conductivity.

8.2.1 Ceramic samples

In ferrites the low conductivity is associated with the simultaneous presence of ferrous and ferric ions on equivalent lattice sites (usually octahedral sites). In such a situation the mechanism of conduction that comes into play is the Verwey type conduction or hopping conduction. The electrical conduction in NiZn Ferrites with the structural formula $Zn_xFe_{1-x}[Ni_{1-x}Fe_{1+x}]O_4$ is explained by Verwey mechanism. The extra electron on a ferrous ion requires only very small energy to move to a similarly situated ferric ion. The valence states of the two ions are interchanged. Under the influence of an electric field these extra electrons can be considered to constitute the conduction current by hopping or jumping from one iron ion to the other. Depending on the sintering conditions such ions with different valence states can be produced during preparation of ferrite samples. For example when ferrites containing nickel are cooled from an elevated temperature in an oxygen atmosphere Ni^{3+} ion are formed by oxygen absorption. Hence hole hopping between Ni^{2+} and Ni^{3+} on B site also contribute electric conduction in nickel zinc ferrites. Also a partial reduction of Fe^{3+} to Fe^{2+} ions is possible at elevated firing temperatures of the order of 1000K.

The variation of AC conductivity with frequency at room temperature for the ceramic samples of NZF is given in Fig. 8.1. The ac conductivity shows an increasing trend with increase in frequency for all samples. But at high

frequencies (for frequencies beyond 5MHz) the ac conductivity values show a decreasing trend. This behaviour can be explained as follows.

The dielectric structure of ferrites is given by Koops Phenomenological theory and Maxell-Wagner theory. According to this theory dielectric structure was formed by a first layer of fairly well conducting ferrous ions, which is separated by a thin layer of poorly conducting grain boundary formed by oxygen ions. At lower frequencies these grain boundaries are more active and hence hopping of Fe^{2+} and Fe^{3+} ion is less at lower frequencies. As the frequency of the applied field increases the conductive grains become more active by promoting the hopping between Fe^{2+} and Fe^{3+} ions, there by increasing the hopping conduction. Thus we observe a gradual increase in conductivity with frequency. But at higher frequencies the frequency of the hopping ions could not follow the applied field frequency and it lags behind it. This causes a dip in conductivity at higher frequencies.

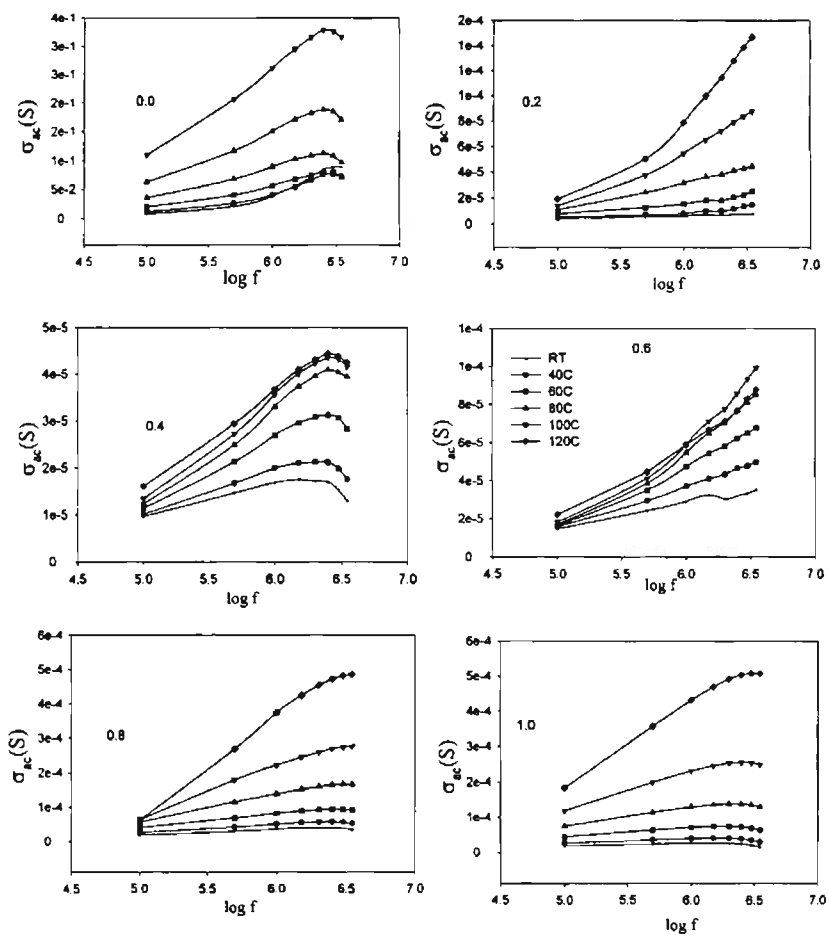


Fig.8.1 Variation of σ_{ac} with frequency

It is well known that ac conductivity σ_{ac} is temperature and frequency dependent and is related to the dielectric relaxation caused by the localized electric charge carriers. It can be written in the power law as

$$\sigma_{ac}(\omega) \propto \omega^n$$

where $\omega = 2\pi f$ is the angular frequency and n is dependent on composition and temperature. The $\log \sigma_{ac}$ versus $\log \omega$ were plotted and the value of n for different compositions at various temperatures were evaluated for ceramic samples. It was found that n lies in the range 0.2 to 0.73 for all compositions at all temperatures. This also confirms the hopping mechanism of conduction in the present system.(201-208)

8.2.2 Blank natural rubber

In most polymers it is difficult to detect any electronic conductivity and most of the conductivity observed is due to impurity ions such as catalyst residues, dissociable end groups and degradable products. Unvulcanised natural rubber is nonconducting and the vulcanized rubber contains different compounding ingredients which may act as carriers for conduction. Also polymers are known to be semicrystalline and natural rubber can be thought of as a continuous matrix of an amorphous polymer in which properties are modified by the crystalline regions which act as the reinforcing centers. As far as the electrical properties are considered the effect of crystalline centers is to lower the conductivity. If the conduction is ionic, ion mobility through the crystalline region will be low and in the case of electronic conduction the crystalline amorphous interface may act as a trapping region. Thus it can be considered similar to Maxwell-Wagner two layer model.(211-213)

The variation of AC conductivity with frequency for blank NR is given in fig 8.2. It can be noted that the ac conductivity increases with increase in frequency and drops after reaching a maximum at higher frequencies. At lower frequencies the crystalline- noncrystalline interface may be more active and as the frequency increases the ions are able to move across this interface which in turn will increase the conductivity. High frequency limit is reached when applied frequency is greater than maximum hopping rate.

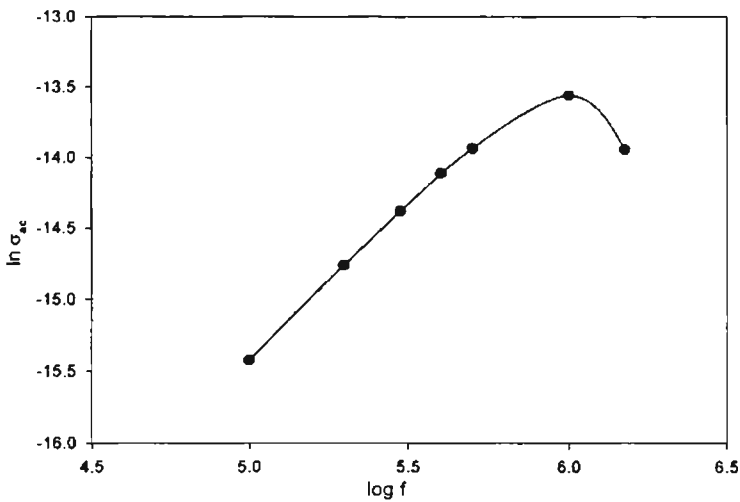


Fig.8.2 Variation of ac conductivity for blank NR

8.2.3 Composite samples

In the case of composite samples too the similar behaviour is observed for the variation of conductivity versus frequency and this can be explained based on the interfacial polarization itself. Figure 8.3 show the variation of AC conductivity with frequency for rubber ferrite composites containing nickel zinc ferrites in natural rubber. It is also observed that the variation of ac conductivity with frequency retains the same pattern for different loadings of the filler.

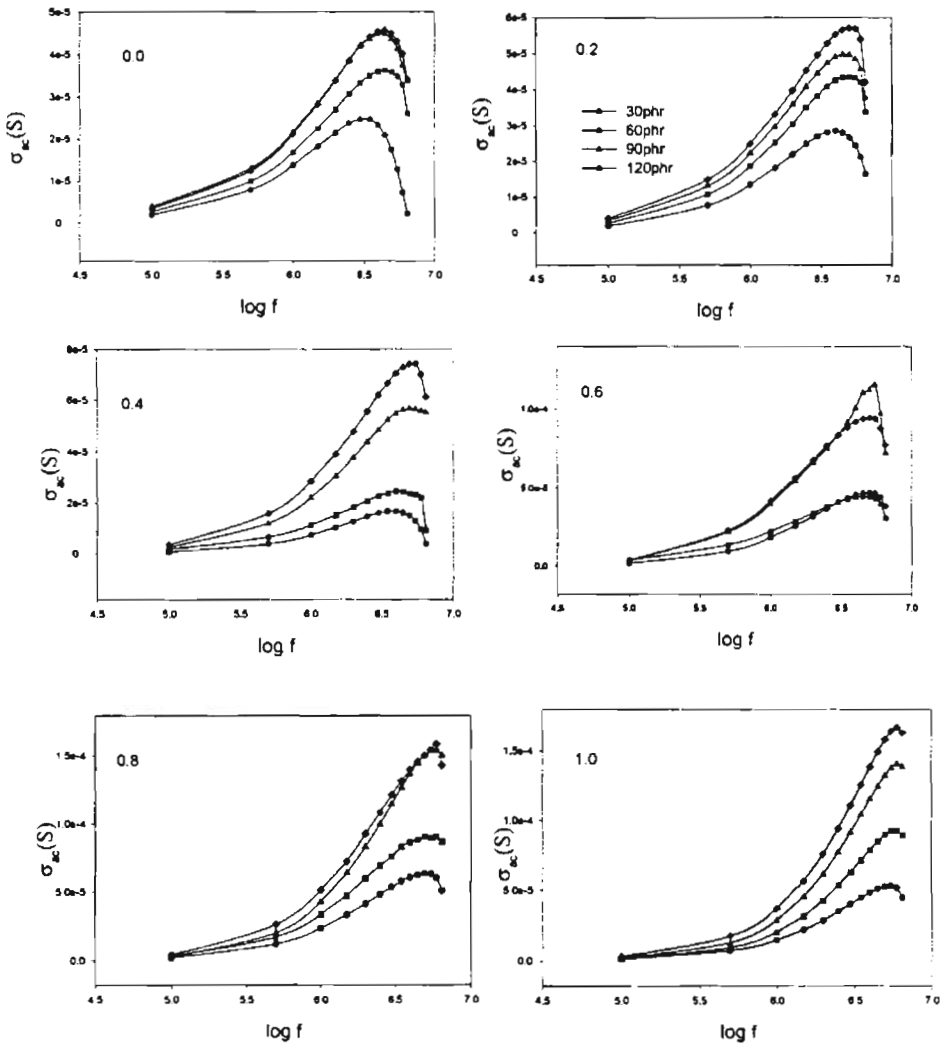


Fig.8.3 Variation of σ_{ac} with frequency for composite samples

8.2.3 Compositional dependence

8.3.1 Ceramic samples

The variation of conductivity with composition (zinc content) for ceramic nickel zinc ferrites at room temperature is shown in figure.8.4. It can be seen that the ac conductivity increases with increase of composition. The variation pattern remains the same for all frequencies. The conduction mechanism in ferrites can be expressed in terms of electron hopping between ferrous and ferric ions on the octahedral site for n-type semiconductor ferrites and in terms hole hopping for p-type ferrites (Verwey type of conduction). In $Ni_{1-x}Zn_xFe_2O_4$ at $x=0.0$ the hole

hopping ($\text{Ni}^{2+} \leftrightarrow \text{Ni}^{3+}$) at B site is the prominent mechanism. As the zinc content increases Ni content at the B site decreases and hence hole hopping decreases. But at the same time the Fe content at the B site increases which in turn will increase the conductivity due to electron hopping ($\text{Fe}^{3+} \leftrightarrow \text{Fe}^{2+}$). At higher sintering temperatures the evaporation of zinc will contribute some Fe^{2+} ions to the B site and this will localize the hopping electrons and will decrease the $\text{Fe}^{3+}/\text{Fe}^{2+}$ ratio which in turn will result in a decrease in the AC conductivity at $x=1.0$ or for zinc ferrite(188-195).

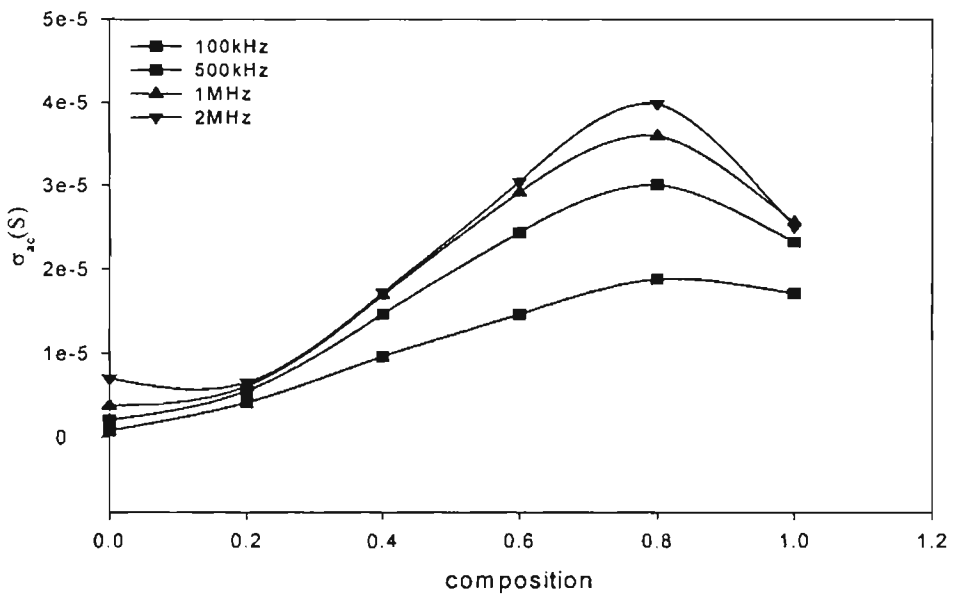


Fig.8.4 Variation of ac conductivity with composition

8.3.2 Composite samples

Compositional dependence of ac electrical conductivity for rubber ferrite composites was also studied at different frequencies and also at various temperatures. The variation pattern of AC conductivity with composition for rubber ferrite samples at 1MHz is shown in Fig.8.5. It is found that the variation is almost the same as that of the ceramic samples for higher loadings of the filler. But for lower loadings a slight decrease for $x=0.4$ is observed. This decrease is more prominent at 30phr and becomes less at 60phr. It may be noted that the conductivity of the matrix NR is very small compared with that of the filler and hence conductivity variation with composition is generally governed by the compositional variation in the conductivity of the filler. From the graph it may be

noted that the ac conductivity increases with increase in zinc content except for a small decrease at $x=1.0$. These results suggest that the ac conductivity of the rubber matrix can be suitably modified by an appropriate choice of the composition and with the required loading of the filler.

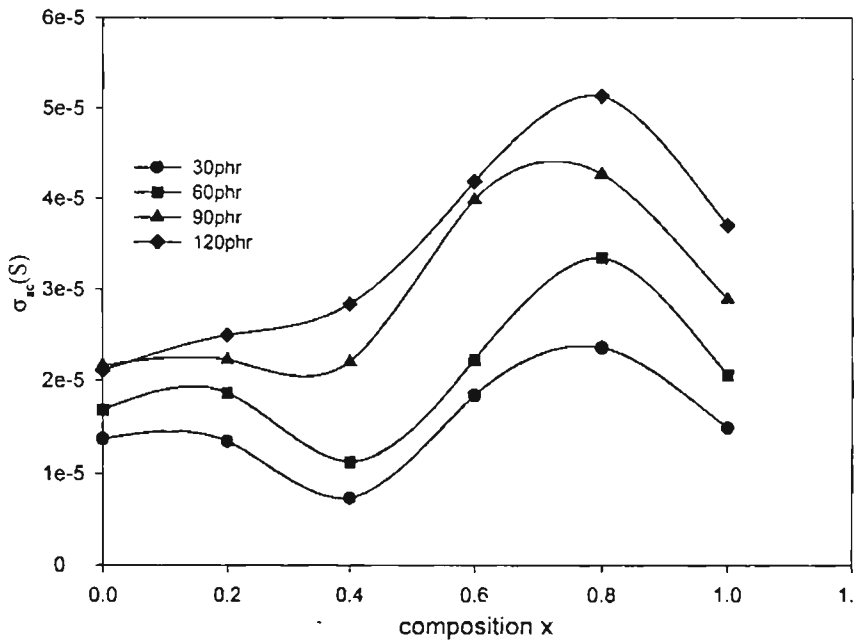


Fig.8.5 Variation of AC conductivity with composition for RFC

8.4 Loading dependence

In RFCs containing NZF an increase in conductivity was observed with increase of the volume fraction of the filler. A maximum conductivity is observed for a maximum volume fraction of 120phr. This is same for all compositions (that is for all x values). Graphs showing the variation pattern is depicted in Fig.8.6. At lower loadings the conductivity of the composites differs slightly from that of the host polymer. At percolation threshold conductive paths are formed and the conductivity increases sharply. Above percolation threshold it increases slowly. Here no such sudden change in conductivity is observed by adding higher volume fraction of the filler and it was found that the percolation threshold was not yet reached even for a loading of 120phr. From the graphs it is obvious that the conductivity increases with increase of loading of the filler. This means that the filler modifies conductivity of the matrix. It may also be noted that the parameters like particle size, structure, aggregation, surface contamination and matrix filler interaction can have remarkable influence in the conductivity of the composites.

However from our magnetic and dielectric studies has been found that the matrix filler interaction is very little in the system under study.

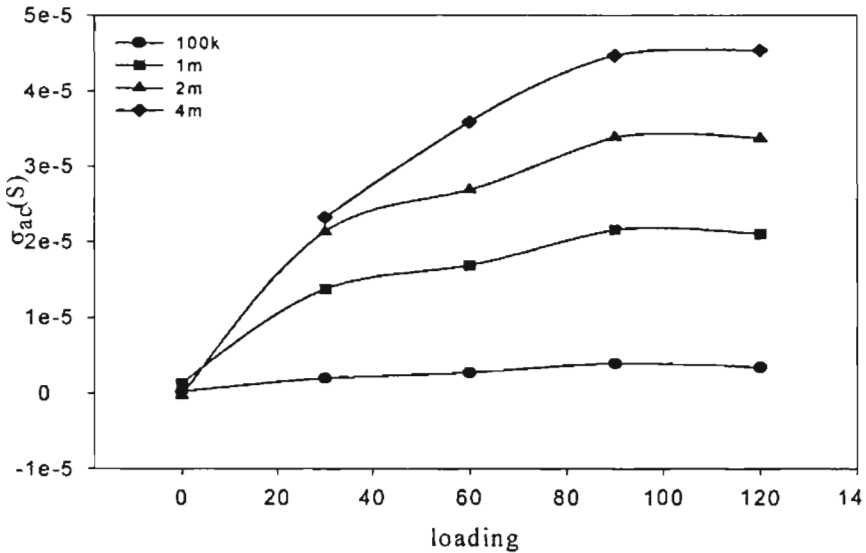


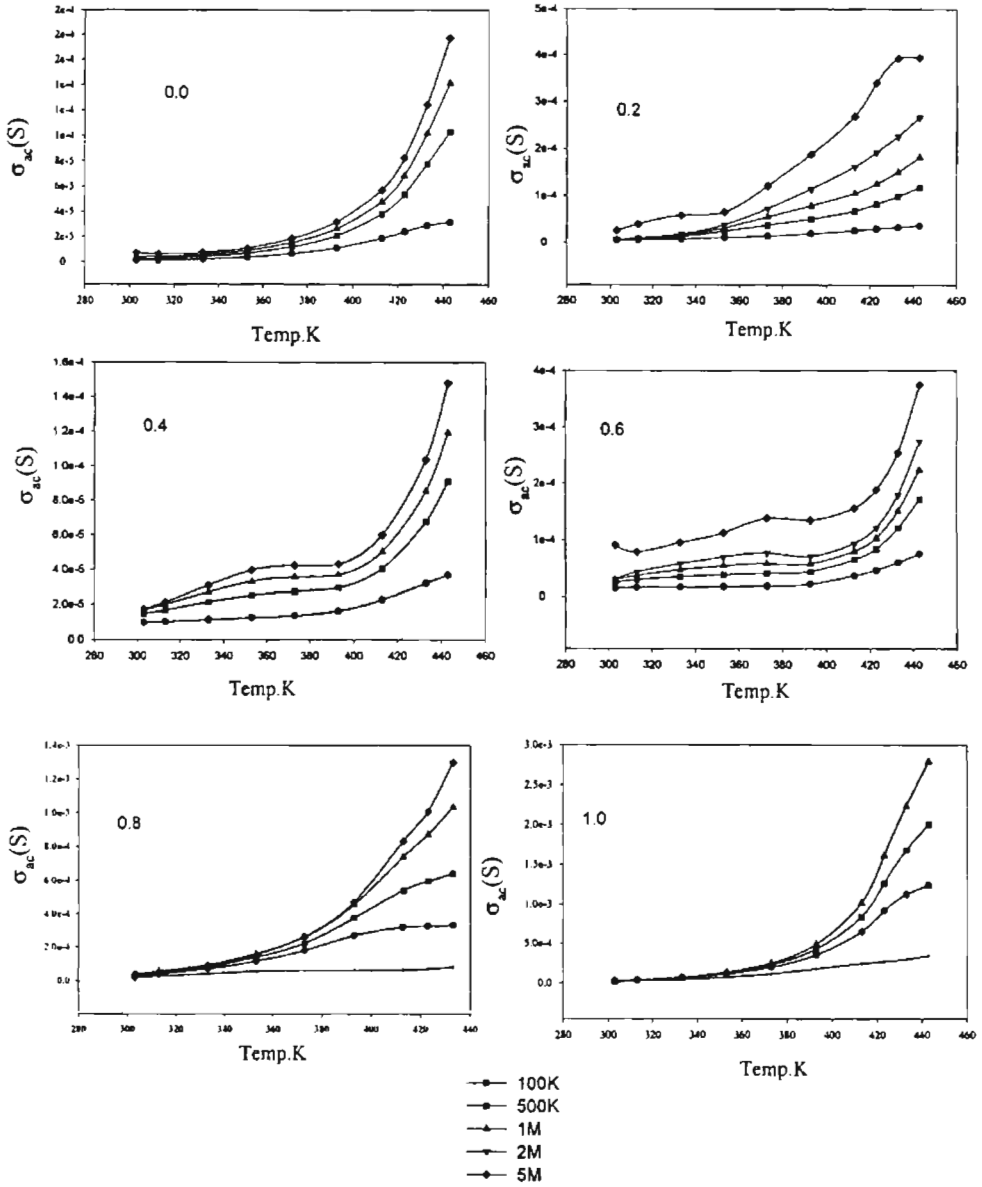
Fig 8.6 Variation of ac conductivity with loading $nzf0.0$

8.5 Temperature dependence

8.5.1 Ceramic samples

The effect of temperature on the ac electrical conductivity of ceramic nickel zinc ferrite studied in the range 303K to 393K. It was observed that the conductivity increases with increase of temperature for all ceramic nickel zinc samples. At low frequencies the variation is very minimal but at higher frequencies the variation is more. The variation pattern of conductivity with temperature for different compositions are shown in Fig.8.7. The influence of temperature on conductivity can be explained by considering the mobility of charge carriers responsible for hopping. As temperature increases the mobility of hopping electrons also increases thereby increasing conductivity. In the present case the electrons which are involved in hopping gets more energy and their mobility increase.

Fig. 8.7 Variation of ac conductivity with temperature



8.5.2 Blank NR

The temperature dependence of conductivity for blank natural rubber was also noted. It shows that the conductivity increases as the temperature is increased. The change is showed graphically in Fig.8.8. A reduction in conductivity at high temperature was observed for blank NR. This may be due to the thermal expansion of the polymer. At higher temperature the polymer density is reduced by thermal expansion and thus reduce the conductivity.

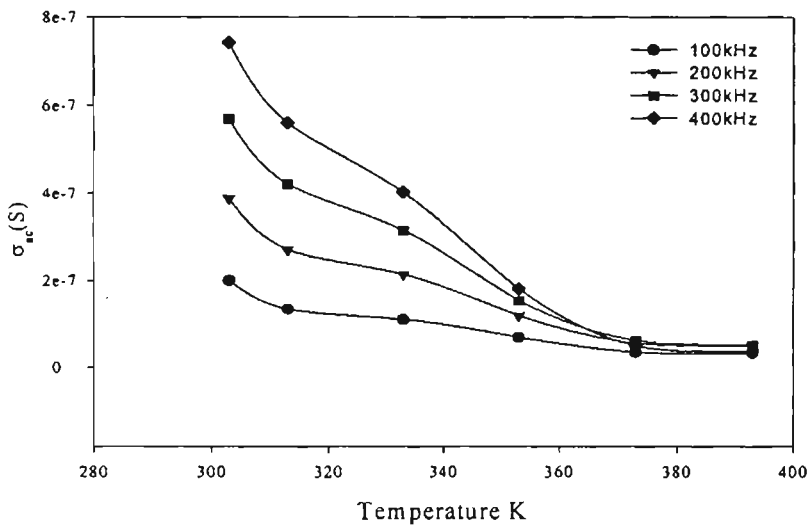


Fig.8.8 Variation of ac conductivity with Temperature for Blank NR

8.5.3 Composite samples

The effect of temperature on the ac electrical conductivity of the rubber ferrite composites were also studied in the range 303K to 393K. Variation pattern is shown in Fig.8.9. It was observed that the conductivity increases with increase of temperature for the composite samples also. A reduction in conductivity was observed at higher temperature for the composite samples also. The conductivity values of composites are found to be larger than the blank matrix.

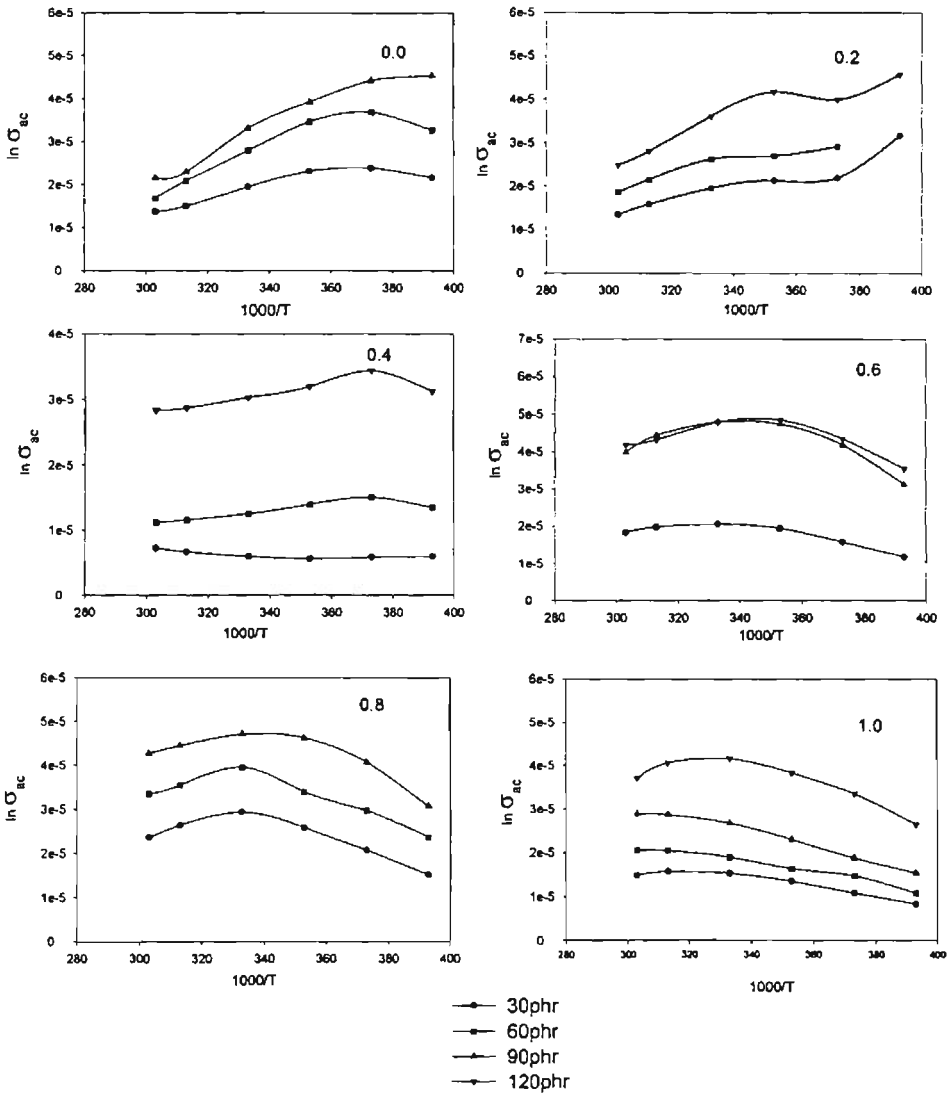


Fig.8.9 Variation of $\ln \sigma_{ac}$ with temperature

8.6 Activation energy for conduction

Activation energy for conduction can be calculated from the slope of $\ln \sigma_{ac}$ vs $10^3/T$ graphs according to the relation

$$\sigma_{ac} = \sigma_0 \exp \left(\frac{-E_a}{kT} \right)$$

Where σ_0 is a constant, E_a is the activation energy, k is Boltzman's constant and T the temperature in degree absolute.

The activation energy for conduction was calculated for ceramic and composite samples. The variation of activation energy with composition for the ceramic samples is shown in Fig.8.10.

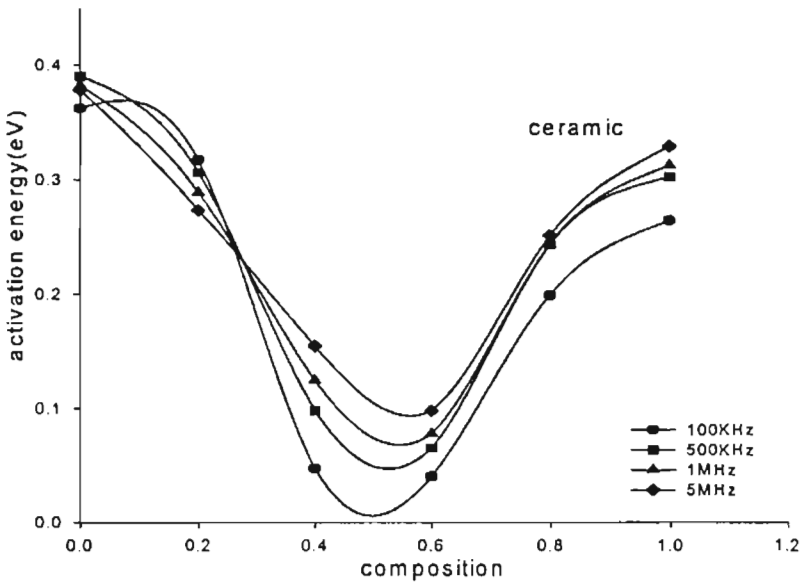


Fig.8.10 Activation energy for conduction for ceramic NZF

It can be seen the variation in activation energy with composition is almost opposing to the variation in conductivity with composition for the ceramic samples. This also supports the compositional dependence of conductivity. Similarly the activation energies for all filler incorporated rubber composites were also noted and Table 8.1 summarizes the value of activation energy for the composites calculated at 1 MHz. Form the table it can be seen that the activation energy for composites is less than the activation energy for the filler.

Composition (x)	Activation energy in eV			
	30phr	60phr	90phr	120phr
0.0	0.097	0.122	0.127	0.074
0.2	0.105	0.101	0.103	0.097
0.4	---	0.044	0.018	0.028
0.6	0.035	0.13	0.056	0.036
0.8	0.062	0.048	0.03	----
1.0	0.043	---	---	0.0568

Table 8.1 Activation Energy values for Composite samples

The low conductivity in polymers, even for their low activation energies can be attributed to the low mobility of carriers in the polymer. There are reports that the activation energy for conduction of inorganic semiconductor is higher than the corresponding activation energy of conductance of polymeric semiconductors (213). For example for germanium with a conductivity 0.1 to $0.01 \text{ ohm}^{-1}\text{cm}^{-1}$, the activation energy for conductance is about 0.6eV and for an organic semiconductor with the same conductivity the activation energy of conductance is between 0.1 and 0.03eV . These factors may account for the low activation energy and low conductivity for the composite samples.

8.7 Conclusion

Ceramic NZF and composites containing NZF in NR have been prepared and their ac conductivity have been evaluated from the dielectric measurement. Variations of ac conductivity with frequency, temperature, composition and loading have been studied and the results have been correlated. Activation energy for conduction is also evaluated for the ceramic and composite sample.

CHAPTER 9

SUMMARY AND CONCLUSION

Nanomaterials and nanocomposites have a major role to play in the coming century as far as the technology is concerned. Needless to mention that, the composites that are prepared by mechanical means will continue to contribute its might as far as applications are concerned. Among the nanomaterials magnetic nanocomposites is all the more important since it provides scientists and engineers a chance to improve upon the existing and search for new replacements with improved/modified performance characteristics. Since the entire field of nanocomposites is in its infancy, a lot more needs to be understood from the fundamental view point. Phenomena like superparamagnetism, spin glass behaviour and spin clusters is growing into a separate branch in magnetism owing to its predominant role in determining the magnetic and electrical properties at the nanolevel.

In the present work the focal theme was on preparing and characterising composites based on spinel ferrites. In that we have divided the work into two categories mainly on the nanocomposites based on $\gamma\text{-Fe}_2\text{O}_3$ and then on rubber ferrite composites based on nickel zinc ferrites. Chapter 1 to Chapter 3 dealt with the general aspects of the subject including the theory and experiments carried out for preparation and characterisation of the samples.

Chapter 4 deals with the preparation and characterisation of nanocomposites based on $\gamma\text{-Fe}_2\text{O}_3$ by the method of ion exchange. The conditions have been optimised and standardised. It has been found that the employment of strong ion exchange resin and a concentrated solution of FeSO_4 with H_2O_2 is ideal for incorporating an inorganic magnetic component in the matrix. Though similar experiments were carried out with weak ion exchange resins it is found that as far as the magnetic yield is concerned it is far behind strong ion exchange resin. The cycling experiments carried out on this sample shows that the cycling increases the yield of magnetic component is enhanced or in turn increases the M_s of the composites. This is desirable because applications demand specific M_s and this can be achieved by selecting the number of cycles. It is to be noted that in our set

of experiments a maximum M_s of $9.18 \text{ Am}^2/\text{kg}$ has been obtained. Though this is well below the theoretical limit of $16 \text{ Am}^2/\text{kg}$, for the strong ion exchange resin of sulphonated polystyrene, possibility exists to enhance the magnetic characteristic by further cycling. Since ion exchange resins with various pore sizes are available and since the pore size limits the growth of the particle this method of ion exchange can be successfully employed to prepare magnetic nanocomposites with various particle dimension.

In application involving magnetic nanocomposites where H_c is a determining factor it would be appropriate to incorporate cobalt into the $\gamma\text{-Fe}_2\text{O}_3$, thereby increasing the coercivity. It is known from literature (215) that cobalt because of its uniaxial anisotropy, enhances the coercivity to a large extent. It has been reported for bulk $\gamma\text{-Fe}_2\text{O}_3$ that even a dopant percentage of cobalt of the order of 2-8 atomic percentage increases the coercivity of $\gamma\text{-Fe}_2\text{O}_3$ by an order of one that is from 200 to 2000Oe. Most of the relevant literature related to coercivity enhancing property of the Co containing compounds are carried out in bulk. It would be a good proposition to study the effect of Co in a matrix containing polystyrene and $\gamma\text{-Fe}_2\text{O}_3$ in improving the magnetic characteristics. Since the magnetic component is already in the nanoregime, in most of the case below critical particle size, high coercivity is a hallmark of such systems and it would be interesting both theoretically and fundamentally to delve into the interaction that take place after incorporation of cobalt into the matrix. No morphological studies could be carried out on these samples due to lack of proper microtoming techniques. So scope exist for further investigations on the morphology of nanocomposites.

Imaging applications based on magnetic nanocomposites requires that they are either transparent or coloured. This requirement can be fulfilled by incorporating suitable dyes into the matrix and thereby rendering it useful for optical applications. However it must be mentioned here that technique for the incorporation is to be worked out. Chromium dioxide is a known ferromagnetic compound and is known for its superlative recording potentials as far as the storage applications are concerned. It would be appropriate to see the potential of incorporating chromium dioxide in a matrix of polystyrene. Available literature indicates that no such studies have been carried out.

Another spin off of this method of preparation is that $\alpha\text{-Fe}_2\text{O}_3$ can be successfully incorporated into the matrix by proper oxidation or decomposition of the nanocomposites containing $\gamma\text{-Fe}_2\text{O}_3$. This is important commercially because fine $\alpha\text{-Fe}_2\text{O}_3$ is a very good catalyst for oxidative dehydrogenation reactions(216). These magnetic composites based on $\gamma\text{-Fe}_2\text{O}_3$ can be a useful precursor for the preparation of ferrofluids. The use of ferrofluids for technological for technological applications is ever increasing and hence these nanocomposites could be precursors for the ferrofluids synthesis. If the ion exchange method of preparation of nanocomposites can be modified and extended to matrixes like nylon or molecular sieves, materials with modified properties could be prepared.

Nanocomposites containing $\gamma\text{-Fe}_2\text{O}_3$ exhibit magnetocaloric effect and it would be of interest to study the magnetocaloric effect of this nanocomposite by subjecting them to thermal studies. However no thermal studies were carried out on these samples.

Chapter 5 dealt with the low temperature studies carried out on the nanocomposites samples. Studies carried out on these samples using Mossbauer Spectroscopy and Electron spin resonance spectroscopy indicate that the composite consists of a ferrimagnetic component along with a superparamagnetic component of $\gamma\text{-Fe}_2\text{O}_3$ with traces of nonmagnetic impurities. The evidence gathered from Mössbauer studies indicate that as cycling increases the ferrimagnetic component increases. Reports regarding the exhibition of hysteresis by nanocomposites at room temperature are conflicting and from the present study it is not possible to gather any confirmatory evidence in this regard. Mössbauer studies at room temperature and low temperature suggest superparamagnetic relaxation of nanoparticles. This is to be substantiated by other experiments. Having confirmed the presence of superparamagnetic particles in the composites, though they exhibit hysteresis at room temperature, the superparamagnetic blocking temperature T_B whether it is less than room temperature or above room temperature could not be ascertained. Possibly low temperature studies below 80K or high temperature studies above room temperature may be undertaken to delve into this.

The second part of the thesis deals with rubber ferrite composites. The investigations were focussed on studies related to the processability, electrical,

magnetic and mechanical properties of the composites. Chapter 6 deals with in details the processability and magnetic studies. The studies carried out on these samples by evaluating the cure parameters indicate that processability is not affected for higher loadings of the filler. The flexibility also is not affected upto a maximum of 120phr loading. Evaluation of the magnetic parameters indicate that the percolation threshold is not reached and the homogeneity of the sample is intact with no agglomeration or segregation on the surface of the composites. The formulation of a semi empirical relation of the form

$$\sigma_{rfc} = (1 + 0.2x) \sigma_{cer. max.} \cdot W_2 \cdot \exp\left[-0.5\left(\frac{x - x_0}{b}\right)^2\right] \dots\dots\dots(9.1)$$

will help in tailoring the saturation magnetisation of the composites. The semiempirical relation has been applied to other systems namely nickel zinc ferrite in butyl rubber and manganese zinc ferrite in natural rubber and the observed and calculated values are in excellent agreement. This relation requires only the saturation magnetisation of that composition (x vs M_s) which exhibit maximum magnetisation for a series resembling $Ni_{1-x}Zn_xFe_2O_4$. Scope also exist to extend this formula for tailoring the magnetic properties of composites containing similar mixed ferrites. One of the criteria is that the graph depicting the composition versus M_s in the series should necessarily be Gaussian in nature. The coercivity of the composites have been found to be the same as that of the corresponding ceramic component. This indicate that the possibility of the matrix interacting with the filler is minimal. Homogeneous sheets of the composites could be moulded by this method of mixing and the recipe adopted. Further, scope also exists for incorporating this filler in matrices like nitrile rubber, polystyrene, polyurethane etc. However specific recipe for compounding is to be worked out.

Mouldability and flexibility is an added advantage of these composites. Most of these composites are potential microwave absorbers and gaskets for EMI shielding could be moulded by using this method of preparation. Permeability is a determining factor as far as the microwave absorbing properties are concerned. Since no permeability studies were carried out on these samples, investigations on the determination of permeability could be undertaken as an extension of the present work. Nanocrystalline ferrites can be prepared and incorporated in the matrix. It will be interesting to see whether they form magnetic nanocomposites.

Chapter 7 dealt with the dielectric properties of the rubber ferrite composites. The dependence of dielectric permittivity with temperature, frequency, composition and temperature were studied and correlated. Tailoring of dielectric properties of the composites requires that simple equations connect the dielectric properties of the composites with that of the matrix and filler. Two semi empirical formulae of the form

$$\log \varepsilon^* = y_1 \log \varepsilon_1 + y_2 \log \varepsilon_2 \dots\dots\dots(9.2)$$

and

$$\varepsilon^* = \frac{\varepsilon_1 \varepsilon_2}{\varepsilon_1 y_2 + \varepsilon_2 y_1} \dots\dots\dots(9.3)$$

seems to be useful for the prediction of dielectric properties of the composites. These two semi empirical relationships have been applied to the present system under study and it has been found that they are in agreement with the observed value.

Loading of the magnetic filler in the matrix reveals that the dielectric permittivity can be enhanced appreciably and the dielectric property can be tailored by employing one of the equations given by equation 9.2 or 9.3.

The evaluation of the mechanical properties of this composite samples indicate that the mechanical properties could be enhanced by incorporation of the fillers. The tensile data indicate that the magnetic filler act as a semi reinforcing filler too. The composition corresponding to $x=0.4$ and 0.6 for a maximum loading gives optimum strength, maximum magnetic characteristics and minimum hardness. This modification will aid in the design of composite materials for possible applications.

The variation of permittivity with frequency resembles the theoretical curve given by the equation of the form

$$\varepsilon(\omega, T) = \left[(1+x) \frac{(\varepsilon_{hf} x(x\sigma_{lf}^2 + \sigma_{hf}^2) + \omega^2 \varepsilon_0^2 \varepsilon_{hf}^3 (1+x))}{(x^2 (\sigma_{lf} + \sigma_{hf})^2 + \omega^2 \varepsilon_0^2 \varepsilon_{hf}^2 (1+x)^2)} \right] \dots\dots\dots(9.4)$$

comparison of calculated and observed values was not possible since no studies pertaining to the grain size and grain boundary could be carried out in this work. Scope exists for carrying out the morphological studies on these samples. This is possible by subjecting the samples to electron microscopic studies.

However, the dielectric dispersion could be fitted in to a general equation of the form

$$\epsilon = \frac{\epsilon_{ij} - b \log f}{1 - c \log f}$$

and it was found that the equation fits very well with the observed values. It can be said intuitively that the constants b and c are related to the grain size or grain boundary. This demands further investigation for confirmation.

The temperature dependence of dielectric constant were also studied and it was observed that composites are stable upto a maximum temperature of 120°C with no visible sign of degradation.

From the cure time and tensile studies it was also observed that the tensile strength is dependent on the cure time. This has been explained as due to the increased crosslinking in the matrix with increase in the time of cure. This information is valuable in the sense that during the evaluation of the processability parameters one gets an idea about the behaviour tensile properties in advance.

As far as the electrical properties are concerned enormous data has been generated which can be used to model equations to predict the dependence of dielectric constant on temperature, frequency, composition and loading.

The magnetic and dielectric properties of these composites are important since microwave absorbing properties of these composites demand a certain dielectric permittivity and magnetic permeability. In the present investigation the dielectric studies were limited in the mid-frequency range that is, upto 8MHz. Scope exist to carry out further measurements using network analyser and evaluate the bandwidth of absorption. There are literature reports suggesting that carbon black is a good additive for enhancing the bandwidth of absorption for microwave applications. The effect of carbon black on the microwave absorbing property will be another futuristic proposition. Inert fillers like precipitated silica can also be used as additives in RFCs and one can study the electrical and magnetic properties of the compounds.

The method of evaluating the ac conductivity from the dielectric measurements is a simple technique. This has been carried out by automating the dielectric measurements and evaluating σ_{ac} by using the relation

$$\sigma_{ac} = 2\pi f \tan\delta \epsilon_0 \epsilon_r .$$

The variation of ac conductivity with temperature, frequency, composition and loading have been studied and correlated. They don't seem to be obeying any mixture equations. The activation energy for conduction is evaluated for both the composite as well as ceramic samples. The activation energy in the case of composites are very low. The low mobility of carriers in the polymer contribute to their low conductivity even for low activation energies. There are reports that the activation energy for conduction of inorganic semiconductor is higher than the corresponding activation energy of conductance of polymeric semiconductors.

Days won't be far when ordinary refrigeration gases, transformer cores and recording media are replaced with environmental friendly techniques based on magnetocaloric effect, transformers based on nanocomposites and other nanomaterials for recording, respectively. One would not be surprised if gamma iron oxide and ferrites based composite materials are the front running materials in this category. Iron oxide based composites are promising and have the potential because of its abundance and relative inexpensiveness. The entire field of refrigeration and hydrogen storage will witness a quite revolution if appropriate technology based on magnetic nanocomposites is developed. RFCs and RFCs based EMI shields and emulsions based on RFCs for antiradar applications have the potential as better substitute for the existing devices. Lossless transformers, high density MRAM etc will be the futuristic gadgets based on these materials. This all requires a fine and thorough understanding of the Physics and Chemistry of nanomaterials especially at the size and temperature that are talked about. This will be an area which will witness a huge research activity in the coming decade.

References

- 1 Smit J and Wijn H P G 1959 Ferrites (Philips Technical library)
- 2 Benjamin Lax, Kenneth J Button, Microwave ferrites and ferrimagnets, Mc Graw-Hill Book Co. (1962).
- 3 Daniel C.Mattis, The theory of Magnetism, Harper and Row Publishers New York 1965.
- 4 Ph.D.Thesis, Adrian Richard Muxworthy, Dept. of Earth Sciences, University of Oxford, 1998.
- 5 Yuji Masumoto, M.Murukami et al Science 291, 2Feb, 2001
- 6 D.Ralph, Science, 291 , 9 Feb 2001, p 9990
- 7 Hartley et al Science 290, 15Dec, 2000
- 8 B.D.Cullity, 'Magnetic Materials' Addison-Weisley Publishing Company, Inc (1972).
- 9 S.Henze, Science 288, 9 June2000, p1805.
- 10 E.C.Snelling and A.D Giles Ferrites For Inductors and Transformers, Research studies press. John Wiley and sons,1983.
- 11 D.P.E.Dickson, Biological Application, Nanophase Materials – Synthesis properties and applications (G.C.Hadjipanayis and R.W. Seigel (Edt.)), Kluwer Academic Publishers (1994) p729.
- 12 J.Douglas Adam, Magnetic Thin film devices (Vol4. Handbook of Thin film devices (Edt.) Maurice Francomb). Academic Press, U.K.2000.
- 13 C.Bergemann,D.Muller-Schulte, J.Oster, L.a Brassard, A.S.Lubbe,. J of MMM 194 (1999) 45-52.
- 14 V.Provenzano and R.L.Holtz, J.Material Science and Engineering A204(1995) 125-134.
- 15 Maurice Gell J.Material Science and Engineering A204(1995) 246-251.
- 16 Staurt M Lee, International Encyclopaedia of composites, VCH Publishers New York (1989), vol 1-6.

References

- 17 H.S.Gokturk, T.J.Fiske and D.M.Kalyon, *J.Appl.Phys.* 73 (10), 15May 1993.
- 18 Gerad Kraus *Reinforcement of Elastomers* . Inter Science Publishers John Wiley & Sons , New York, 1978.
- 19 J.H.Paterson, R. Devine ,A.D.R.Phelps, *J.Magn. Magn. Mater.* 196-197,(1999),394-396.
- 20 Ron Dagani, *Nanostructured Materials Promise To Advance Range of Technologies, Science/Technology*, 1992, p.18-24.
- 21 R. F.Ziolo, E.P.Giannelis, B.A Weinstein, Michela P. O'Horo, B.N.Gaguly, V.Mehrotra, M.W.Russel, D.R.Huffman. *Science* 257, 219(1992)
- 22 D.Chakravorty *Bull.Mat.Sci.*vol 15, no.5, 192 p 411-420
- 23 R.D.Shull and L.H.Bennet, *Nanocomposite magnetic materials, J.Nanaostructured Materials* vol 1(1992),p83-88.
- 24 Stoyen I. Ganchev *Microwave Diagnosis of Rubber compounds IEEE Trans. Microwave Theory nd tech.* vol- 42 , no. 1 January 1994.
- 25 Sung Soo Kim and Dae Hee Han *Microwave absorbing properties of Sintered Ni-Zn Ferrite IEEE Transactions on Magnetics* vol.30 No.6 November 1994.
- 26 S.A.Mirtaheri, J.Yin, H.Seki, T.Mizumoto and Y.naito, *The Trans. The IEICE* , Vol. E72 No.12 (1989) p1447-1452.
- 27 D.Y.Kim, Y.C.Chung, T.W.kang and K.C.Kim, *IEEE Trans. Magn.* Vol. 32 , No.2 (1996) p555-558.
- 28 Y.Naito, J.Yin, T.Mizumoto, *Elec. Commun. Japan* , Part 2 Vol. 71, No.7 (1988) p77-82.
- 29 Naito Y and Suetake K , *IEEE Trans. Micro. Theo. Tech.* , 19 (1971) 65.
- 30 Gruberger W, Spreingman B, Brusberg M, Schmit M and Jahnke R , *J. Mag. Mag. Mat.* 101 (1991) 173.
- 31 Z.Osawa,K.Kawauchi, M.Iwata,H.Harada, *J.Mater.Sci.* 23, (1998), 2637-2644..

References

- 32 S.A.Mirtaheri, T.miazumoto and Y.Naito The Trans. Of the IEICE, vol E73, no.10,1990
- 33 T.Nakamura, T.Tsutaoka, K.Hatakeyama, J.Mag. Mag. Mat. 138,(1994) 319-328.
- 34 M.R.Anantharaman, P.Kurian, B.Banerjee, E.M.Mohammed, and M.George: Kautschuk Gummi Kunststoffe, (Germany), 49,6/96, 424-426.
- 35 M.R.Anantharaman, S.Jagatheesan, S.Sindhu, K.A.Malini, C.N.Chinnasamy, A.Narayansamy, P.Kurian and K.Vasudevan. Plastic, Rubber and Composites processing applications, 1998 vol 27 No.2 , 77.
- 36 M.R.Anantharaman, S.Sindhu, S.Jagatheesan, K.A.Malini and Philip Kurian Journal of Physics D Applied Physics 32 (1999) P 1801-1817
- 37 F.Brailsford , Physical principles of magnetism, D Van Nostrand Co. Ltd. (1966).
- 38 D.Hadfield, Permanent Magnets and Magnetism, John Wiley and sons, Inc. London 1962.
- 39 H.V.Keer Principles of solid state physics Willey Eastern Ltd. New Delhi (1993)
- 40 J.Crangle, The Magnetic Properties of Solids, Edward Arnold (Publishers) ltd, 1977.
- 41 Soshin Chikazumi, Physics of magnetism , John Wiley and sons, Inc. New York
- 42 Ami E. Berkowitz and Eckart Kneller, Magnetism and Metallurgy, Academic Press Inc. 1969.
- 43 C.P.Bean and J.D.Livingstone, J.Appl.Phys. 30, (1959) p120
- 44 C.P.Bean, J.Appl. Physics vol.26, no.11, (1955), p1381.
- 45 C.R.K.Murty, magnetism and Basalts, Geological Society of India. Bangalore 1993.
- 46 S.Morup, Europhy. Letters, 28(9)(1994)p671-676.
- 47 S.Morup J.Mag.Mag.Mater.37(1983)39-50.

References

- 48 V.R.K.Murthy, B.Viswanathan, Ferrite Materials, Science and Technology (Narosa Publishing House) 1990
- 49 Charles Kittel, Introduction to Solid State Physics, John Wiley and Sons, New York, 1997.
- 50 K.J.Standley, Oxide magnetic materials. Clarendon Press, Oxford, 1972.
- 51 A.D. Roberts Natural Rubber Science and Technology Oxford University Press Newyork P.556. 1998.
- 52 Allen H.Morrish, Morphology and Physical properties of gamma iron oxide, p173-193.
- 53 L.Bateman(Edt.) The Chemistry and Physics of Rubber like substances. Applied Science Publishers,Ltd.London,1963.
- 54 Ferdinand Rodrigues , Principles of Polymer systems, McGraw Hill Inc. 1970.
- 55 A.Tager, Physical Chemistry of Polymers, Mir Publishers, Moscow, 1978.
- 56 G.C.Hadjipanayis and R.W. Seigel (Edt) Nanophase Materials – Synthesis properties and applications, Kluwer Academic Publishers (1994)
- 57 Y.Shi, J.Ding, X.liu and J.Wang J.Magn.Magn.Mater. 205 (1999) 249-254
- 58 D.Niznansky,J.L.Rehspringer and M.Drillon, IEEE Trns. On magnetics, vol30,no2. (1994)821-823
- 59 W.Gong, G.C.Hadjipanayis and R.F.Krause, J.Appl.Phys. 75 (10) 1994, 6649-6651.
- 60 R.F Ziolo, E.P.Giannelis and R.D.Shull, J.Nanostructured materials, vol.3,(1993),pp85-92.
- 61 J.K.Vassilovu, V.Mehrotra, M.W.Russel and E.P.Giannelis, Mater. Res.Soc. Symp.Proc.206,561(1991).
- 62 E.S.Watson, M.J.O'Neill, J.Justin and N.Brenne, Anl.Chem.36, (1964) 1233
- 63 Simon Foner, Rev. Sci. Instrum. Vol. 30, No.7 (1959) p548-557.

References

- 64 Joseph A. Pesch, Rev. Sci. Instrum, Vol.54, No.4 (1983)p480.
- 65 R.V.Krishnan and A.Banerjee, Rev. Sci. Instrum., Vol.70 No.1 (1999)p85
- 66 Arthur I. Vogel, Quantitative Inorganic Analysis, Third Edition, The English Language Book Society and Logmans, (1968) London.
- 67 N.N.Greenwood and T.C.Gibb, Mossbauer Spectroscopy, Chapman and Hall, London 1971.
- 68 Philip Gutlich, Ramer Link and Alfred Trautium, Mossbauer Spectroscopy and transition metal chemistry. Springer Verlag, Germany, 1998.
- 69 S.G.Cohen and M.Pasternak, Prospectives in Mossbauer Spectroscopy, Plenum Press, New York, 1973.
- 70 Metals Handbook, 9th Edition, Vol.10, Materials Characterisation, American Society for Metals. 1986.
- 71 Wertz J.E., Bolton J.R. *Electron spin resonance*. - New York, McGraw-Hill Book Company, 1972.
- 72 Walter Gordy, Theory and applications of Electron Spin resonance Spectroscopy,. John Wiley and Sons, Inc. 1980.
- 73 Raul Valenzuela, Magnetic ceramics, Cambridge University press, New York, (1994
- 74 D.C.Khan, M.Misra, Bull. Mater. Sci. 7 (1985) p253.
- 75 K.Ishino, Y.Narumiya, Cerm. Bull. 66 (1987) p1469.
- 76 B.V.Bhise, M.B.Dangare, S.A.Patil, S.R.Sawant, J. Mater. Sci. Lett. 10 (1991) p 922.
- 77 Cullity B.D Elements of X-ray diffraction 2nd edn.1978, Philippines, Addison-Weisley Publishing Company, Inc.
- 78 Ph.D.thesis, Sindhu.S., Cochin University of Science and technology, Cochin-22, 2001.
- 79 C.M. Blow and C.Hepburn Rubber Technology and Manufacture. Second edition. Butterworth Publication, 1985.
- 80 George G Winspear (Edt.), The Vanderbilt Rubber Handbook R.T.Vanderbilt Company Inc. Noew York, 1958.

References

- 81 Vishu Shah, handbook of plastic testing technology, John Wiley and sons inc USA 1998.
- 82 A.W.Allen, Natural Rubber and the Synthetics, Granada Publishing Ltd. 1972
- 83 ASTM D 2084-95.
- 84 Steven Blow. Hand book of Rubber Technology, Galgotia Publishing Pvt. Ltd. 1998.
- 85 Charles A Harper, Handbook of Plastic, Elastomers and Composites (2nd Edition) McGraw Hill Inc.1992.
- 86 A.Goswami, Thin Film Fundamentals, New age international Publishers Ltd. New Delhi (1996)
- 87 S.Gangopadhyay, G.C.Hadjipanyas, C.M.Soresen and K.J.Klabunde, Nanophase Materials – Synthesis properties and applications (G.C.Hadjipanayis and R.W. Seigel (Edt.)), Kluwer Academic Publishers (1994) p573.
- 88 J.J.Ritter, D.B.Minor, R.D.McMicheal and R.D.Shull. Nanophase and Nanocrystalline Structures, Edt. R.D.Shull and J.M.Sanchez. The Minerals, Metals & Materials Society, 1994.
- 89 E.M.Chudnovsky and L.Gunther, Phys.Rev.B 37, (1988) p9455.
- 90 R.D.McMicheal, R.D.Shull, L.J.Swartzendruber. L.H.Bennett and R.E. Watson. J. Magn. Mater. 111 (1992) p29
- 91 K.A.Gschneidner, JR. and V.K.Pecharsky, J.Appl.Phys.,85, no.8, 15 April (1999) p 5365.
- 92 R.D.Shull, J.J.Ritter, A.J.Shapiro,. MRS Symposium Proc. 132 (1989) p179.
- 93 R.D.Shull, J.J.Ritter and L.J.Swartzendruder, J.Appl.Phys. 69 (1991)p 5414
- 94 A.Gavrin and C.L.Chein, J.Appl.Phys. 67 (1990) p938 .
- 95 J.K.Vassiliou, V.Mehrotra, M.W.Russell, E.P.Giannelis, R.D.Mcmicheal, R.D.Shull and R.F.Ziolo J.Appl.Phys.73 (10),15 May 1993, p5109.

References

- 96 R.F.Ziolo, E.P.Giannelis, and R.D.Shull, Nanostructured Materials, vol.3. (1993) p95-92
- 97 R.D.Shull, J.J.Ritter, A.J.Shapiro, L.J.Swartzendruder and L.H.Bennet J.Appl.Phys.67(9) 1May1990, p4490
- 98 R.D.Shull, J.J.Ritter, A.J.Shapiro, L.J.Swartzendruder and L.H.Bennet MRS Symposium Proc. 206 (1991) p455-460
- 99 Jen-Hwa Hsu, Yi-Hong Huang, J.Mag.Mag.Mater. 140-144 (1995) 405-406.
- 100 Michel F.Bent, Borge I.Persson and DAVID G.Agresti, Computer Phy.Comm.1 (1969) p 67.
- 101 C.M.Lukehart, S.B.Milne, S.R.Stock, R.D.Shull, J.E.Witting, Mater.Sci.Engg. A204 (1995) 176-180.
- 102 T.Ambrose,A.Gavrin and C.L.Chien, J.Mag.Mag.Mater.116 (1992) L311-L314.
- 103 S.Roy, D.Das and D.Chakravorty, J.Appl. Phys. 74(7), 1993 p474.
- 104 W.J.Ping and L. H. Lie J.Mag. Mag. Mat. 131(1994)54-60.
- 105 D.T.Pierce, R.J.Celotta,J.Unguris and H.C.Seigmann, Phy.Rev.B26(1982)2566.
- 106 A.Chatterjee, D.Das, D.Chakravorty and K Choudhury, Appl.Phys.Letters 57(13),(1990), p13601362.
- 107 J.M.Daniels and A Rosencwaig, Can.J.Phys. vol48,(1970)p380
- 108 G.A.Sawatzky,F.Vander Woude and A.H.Morrish, Phys. Rev, vol187,no.2,(1969)p747.
- 109 A.P.Amulyavichus and I.P.Suzdalev, Sov.Phys.JETP, vol37,No.5(1973)
- 110 U.Gonser,H.Weidersich and R.W.Grant, J.Appl.Phys.vol.39, no.2, part (II) (1998), 1004-1005.
- 111 A.Hartridge, A.K.Bhattacharya ,C.K.Majumdar, D.Das and S.N.Chintalapudi, J.Mag.Mag.Mat.183(1998) L1-L4.
- 112 S.Morup, M.B.Madsen and J.Franck, J.Villadsen and C.J.W.Koch, J.Mag.Mag. Mat. 40(1983)163-174.

References

- 113 S.Morup, C.A.Oxborrow, P.V.Hendriksen, M.S.Pedersen, M.Hanson, C.Johansson, *J.Mag.Mag.Mat.*140-144(1995)409,410.
- 114 J.G.Lee, J.Y.Park and C.S.Kim *J.Mat.Science* 33(1998)3965-3968
- 115 F.Gazeau,J.C.Bacri,F.Gendron et al *J.Magn.Mag.Mat.* 186(1998)175-187
- 116 V.K.Sharma and F.Waldner, *J.Appli. Phys.*48,no10(1977)4298-4302.
- 117 R.V.Upadhyay, D.Srinivas, R.V.Mehta and P.M.Trivedi, *Pramana J.of Physics* vol45, no.5, (1995), 419-430
- 118 K.Nagata and A.Ishihara, *J.Mag.Mag.Mater.* 104-107(1992)1571-1573
- 103 Maurice Morton, *Rubber Technology*(2nd Edition) American Chemical Society, Van Nostrand Reinhold Company New York, 1973.
- 104 J.Brandrup, E.H.Immergut, E.A.Geulte (Editors) *Polymer Handbook* (4th Edition) John Wiley and Sons New York., 1997.
- 105 MITSUO SUGIMOTO *Journal of American Ceramic Society* . vol 82 No 2 P 269- 279 February 1999.
- 106 Jozef Slama, Anna Gruskova, Ludovit Keszesh, Mojmir Kollar, *IEEE Trans. Mag.* Vol. 30 No.2 (1994) p1101-1103.
- 107 Z.Osawa, K.Kawaguchi, M.Iwata, H.Harada, *J. Mater. Sci.* 23 (1988) p 2637- 44
- 124 H.Takei, H.Tokumasu, H.Rikukawa and I.Sasaki, *IEEE Trans. Mag.* Vol MAJ 23 (1987) p3080-3082.
- 125 A.M.Sankpal, S.S.Suryavanshi, S.V.Kakatbar, G.G.Tengshe, R.S.Patil, N.D.Chaudhari, S.R.Sawant, *J. Mag. Magn. Mater.* 186 (1998) p349-356.
- 126 ASTM 10- 325 (Ni ferrite) *Nat. Bur. Stands (U.S) circ.* 539 – 1044 (1960).
- 127 J.C. Anderson , K.D.Leaver, *Materials science*,– Thomas Nelson and sons Ltd. , 1969, Great Britain.
- 128 Hugh St.C.O’Neill and Alexandra Navrotsky *Simple spinels*: vol 68, p181-194 , 1983
- 129 W.J.S. Naunton(Edt.) *The Applied Science of Rubber*, Edward Arnold Publishing Ltd. 1961.

References

- 130 L.K.Leung, B.J.Evans, A.H.Morrish, *Phys. Rev. B*, 8 No.1 (1973) p29
- 131 V.C.Wilson and J.S.Kasper, *Phys. Rev.* 95, 1408 (1954),
- 132 N.S.Satyamurthy, M.G.Nater, S.I.Yousef, R.J.Begum and C.M.Srivastava, *Phys. Rev.* 181, 969 (1969),
- 133 V.I.Goldonskii, V.F.Belov, M.N.Devisheva and V.A.Trukhtanov, *Sov. Phys. JETP* 22, 1149 (1966),
- 134 T.Kamiyama, K.Haneda, T.Sato, S.Ikeda and H. Asano, *Solid State communications* Vol. 81, No.7, (1992) pp 563 – 566
- 135 T.Sato, K.Haneda, N.Seki and T.Iijima, *Appl. Phys. A* 50 (1990) 13-16
- 136 B.Jayadevan, K.Tohji and K.Nakatsuka, *J. Appl. Phys.* 76 No.10 (1994) p 6325-6327.
- 137 A.E.Berkowitz, R.H.Kodama, S.A.Makhlouf, F.T.Parker, F.E.Spada, E.J.McNiff Jr.,S.Foner, *J.Mag.Mag.Mater.*196-197(1999)591-594.
- 138 R.H.Kodama and A.E.Berkowitz , *Physical Review*,v 59, No.9, March 1999, p6321-6336.
- 139 C.N.Chinnasamy, A.Narayanasamy, N.Ponpandian, Justin Joseph (*Phys. Rev. B* in press).
- 140 M.R.Anantharaman,K.A.Malini, S.Sindhu, E.M.Mohammed and P.Kurian (pvt.communication)
- 141 Z.Gigbi and L.Jilken , *J. Magn. Magn. Mater.* 37 (1983) 267,
- 142 D.R.Saini, A.V.Sheony and V.M. Nadkarni, *J. Appl. Polym. Sci.* 29 (1983) 4123
- 143 Kuanr B K, Singh P K, Kishan P, Kumar N, Rao S L N, Prabhat K Singh, Srivastava G P 15 April *J.Appl.Phys.* 63(8) (1988)p3780-3782.,
- 144 El Hiti M A , *J.Mag. and Mag. Mat.* 164 (1996) p 187-196.,
- 145 Josyulu O and Sobhanadri J , *Phys.Status Solidi(a)* 59 (1980) p323.,
- 146 Ahmed M A, El Hiti M A, Mosaad M M and Attia S M , *J. Magn. Magn. Mater.* 146 (1995) p84.,
- 147 Murthy V R K and Sobhanadri J , *Phys. Status Solidi(a)* 36 (1976) p133.

References

- 148 Reddy P V and Rao T S , J. Less. Common. Met. 86 (1982) p255
- 149 Charles Phelps Smyth, Dielectric Behavior and Structure, Mc Graw-Hill Book Company, Inc., 1955
- 150 M.Safari Ardi, W.Dick amd D.H.MacQueen, J.Plastics, Rubber Composites, Processing and Applications, vol.24, 3, 1995, 157-164.
- 151 M.A.Abdeen, die. Beh. In NZF, J of MMM, 192, 1999, p 121-129
- 152 V.P.Miroshkin, Ya.P.Panova and V.V.Passynkov, Phys. Stat. Sol.(a) 66, 779 (1981).
- 153 S.A.Mazen M.H.Abdallah, M.A.Elghandoor and H.A.Hashem, Phys. Stat.Sol.(a) 144,461(1994).
- 154 C.G.Koops , Phys. Rev. 83 (1951) p 121-124
- 155 Tareev B 1979 Physics of Dielectric Materials (Mir Publishers) Moscow
- 156 N.Saxena, B.K.Kuanr, Z.H.Zaidi and G.P.Srivastava,. Phys.Stat. Sol(a) 127. 231(1991)
- 157 F. Haberey, H.J.P.Wijn, Phys. Stat. Sol. (a) 26 (1968) 231
- 158 Rezlescu.N and Rezlescu. E. Physica status solidi (a) 23 (1974) 575
- 159 Chandra Prakash and Baijal J.S, J. Less. Commn. Metals 107 (1985) p 51
- 160 Van Gitert L.G. , J. Chem. Phys. 24 (1956) p 306.
- 161 Patil R.S., Kakatkar S.V, Maskar P.K. , Patil S.A and Sawant S.R, Ind. J. Pure Appl. Phys. 29 (1991) p 589 – 592.
- 162 Chandraprakash and Baijal J.S., J. Less Commn. Metals 106 (1985) p 257
- 163 Elhiti M.A, Ahmed M.A, Mosaad M.M and Attia S.M , J. Mag. Mag. Mater. 150 (1995) p399-402
- 164 Shaikh A.M., Bellad S.S. and Chougule B.K J. Mag. Mag. Mater. 195 (1999) p384-390.,
- 165 J.J.O'dwyer, The theory of electrical conduction and breakdown in solids, Clarendon Press, Oxford.1973.
- 166 Frank E Karasz 1972 Dielectric Properties of Polymers (Plenum Press) New York

- 167 Musal Jr. H M, Hahn H T and Bush G G J.Appl. Phys.63(8) (1988)
p3768-3770.
- 168 Ki Chulhan, Hyung Do Choi, Tak Jin Moon, Wang Sup Kim and Kyung
Yong Kim J.Mater.Sci. 30(1995) p3567-3570.
- 169 R.D.Deanin, Polymer structure, Properties and Applications, Cahners
Books, Cahners Publishing Company, Inc. 1972.
- 170 J.P.Suchet, Electrical Conduction In Solid Materials, Pergamon Press,
1975
- 171 Andrej Žnidaršič and Miha Drofenik J. Ame. Ceram. Soc. 82 (1999) p
359
- 172 Yootarou Yamazaki and Minuru Satou Jap. J. Appl. Phy. 12 No.7
(1973) p998-1000.,
- 173 Ahmed M.A. and Elhiti M.A 1995 Journal de Physique III 5 775- 781.,
- 174 Abdeen A.M , J. Mag. Mag. Mater. 192 (1999) p121 – 129
- 175 Ahmed M.A, Elhiti M.A, El Nimr M.K and Amer M.A , J. Mag. Mag.
Mater. 152 (1996) p391-395.,
- 176 Pal M, Brahma P and Chakravorty D , J. Phys. Soc. Jap. 63 No.9
(1994) p3356- 3360
- 177 Brockman F.G and White R.P , J. Amer. Ceram. Soc. 54 (1971)
p183
- 178 Abdeen A.M , J. Mag. Mag. Mater. 185 (1998) p199 – 206.,
- 179 Elhiti M.A , J. Mag. Mag. Mater. 164 (1996) 187 – 196.,
- 180 Pal M, Brahma P and Chakravorty D , J. Mag. Mag. Mater.152 (1996)
p370- 374.
- 181 Samokhvalov A.A and Rustamov A.G , Soviet Physics – Solid State 6
No.4 (1964) 749 – 752
- 182 G.K.Joshi, S.A.Desh Pande, A.Y. Khot, S.R.Sawant, J. Appl. Phys. A
61 (1987) 251
- 183 Radhapiyari Laishram, Sumithra Phanjoubam, HNK Sarma and Chandra
Prakash, J of Phys,D:Appl. Phy.32 (1999) p 2151-2154
- 184 R. Satyanaryana, S.R. Murthy, T.S.Rao, J. Less Commn. Met. 90
(1983) 243

References

- 185 G.K.Joshi, A.Y.Khot, S.R.Sawant, Solid State Commun. 65 (1988) 1593
- 186 H.D.Patil, R.V.Upadhyay, N.R.Shankamar, R.G.Kulkarni, Solid State Commun. 81 (1992) 1001
- 187 R.B.Jotamia, R.V.Upadhyay, R.G.Kulkarni, IEEE Trans. Magn. 28 (1992) 1889
- 188 C.Prakash, J.S.Bijal, P.Kishan, J. Less- common Met. 106 (1985) 243
- 189 J.S.Bijal, S. Phanjouban, d.Kothari, C.Prakash, P.kishan, Solid State Commun. 83 (1992) 679
- 190 P.V.Reddy, T.S.Rao, S.M.D. Rao, J. Less Commn. Met. 79 (1981) 191
- 191 E. Iguchi, A. Tamenori and N.Kubota, Phys. Rev. B , 45 (1992) 697
- 192 E.Iguchi, N. Kubota, T.Nakamori, N. Yamamoto and K.J.Lee, Phys. Rev. B 43 (1991) 8646
- 193 N.F.Mott, J. Non. Cryst. Solids 1 (1968) 1
- 194 D.Chakravorthy and A.Srivastava, J. Phys. D : Appl. Phys. , 19 (1986) 2185
- 195 D.Emin and T.Hostein , Ann. Phys. N.Y. , 53 (1969) 439
- 196 W.A.Philips , Phil. Mag. , 34 91976) 983
- 197 S.R. Elliott , Adv. Phys. 36(2) (1978) 135
- 198 G.E.Pike , Phys. Rev B 6 (1972) 1572
- 199 A.R. Long , Adv. Phys. 31 (1982) 553
- 200 L.G.Austin and N.F. Mott , Adv. Phys. 18 (1969) 41
- 201 M.A.El Hiti, J. Phys. D: Appl. Phys. 29(1996) 501
- 202 M.A.El Hiti Phase Trans. 54 (1995) 117
- 203 M.A.Ahmed, M.A.El Hiti, M.K.El Nimr, M.A.Amer, J. Magn. Magn. Mater. 152 (1996)391
- 204 M.A.El Hiti, M.K. El Nimr, M.A. Ahmed, Phase Trans. 54 (1995) 137
- 205 M.M.Mosaad, M.A.Ahmed, M.A.Ahmed, J. Magn. Magn. Mater. 150 (1995) 51
- 206 M.A.Ahmed, M.A.El Hiti , M.M.Mosaad, S.M.Ahmed, J. Magn . Magn. Mater. 146 (1995) 84

References

- 207 M.A.El Hiti, J.Magn. Magn. Mater. , 164 (1996) 187
- 208 M.A.El Hiti, J. Magn. Magn. Mater. 136 (1994) 138
- 209 Largeteau, J.M. Reau and J.Raves , Phys. Stat. Sol. (a) 121 (1990) 627
- 210 M.El-Saadway and M.M.Barakat, J.Mag.Mag.Mat. 205(1999)p319-322.
- 211 D.A.Seanor (edt.) Electrical properties of Polymers , Academic press
New York, 1982.
- 212 James M.Margolis, (Edt), Conductive Polymers and Plastic, Chapman
and Hall, New York, 1989.
- 213 Ya.M.Paushkin, T.P.Vishnyakova, A.F.Lunin, S.A.Nizova, Organic
Polymetric Semiconductors , Keter Publishing House Jerusalem Ltd,
1974
- 214 M.P.Sharroock, L.Josephson IEEE, Tran.Mag. vol. Mag-22,No.5 1986.
- 215 H.H.Kung and M.C.Kung, Advances in Catalysis.33 (1984)159.

ANNEXURE I

STUDIES ON THE INFLUENCE OF DOPANTS ON THE PROPERTIES OF MAGHEMITE

A1.1 Introduction

Maghemite ($\gamma\text{-Fe}_2\text{O}_3$) and materials derived from $\gamma\text{-Fe}_2\text{O}_3$ in the acicular form find applications as a magnetic storage medium⁽¹⁾. About 90% of audio/video and computer diskettes employ these needle shaped gamma ferric oxides either in the particulate or thin film form⁽²⁾. The $\gamma\text{-Fe}_2\text{O}_3$ is a widely used material for recording media because it has the ideal combination of hysteresis loop parameters such as saturation magnetisation (M_s), coercivity (H_c) and squareness ratio (M_r/M_s). It is generally preferred in the form of acicular single domain particles⁽³⁾. The need for single domain particles is for obtaining optimum value of coercive force⁽⁴⁾. The acicular shape is for better alignment of particles while on recording which in turn is related to signal to noise ratio⁽⁵⁾. Gamma ferric oxide is also used as a potential catalyst in petrochemical industry⁽⁶⁾. Hence studies relating to gamma ferric oxide and gamma ferric oxide based materials are commercially very important. It has also been discovered recently that polymer nanocomposites containing gamma iron oxide exhibit novel properties like superparamagnetism and are potential materials for magnetic refrigeration^(7,8).

Gamma ferric oxide is a vacancy ordered spinel having the structure $\text{Fe}^{3+}[(\text{Fe}^{3+})_{5/3}\square_{1/3}]\text{O}_4$ where the vacancies are exclusively concentrated on the octahedral sites⁽⁹⁾. These vacancies give scope for doping gamma ferric oxide with cations having octahedral site preferences, thereby leading to modification of magnetic properties without altering its basic structure. This will lead to thermal stability⁽¹⁰⁾. There are also reports stating that $\gamma\text{-Fe}_2\text{O}_3$ exhibits a structure similar to hydrogen ferrite having the formula $\text{Fe}_8[\text{H}_4\text{Fe}_{12}]\text{O}_{32}$ ⁽¹¹⁾. The addition of dopants into the $\gamma\text{-Fe}_2\text{O}_3$ lattice has been known to modify the magnetic properties⁽¹²⁾. Here in this study pure and doped acicular $\gamma\text{-Fe}_2\text{O}_3$ have been prepared using acicular ferrous oxalate dihydrate precursors⁽¹³⁾. Dopants like magnesium, nickel

and gadolinium were incorporated in to the lattice. These were then characterised using XRD, UV-VIS-NIR, FTIR and magnetic measurements. Doping may effect changes in symmetry and also on the optical bandgap. Changes if any, introduced by doping can be detected by using spectroscopy as an analytical tool.

A1.2 Experimental Details

A1.2.1 Synthesis of gamma iron oxide containing dopants

Gamma ferric oxide containing dopants were prepared in the form of acicular particles by employing acicular oxalate precursors⁽¹⁴⁾. The oxalate precursors containing the appropriate dopants were decomposed in an inert atmosphere containing oxygen free nitrogen at around 400°C to yield Fe₃O₄ which was then carefully oxidised to doped gamma ferric oxide at around 200°C. The preparation scheme is depicted in the form of a flow chart (FigA1.1).

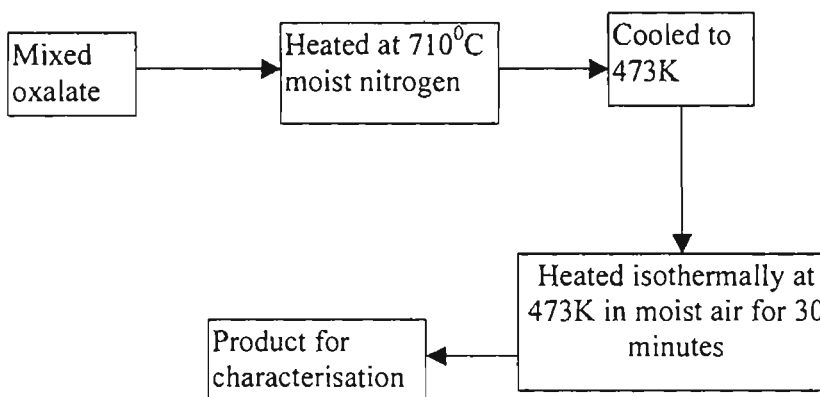


Fig.A1.1 Preparation details of doped acicular gamma ferric oxide(Schematic)

A1.2.2 Characterisation

A1.2.2.1 Structural studies;

Powder diffractograms were recorded on a Philips PW1140 diffractometer using CuK_α radiation. The lattice parameters for pure and doped γ-Fe₂O₃ were evaluated assuming cubic symmetry.

A1.2.2.2 Morphology studies :

The optical micrographs and TEM of some representative samples were recorded by using optical microscope (Versamet2) and TEM (Philips EM 301) respectively.

A1.2.2.3 Magnetisation measurements:

Magnetisation measurements on magnesium and nickel doped samples were carried out by using hysteresis loop tracer (HLT)⁽¹⁵⁾. Magnetic properties such as saturation magnetisation, coercivity and squareness ratio were evaluated by using HLT.

A1.2.2.4 Spectroscopic studies :

UV-VIS-NIR absorption spectra of pure and doped γ -Fe₂O₃ samples were charted by using Hitachi UV-VIS-NIR spectrophotometer (model U3410). The optical band gap of these samples was evaluated from the spectra by noting the wavelength λ_g corresponding to the absorption edge. The energy corresponding to this wavelength was calculated using the formula

$$E_g = hc/\lambda_g$$

FTIR spectra of these samples were also recorded to find out different IR absorption bands. The spectrum was charted on a FTIR spectrophotometer (Schimadzu 8101) in the range 1500-400 cm⁻¹.

A1.3. Results and Discussion

A1. 3.1 Structural studies

X-ray powder diffractograms were recorded for pure and doped compositions. Lattice parameters for pure and doped samples were calculated under the assumption that they crystallize in the spinel structure. The details are given in Tables A1.1, A1.2 and A1.3 for magnesium, nickel and gadolinium doped samples respectively. The lattice parameters were found to be 0.833nm, 0.830nm and 0.832nm for Mg, Gd and Ni doped samples. It can be seen that doping do not effect any notable change in lattice parameter. The absence of any increasing or decreasing trend in lattice parameter with increase in dopant concentration can be attributed to the following.

Table A1.1-Lattice parameter, magnetisation data and optical bandgap for magnesium doped γ -Fe₂O₃ samples.

Dopant concentration in atomic %	Lattice parameter in nm	Saturation magnetisation Ms in Am ² /Kg	Coercivity Hc in A/m	Optical bandgap in eV
0	0.834	77	19900	1.84
1	0.833	89	25950	1.83
2	0.833	100	21492	1.83
4	0.833	76	18308	1.85
6	0.833	91	21492	1.81
8	0.834	81	16716	1.84
10	0.833	80	15920	1.84
16	0.833	86	15920	1.84

Table A1. 2 - Lattice parameter, magnetisation data and optical bandgap for nickel doped γ -Fe₂O₃ samples.

Dopant concentration in atomic %	Lattice parameter in nm	Saturation magnetisation Ms in Am ² /Kg	Coercivity Hc in A/m	Optical bandgap in eV
0	0.834	77	19900	1.84
1	0.832	83	17910	1.83
4	0.832	78	19900	1.72
8	0.832	73	18308	1.72
16	0.834	74	19900	1.83

Table A1.3 - Lattice parameter and optical bandgap for gadolinium doped γ -Fe₂O₃ samples

Dopant concentration in atomic %	Lattice parameter in nm	Optical bandgap in eV
0	0.834	1.84
1	0.830	1.93
2	0.834	1.82
4	0.834	1.84
6	0.832	1.69
8	0.833	1.85

These cations have the right ionic radii to fill the octahedral voids of the spinel lattice. An ideal close packed structure consisting of rigid ions in the tetrahedral interstices should permit ions with maximum ionic radii of 0.04nm and whereas the octahedral ones can have a maximum radius of 0.073 nm^(9,16). Since the ionic radii of nickel, magnesium and gadolinium are greater than 0.04nm, it is right to assume that they occupy octahedral sites. Normally in order to accommodate larger sized ions the lattice should expand. Since we do not observe any increase in lattice parameter it is presumed that these ions occupy octahedral vacancies.

A1.3.2 Morphological studies

The optical and TEM micrographs of some representative samples are shown in Figs. A1.2(a) and A1.2(b). These micrographs confirm the acicular nature of the precursors as well as that of maghemite.



Fig A1.2.a. Optical Micrograph of acicular ferrous oxalate dihydrate precursors
 b. TEM of gamma iron oxide prepared using the precursors.

A1.3.3 Magnetic measurements

Saturation magnetisation (M_s) and coercivity (H_c) of pure as well as magnesium and nickel doped samples are listed in Tables A1.1 and A1.2 for magnesium and nickel doped samples respectively. Doped gamma ferric oxide exhibits higher saturation magnetisation than that of pure gamma ferric oxide. Theoretically one should expect a steady increase in M_s with increase in dopant concentration. The expected gradual increase in M_s is not observed probably because due weightage for particle size effects is not given. Moreover, the presence of superparamagnetic particles even in small quantities can bring down

the saturation magnetisation value considerably. Since the particle size measurements have not been carried out it is hard to conclude that only superparamagnetic particles are responsible for reduction in saturation magnetisation. It is also possible that some amount of alpha iron oxide is present in these samples which is out of the detectable limits of XRD. These doped samples exhibit a relative increase in saturation magnetisation with respect to pure $\gamma\text{-Fe}_2\text{O}_3$. Since the dopant concentration is very small and a thorough chemical analysis is not performed on these samples, these inferences are only tentative. Coercivity (H_c) largely depends on magnetocrystalline anisotropy, and in this case it does not show any specific trend.

A1.3.4. Spectroscopic studies

Absorption spectra were recorded to determine the influence of dopants on the bandgap of these materials. From the UV-VIS-NIR absorption spectra the optical bandgap for pure and doped $\gamma\text{-Fe}_2\text{O}_3$ were calculated and are listed in Tables A1.1, A1.2 and A1.3 for magnesium, nickel and gadolinium doped samples respectively. The bandgap calculation employing the method of absorption edge involves an error of <2%. It is seen that pure $\gamma\text{-Fe}_2\text{O}_3$ exhibits a bandgap of 1.84eV, while doped compositions except 6% gadolinium and 4 and 8% nickel doped samples have almost the same bandgap as that of pure $\gamma\text{-Fe}_2\text{O}_3$. This gives complementary evidence to the inference drawn from the structural characterisation that no significant structural changes are effected by doping. In the case of 6% gadolinium and 4 and 8% nickel doped samples the bandgap is found to be less than that of pure gamma ferric oxide. This may be due to the presence of alpha ferric oxide which may be present in the form of impurities.

Spectroscopy has been a valuable tool for detecting the fundamental vibrations of OH stretching⁽¹⁷⁾. This is especially true for determining the OH vibrations on oxide surfaces. Extensive investigations were carried out on $\gamma\text{-Al}_2\text{O}_3$ which resemble the structure of $\gamma\text{-Fe}_2\text{O}_3$. On alumina surfaces three bands are detected in the range 3700 to 3800 cm^{-1} . However at higher resolutions 5 bands can be observed. The five OH stretching bands which were observed during dehydroxylation of $\gamma\text{-Al}_2\text{O}_3$ surfaces were attributed to OH groups in distinct lateral surface environments. Thus the high wave number band at 3800 cm^{-1} was

assumed to be characteristic for OH group with four oxide neighbours in the surfaces whereas the lowest band at 3700cm^{-1} correspond to the OH group that has no oxide neighbours. The other OH groups which give rise to intermediate wave numbers at 3711 , 3744 and 3780cm^{-1} were assumed to be located at one, two and three nearest neighbour oxide ions respectively. If gamma ferric oxide crystallizes in the hydrogen ferrite structure as predicted by researchers⁽¹⁸⁾, then bands due to OH should have been present in the spectra. We did not detect OH bands in the FTIR spectra. Our attempts to detect OH overtones in UV-VIS-NIR spectra was also in vain. Thus it may be noted that these conclusions drawn from the structural studies also points to the formation of a vacancy ordered spinel structure of gamma ferric oxide. This leads us to believe that gamma ferric oxide prepared via the oxalate precursor route has crystallised in the vacancy ordered spinel structure.

Normally compounds exhibiting spinel structure should possess four IR active modes leading to four IR bands in the spectra^(19,20). In the spinel lattice every oxygen anion is bonded to three octahedral and one tetrahedral cations as shown in Fig.A1.3. The three octahedral bonds are perpendicular to each other and hence provide an isotropic field. The tetrahedral cation C_T introduces a restoring force in a direction along C_T -O bond and this appears as stretching vibration of the tetrahedral group. Considering the vibration of oxygen atom at right angles with the preceding one this restoring force due to tetrahedral cation C_T will be negligible. This leads to ν_2 mode which can be considered as the stretching vibration of the octahedral group. Two other modes ν_3 and ν_4 are related to the displacement of cations in the lattice.

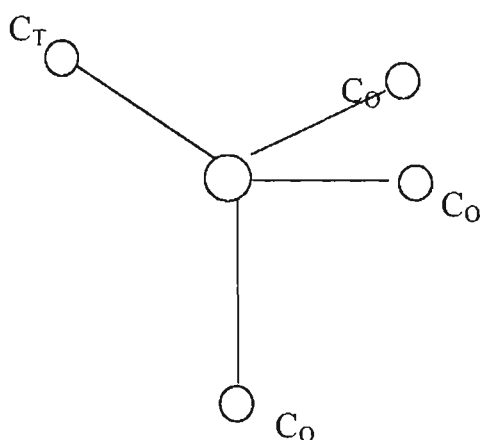


Fig.A1.3. Bonding of tetrahedral and Octahedral cations with oxygen in the spinel lattice.

FTIR spectra of the pure as well as doped gamma ferric oxide were charted in the range $1500-400\text{ cm}^{-1}$ and a representative spectrum is shown in Fig.A1.4. Bands characteristics of these samples were obtained in the range $700-400\text{ cm}^{-1}$. Peaks were obtained at around 636 , 555 and 443 cm^{-1} . Bands at 636 and 555 cm^{-1} may be assigned to the stretching vibrations of tetrahedral and octahedral groups respectively. The bands related to ν_3 and ν_4 can be assigned to the motion of Fe^{3+} ions to the tetrahedral sites against those at the octahedral sites and the O-Fe-O bonding mode of the tetrahedral to octahedral mode respectively. These bands are reported to be at 268 cm^{-1} and 178 cm^{-1} which could not be detected because of the instrument limitations. The band at around 440 cm^{-1} may be assigned to the alpha phase of iron oxide that may be present in the sample. However discrepancy exists in the 4 and 8% nickel doped samples, which may be due to impurities present in minute amounts.

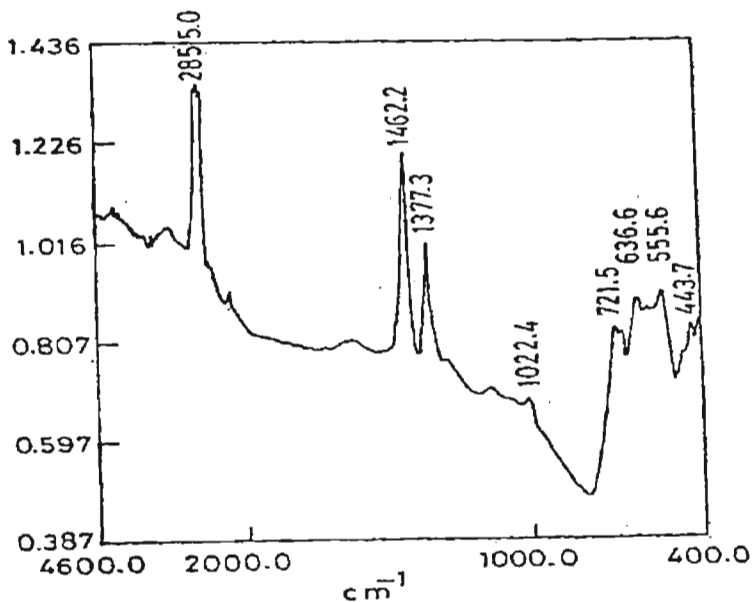


Fig.A1.4 A representative FTIR spectrum (1 % Mg doped $\gamma\text{-Fe}_2\text{O}_3$)

A1. 4. Conclusion

The present studies conducted on doped gamma iron oxide indicate that saturation magnetisation (M_s) can be modified by an appropriate choice of cations. The advantage of employing oxalate precursor route is that doped oxides can be prepared in the acicular form. It can be concluded that spectroscopic studies can be used in conjunction with X-ray diffraction for evaluating the role of dopants and its effect, if any on the crystal structure. Though literature reports on the γ - Fe_2O_3 are varied our investigations indicate that it crystallises in the vacancy ordered spinel structure.

A1. REFERENCES

1. Bate G, & Alstad J K, *IEEE Trans. on Magn.* 5 (1969) 823.
2. Koster E, *J. Magn. and Magn. Mater.*, 120(1993)1.
3. Bate G, *J. Magn. and Magn. Mater.*, 100(1991)413
4. Cullity B D, '*Introduction to magnetic materials*', Addison Wesley Publishing Company, The Philippines. (1972),339.
5. Seshan K, Chakrabarty D K & Biswas A B, *Phys. Status Solidi (a)*, 63(1981) K123
6. Harold H Kung & Mayfair C Kung, *Adv. Catalysis*, 33 (1984)159.
7. R.F Ziolo, et al, *Science*, 257 (1992) 219.
8. J.K Vassiliou, et al *J.Appl.Phys.*73(1993), 5109.
9. Raul Valenzuela, '*Magnetic ceramics*', (Cambridge University press, New York), (1994)3.
10. Ramachandra Bhat, Anantharaman M R, & Keer H V, *Indian J of Chem.* 28A (1989) 649.
11. Braun P B, *Nature* 170 (1952)1123.
12. Gougeon M, Dupuy O, Sarda Ch, et al *J. Mag. and Mag. Mater.*, 120 (1993) 40.
13. Anantharaman M R, Joseph K V & Keer H V, *Bull. of Mater.Sci*, 20(1997) 975.
14. Ph D Thesis, Anantharaman M R, IIT Bombay, 1984.
15. Likhite S D, Radhakrishnamurty C & Sahasrabudhe P, *Rev Sci Instrum*, 36(1965)1558.
16. *Ferrite Materials, Science and Technology*, Edited by B Viswanathan, V R K Murthy (Narosa Publishing House, New Delhi), (1990)4 .
17. Knozinger H & Ratnasamy P, *J Cat Rev Sci Engg* 17 (1978) 31.
18. Nikumbh A N, Rane K S & Mukhedkar A J, *J Mater Sci*, 17(1982) 2503.
19. Gillot B & Bouton F, *J Solid State Chem* 32(1980)303.
20. Gledhill G A, Hamilton A A, Nikolic P M et al. *Science of Sintering*, 24 (1992) 15.

Annexure II

Papers Published/ Communicated in Journals

1. On the magnetic properties of ultrafine zinc ferrites.
M.R.Anantharaman, S.Jagatheesan, K.A.Malini, S.Sindhu, A.Narayanasamy, C.N.Chinnasamy, J.D.Jacobs, Reijne, K.Seshan, R.H.H.Smits, and H.H.Brongersma, *Journal of Magnetism and Magnetic Materials*, **189** (1998) p 83-88.
2. Investigations on the cure characteristics and magnetic properties of Rubber ferrite Composites, M.R.Anantharaman, S.Jagatheesan, S.Sindhu, K.A.Malini, A.Narayanasamy, C.N.Chinnasamy, Philip Kurian and K.Vasudevan, *International Journal of Plastics, Rubber and Composites-Processing and Appl*, **27**, No.2 (1998) p 77-81.
3. Dielectric properties of rubber ferrite composites containing mixed ferrites, M.R.Anantharaman, S.Sindhu, S.Jagatheesan, K.A.Malini, and Philip Kurian, *J. Phy D: Applied Physics*, **32** 15(1999) p 1801- 1810.
4. Studies on the influence of dopants on the properties of maghemite –A tape material, M.R.Anantharaman, K.A.Malini, P.D.Sindhu, S.Sindhu and H. V. Keer, *Indian Journal of Pure and Applied Physics*, **37** (1999) p 842-847
5. Effect of cycling on the magnetization of ion exchanged nanocomposites based on polystyrene, K.A.Malini, M.R.Anantharaman, S.Sindhu, C.N.Chinnasamy, N.Ponpandian, A.Narayanasamy, M.Balachandran & V.N.Sivasankara Pillai, *Journal of Materials Science*, **36** (2001) 821-824.
6. Preparation and spectroscopic characterisation of plasma polymerised poly aniline thin films. Minimol Augustine, Mini Sebastian, Malini.K.A., Samkumar M.C., Joseph M.J., Tenson Joseph, D.Sakthikumar, S.Jayalekshmy, T.M.A. Rasheed and M.R.Anantharaman. *Indian Journal of Pure and Applied Physics*, **34**, (1996), 966-971
7. Evaluation of mechanical and Dielectric properties of RFCs containing $Ni_{1-x} Zn_xFe_2O_4$ in NR matrix, K.A.Malini, E.M.Mohammed, S.Sindhu, P.Kurain and M.R.Anantharaman (*Plastics rubber composites processing and applications- Under revision*)
8. Calculation of ac conductivity of rubber ferrite composite from dielectric easurements, S.Sindhu, M.R.Anantharaman, Bindu P Thampi,

- S.Jagatheesan, K.A.Malini and Philip Kurian (*Communicated to Journal of Materials Science*).
9. Magnetic and processability studies on rubber ferrite composites based on natural rubber and mixed ferrite, K.A.Malini, E.M.Mohammed, S.Sindhu, P.A.Joy, S.K.Date, S.D.Kulkarni, P.Kurian and M.R.Anantharaman (*Communicated to Journal of Materials Science*).
 10. Tailoring magnetic and dielectric properties of rubber ferrite composites containing mixed ferrites, M.R.Anantharaman, K.A.Malini, S.Sindhu, E.M.Mohammed and P. Kurian (*Communicated to Bull. Mater.Science*)

Papers presented in conferences / Seminars

1. Studies on the influence of dopants on the properties of maghemite. K.A.Malini, P.D.Sindhu, and M.R.Anantharaman. DAE SSP-97 held at Cochin University of Science and Technology, Cochin, India during Dec.1997.
2. Preparation and characterisation of magnetic nanocomposites. K.A.Malini, V.N.S.Pillai, C.N.Chinnasamy, A.Narayanasamy, P.Kurian and M.R.Anantharaman. MRSI Annual General Meeting at IIT Madras during February 1998.
3. Synthesis of magnetic nanocomposite based on iron oxide and evaluation of their properties. K.A.Malini, V.N.S.Pillai, C.N.Chinnasamy, A.Narayanasamy, P.Kurian and M.R.Anantharaman. Advances in Polymer Technology-98 (APT-98) at PS&RT , CUSAT during March 1998.
4. Investigations on Rubber ferrite composites.
S.Sindhu, M.R.Anantharaman, S.Jagatheesan, K.A.Malini, P.Kurian and K.Vasudevan, National Symposium on Advances in Polymer Technology held at CUSAT, India, during March 27-28 , 1998.
5. Magnetic and Dielectric properties of rubber ferrite composites. , S.Sindhu, S.Jagatheesan, M.R.Anantharaman, K.A.Malini, C.N.Chinnasamy, and A.Narayanasamy. National Seminar on Magnetism and Magnetic Materials held at CUSAT, India during February 22-23 1999.

6. Calculation of AC Conductivity from Dielectric Measurements and Studies on the AC Conductivity of Rubber Ferrite Composites. S.Sindhu, Bindu P. Thampi, K.A.Malini, E.M.Mohammed, P.Kurian and M.R.Anantharaman, DAE SSP symposium held at Kalpakkam, India during 20-24 December 1999.
7. Tailoring magnetic and dielectric properties of rubber ferrite composites containing mixed ferrites. M.R.Anantharaman, S.Sindhu, K.A.Malini, E.M.Mohammed, and P.Kurian, National Seminar on current trends in materials science, held at Mahatma Gandhi University, Kottayam, India during 23-24 March 2001.
8. Preparation and spectroscopic characterisation of plasma polymerised poly aniline thin films. Minimol Augustine, Mini Sebastian, Malini.K.A., Samkumar M.C., Joseph M.J., Tenson Joseph, D.Sakthikumar, S.Jayalekshmy, T.M.A. Rasheed and M.R.Anantharaman. National Seminar on Developments of Electronic Materials and their Applications held at Shivaji University, Kolhapur. India during March 1995.